Ruđer Bošković Institute

Croatian Microscopy Society

INNOMOL project

PROCEEDINGS

3rd CROATIAN MICROSCOPY CONGRESS

with International Participation

April 26-29, 2015

Zadar, Croatia

Editors

Andreja Ambriović Ristov, Andreja Gajović, Igor Weber and Ana Vidoš

Publishers

Ruđer Bošković Institute and Croatian Microscopy Society

3rd CROATIAN MICROSCOPY CONGRESS with International Participation: PROCEEDINGS

3rd CROATIAN MICROSCOPY CONGRESS with International Participation

April 26-29, 2015, Zadar, Croatia

Editors: Andreja Ambriović Ristov, Andreja Gajović, Igor Weber and Ana Vidoš

Publishers: Ruđer Bošković Institute and Croatian Microscopy Society

Number of copies: 120

ISBN 978-953-7941-05-5

ORGANIZING COMMITTEE

- *Ivanka Jerić*
- *Jelena Macan*
- *Andreja Ambriović Ristov*
- *Hrvoje Fulgosi*
- *Ana Vidoš*

SCIENTIFIC COMMITTEE

- *Igor Weber*
- *Andreja Gajović*
- *Ivana Bočina*
- *Sanja Štifter*
- *Stefan Terjung*
- *Nenad Tomašić*
- *Oliver Vugrek*

CONGRESS SPONSORS

Platinum Sponsor

Golden Sponsors

Sponsors


assing
PARTNER DELLA RICERCA

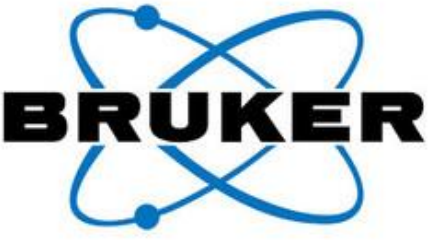
BRUKER


Ansar-analitika d.o.o.
Analytical equipment


ikrolux
www.mikrolux.hr


TESCAN
PERFORMANCE IN NANOSPACE

PROGRAM

PROGRAM OVERVIEW

Sunday, 26. April 2015

17:00	**REGISTRATION & POSTER SET UP** (Lobby)
18:00	**OPENING CEREMONY** (Lecture hall 1)
18:30	**KEYNOTE LECTURE** (Lecture hall 1)
19:30	**WELCOME PARTY** (Lobby)

Monday, 27. April 2015.

9:00-10:20	**PLENARY LECTURES** (Lecture hall 1)
10:20-10.50	COFFEE BREAK
10:50-11:50	**INVITED LECTURES / PARALLEL SESSIONS**
11:50-12:30	**SELECTED LECTURES / PARALLEL SESSIONS**
12:30-13:30	LUNCH BREAK
13:30- 14:10	**EQUIPMENT PRESENTATION**(Lecture hall 1) **INEL / LEICA** **MIKRO+POLO**
14:20-15:20	**INVITED LECTURES / PARALLEL SESSIONS**
15:20-15:40	**EQUIPMENT PRESENTATION / PARALLEL SESSIONS** **JEOL / SCAN**
15:40-16:00	**SELECTED TALKS / PARALLEL SESSIONS**
16:00-17:30	**POSTER SESSIONS / REFRESHMENTS** (Lobby)
19:00	**ZADAR BY NIGHT TOUR**

Tuesday, 28. April 2015

9:00-10:20	**PLENARY LECTURES** (Lecture hall 1)
10:20-10.50	COFFEE BREAK
10:50-11:50	**INVITED LECTURES / PARALLEL SESSIONS**
11:50-12:30	**SELECTED LECTURES / PARALLEL SESSIONS**
12:30-13:30	LUNCH BREAK
13:30-19:00	EXCURSION - NATIONAL PARK KRKA
20:00	GALA DINNER

Wednesday, 29. April 2015

9:00-10:20	**PLENARY LECTURES** (Lecture hall 1)
10:20-10.50	COFFEE BREAK
10:50-11:50	**INVITED LECTURES / PARALLEL SESSIONS**
11:50-12:30	**SELECTED LECTURES / PARALLEL SESSIONS**
12:30	CLOSING
12:50-14:20	LUNCH

Sunday, 26. April 2015

17:00 **REGISTRATION & POSTER SET UP** (Lobby)

18:00 **OPENING CEREMONY** (Lecture hall 1)

18:30 **KEYNOTE LECTURE** (Lecture hall 1)

Rainer Pepperkok: High throughput microscopy to study organelle biogenesis and membrane traffic in mammalian cells

19:30 **WELCOME PARTY** (Lobby)

Monday, 27. April 2015.

9:00-10:20 **PLENARY LECTURES** (Lecture hall 1)

Paul Dyson: Streptomyces development: imaging from outside in

Velimir R. Radmilović: Aberration corrected microscopy of functional oxide nanowires at atomic scale

10:20-10.50 COFFEE BREAK

10:50-11:50 **INVITED LECTURES / PARALLEL SESSIONS**

LIFE SCIENCE
(Lecture hall 1)

Paul Herron: Imaging chromosome segregation in Streptomyces coelicolor

Karim Benihoud: Increased uptake by Kupffer cells and reduced liver transduction and toxicity following serotype 5 adenovirus pseudotyping with serotype 3 fiber

MATERIAL SCIENCE
(Lecture hall 2)

Miran Čeh: High-resolution STEM Investigations of SrO-doped Sr(Ti,Nb)O3 and In2O3-doped ZnO oxide thermoelectrics

Jordi Arbiol: Direct correlation between optical properties at sub-nanometer scale and structure at atomic scale, in-situ performance in a STEM

11:50-12:30 SELECTED LECTURES / PARALLEL SESSIONS

LIFE SCIENCE (Lecture hall 1)	MATERIAL SCIENCE (Lecture hall 2)
Suzana Šegota Nanoparticle clustering within lipid membranes induced by surrounding medium. nanomechanical and thermotropic study on model lipid membranes	**Milivoj Plodinec:** Increased photoconductivity in BaTiO3/TiO2 composites
Vida Čadež: Biomineral structures of aragonite in marine mollusks at the nanoscale: FESEM and AFM studies	**Igor Djerdj:** Novel mixed phase sno2 nanorods for enhancing gas-sensing performance towards isopropanol gas

12:30-13:30 LUNCH BREAK

13:30-14:10 EQUIPMENT PRESENTATION (Lecture hall 1)

INEL / LEICA

MIKRO+POLO

14:20-15:20 INVITED LECTURES / PARALLEL SESSIONS

LIFE SCIENCE (Lecture hall 1)	MATERIAL SCIENCE (Lecture hall 2)
Eva Bártová: Confocal microscopy and DNA repair studies in living cells	**Mariana Klementová:** What can electron diffraction tomography do for you?
Sonja Levanat: Imaging the Hh-Gli signaling network in various tumor types	**Shunsuke Muto** Quantitative element/site-selective microanalysis using high-angular resolution electron channeled x-ray/electron spectroscopy

15:20-15:40 EQUIPMENT PRESENTATION / PARALLEL SESSIONS

LIFE SCIENCE (Lecture hall 1)	MATERIAL SCIENCE (Lecture hall 2)
SCAN / JEOL	**SCAN / JEOL**

15:40-16:00 SELECTED TALKS / PARALLEL SESSIONS

LIFE SCIENCE (Lecture hall 1)	MATERIAL SCIENCE (Lecture hall 2)
Danijela Poljuha: Once upon a time, there were women in microscopy sciences in Croatia	**Ognjen Milat:** Four-dimensional crystallography of Ca.83CuO2 composite crystal; an electron and X-ray diffraction study

16:00-17:30 POSTER SESSIONS / REFRESHMENTS (Lobby)

19:00 ZADAR BY NIGHT TOUR

Tuesday, 28. April 2015

9:00-10:20 **PLENARY LECTURES** (Lecture hall 1)

Jan Faix: Formin-generated actin filaments in the rear of polarized cells are utilized by myosin II to drive motility

Ute Kaiser: Strategies of imaging low-dimensional electron-beam-sensitive objects with low-voltage aberration-corrected TEM

10:20-10:50 COFFEE BREAK

10:50-11:50 **INVITED LECTURES / PARALLEL SESSIONS**

LIFE SCIENCE (Lecture hall 1)	MATERIAL SCIENCE (Lecture hall 2)
Till Bretschneider: Image-based modelling of cellular blebbing	**Manca Logar:** Variation of energy density of states in quantum dot arrays due to interparticle electronic coupling
Alon Kalo: Cellular levels of signaling factors are sensed by β-actin alleles to modulate transcriptional pulse intensity	**Marc Willinger:** In-situ observation of graphene growth dynamics by environmental scanning electron microscopy

11:50-12:30 **SELECTED LECTURES / PARALLEL SESSIONS**

LIFE SCIENCE (Lecture hall 1)	MATERIAL SCIENCE (Lecture hall 2)
Adriana Lepur: Exploring protein-protein interactions of S-adenosyl homocysteine hydrolase (SAHH) using bi-molecular fluorescence complementation (BiFC)	**Tea Zubin Ferri:** Microscopic and micro-spectroscopic techniques for pigment and binder investigation on the „Crucifixion“ of Gianfrancesco da Tolmezzo
Vitalijs Zubkovs: Living cells viability study after 200 kHz laser illumination in a wide-field two-photon microscope	**Nenad Tomašić:** Micro- and nano-features of kaolin aggregates as a result of weathering processes

12:30-13:30 LUNCH BREAK

13:30-19:00 **EXCURSION - NATIONAL PARK KRKA**

20:00 GALA DINNER

Wednesday, 29. April 2015

9:00-10:20 **PLENARY LECTURES** (Lecture hall 1)

Agnes Kittel: Emerging role of extracellular vesicles

Chantal Pichon: E3-14.7K peptide that promotes microtubules mediated transport of plasmid DNA increases polyplexes transfection efficiency

10:20-10:50 COFFEE BREAK

10:50-11:50 **INVITED LECTURES / PARALLEL SESSIONS**

LIFE SCIENCE (Lecture hall 1)	MATERIAL SCIENCE (Lecture hall 2)
Boris Turk: Imaging cathepsins: from cellular processes to in vivo diagnostics	**Boštjan Jančar:** Structural diversity of thermoelectric cobaltates
Marin Barišić: Microtubule detyrosination guides chromosomes during mitosis	**Bella Pecz:** Microscopy of GaN devices beyond the blue LED

11:50-12:30 **SELECTED LECTURES / PARALLEL SESSIONS**

LIFE SCIENCE (Lecture hall 1)	MATERIAL SCIENCE (Lecture hall 2)
Kiyoshi Kobayashi: Near-field optical (SNOM) nanoimaging for glia-synapse correlations and functions	**Ljerka Slokar:** The influence of grain size of waste foundry sands on removal percentage of Copper ions
Srećko Gajović: Multiple imaging modalities to assess the mouse brain after stroke	**Jelena Macan:** Porous yttria-stabilized zirconia for bone implants

12:30 CLOSING

12:50-14:20 LUNCH

Table of content

KEYNOTE LECTURE

High throughput microscopy to study organelle biogenesis and membrane traffic in mammalian cells

Rainer Pepperkok (1)

1) EMBL Meyerhofstr.1, 69117 Heidelberg, Germany

We have developed an organelle knock-out approach in which we remove by laser nano-surgery the entire Golgi complex from living cells and subsequently follow by time-lapse and electron microscopy analysis the “Golgi-less” karyoplast. The data obtained strongly support the hypothesis of a *de novo* Golgi biosynthesis.

In order to identify putative molecules involved in this *de novo* Golgi biogenesis, we have developed and applied functional assays to assess the effect of knock-ins by cDNA over-expression and knock-downs by RNAi, on processes such as constitutive protein transport, Golgi integrity and function of vesicular coat complexes. In order to achieve the throughput that such analyses require we have developed a fully automated high content screening microscopy platform including sample preparation, image acquisition and automated analysis of complex cellular phenotypes. We have applied this technology to genome-wide siRNA screens to identify and characterize comprehensively the genes and their underlying functional networks involved in secretory membrane traffic and Golgi integrity.

PROCEEDINGS OF PLENARY LECTURES

Streptomyces development: imaging from outside in

Paul Dyson (1)

1) Swansea University, Institute of Life Science, College of Medicine, Singleton Park SA2 8PP, Swansea, United Kingdom

Keywords: Streptomyces, development, cell division, microscopy

Streptomyces coelicolor is a model species to understand development in a complex prokaryote. We have used imaging to monitor changes to cell surface properties as the organism goes through its life-cycle. In particular, Atomic Force Microscopy of living cells offers a unique insight into changes in the cell surface during development. Combining genetic approaches with a variety of imaging techniques can provide understanding of complex biological processes. Unlike in other bacteria, cell division genes in *Streptomyces* are not essential. So we have interrogated this biological system to investigate how key cell division proteins function *in vivo*, providing insight into bacterial cell division that *in vitro* assays can overlook. In addition, we have also focused on developmentally regulated Dps proteins that contribute to changes in DNA compaction inside the cells during this life-cycle. We have used imaging to monitor this compaction, changes in gene expression and protein localisation. In addition, DpsA and DpsC can self-assemble into protein nanoparticles. We have used imaging and protein engineering to investigate the functionality of the Dps protein tails in directing and stabilising the assembly process.

References: Del Sol R, Armstrong I, Wright C, Dyson P. Journal of Bacteriology 189 (2007) 2219-25. Mistry BV, Del Sol R, Wright C, Findlay K, Dyson P. Journal of Bacteriology 190 (2008) 5555-66. _x0000_Facey PD, Hitchings MD, Saavedra-Garcia P, Fernandez-Martinez L, Dyson PJ and Del Sol R Molecular Microbiology 73 (2009) 1186–1202

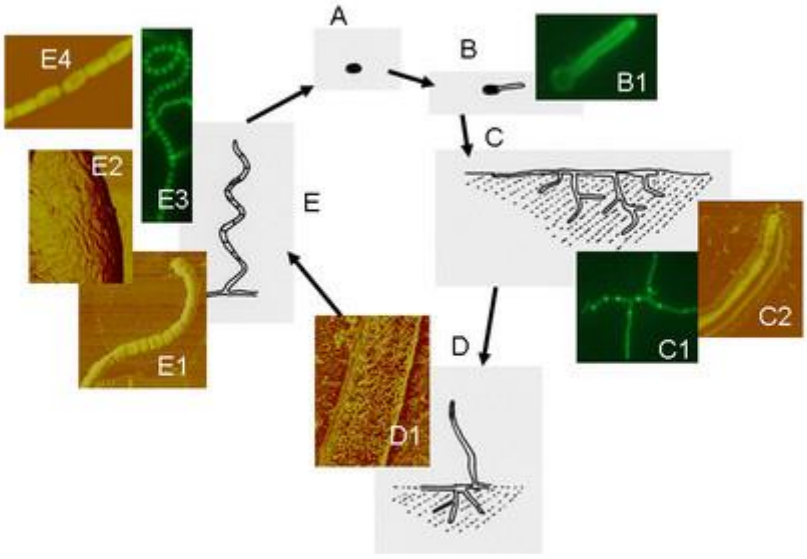

Fig. 1. The life cycle of S. coelicolor. Images were obtained either by fluorescence microscopy of fluo-vancomycin stained hyphae, or by Atomic Force Microscopy. From: P Dyson. Streptomyces. Encyclopedia of Microbiology. (Moselio Schaechter, Editor), pp. 318-332 Elsevier (2009).

Aberration corrected microscopy of functional oxide nanowires at atomic scale

Velimir R. Radmilović (1, 2)

1) Nanotechnology and Functional Materials Center, Faculty of Technology and Metallurgy, University of Belgrade, Karnegijeva 4, 11120 Belgrade, Serbia

2) Serbian Academy of Sciences and Arts, Knez Mihailova 35, 11000, Belgrade, Serbia

Keywords: HAADF, ZnO nanowires, indium diffusion, thermoelectric

Recently we discovered a novel method to produce $M_2O_3(ZnO)_n$ polytypoid nanowires (MZO, where M could be In, Ga, Fe, and other tri-valent metals) by a facile solid state diffusion process and to control their microstructure at atomic level [1,2]. Due to to the decoupling of certain electrical and thermal properties, these polytypoid nanowires, which contain periodic compositional and structural features, typically on the nanometer scale, are promising materials for a variety of applications, including thermoelectrics. The efficiency of energy conversion in thermoelectrics is related to the material-dependent figure of merit, $zT=S2\sigma T/k$, where S, σ, T, and k represent the Seebeck coefficient, electrical conductivity, absolute temperature, and thermal conductivity, respectively. It is predicted theoretically that low dimensional materials can be increase zT [3]. The enhancement can be attributed to two factors: electronic band structure changes (increasing the Seebeck coefficient) and enhanced interface phonon scattering.Using high angle annular dark field (HAADF) scanning transmission electron microscopy (STEM) imaging we performed a detailed structural analysis on the $In_{2-x}Ga_xO_3(ZnO)_n$ nanowires. Fig. 1a is a HAADF image of a IGZO nanowire clearly showing the presence of In-enriched layers (bright lines) perpendicular to the [002] direction. High-resolution (HR)-HAADF image in Fig. 1b shows that the In atoms sit on individual planes and are separated by wurtzite $MZn_nO_{(n+1)}^+$ slabs of varying thickness. The O atoms on the edges of the MO_2^- octahedral layers are each bonded to three In/Ga atoms and one metal atom within the $MZn_nO_{(n+1)}^+$ layer. This creates an inversion domain boundary (IDB) in the wurtzite lattice since the Zn-O bonds on either side of the octahedral layer point with the O atoms toward the In/Ga layer (tail-to-tail configuration). The MO_2^- inclusion layer is also associated with a stacking fault, and the wurtzite lattice on one side of the In/Ga layer is translated by ⅓<100>. In some of the nanowires, partial In/Ga inclusions were observed (Figure 1c). The ends of these partial inclusions are usually associated with edge dislocations with the dislocation line lying at the leading edge of the MO_2^- plane. Moiré images taken along the 002 and 102 reflections clearly show the presence of the edge dislocations. The HAADF imaging allowed us to unambiguously determine the location of indium within the structure and enabled us to evaluate lattice strain and the presence of defects. Based on this analysis we propose that the superlattice structure is generated through a defect-assisted process. One of the greatest advantages of this novel synthesis is the ability to tune the nanoscale features of the polytypoid wires by simply adjusting the amount of metal precursor. Using HAADF imaging we were also able to perform a quantitative analysis of the change in superlattice inclusion density and periodicity with metal deposition. In summary, $M_2O_3(ZnO)_n$ polytypoid nanowires were converted from pure ZnO nanowires using a simple diffusion process that can be used to produce a wide range of ZnO alloys with controllable alloy concentration and inclusion layer density. The single layer inclusion

growth is originated from the surface and propagates though the nanowire by a defect-assisted process. From this study it is apparent that better control of nanometer-scale features could be the key to developing next-generation thermoelectric materials.

References: [1] S.C. Andrews et al., Chemical Science, 2 (2011) 706-714. [2] A.P. Goldstein et al., ACS Nano, 7 (2013)10747-10751. [3] L. D. Hicks and M. S.Dresselhaus, Phys. Rev. B 47 (1993) 16631. TEM has been performed at the National Center for Electron Microscopy, LBNL, Berkeley, supported by the Director, Office of Basic Energy Sciences, Materials Sciences and Engineering Division, of the U.S. Department of Energy under Contract No. DE-AC02-05CH11231, and at FELMI Lab at Technical University in Graz, Austria. VR acknowledges support by the Ministry of Education, Science and Technological Development of the Republic of Serbia, under project No. 172054 and Nanotechnology and Functional Materials Center, funded by the EC FP7 regpot project No. 245916.

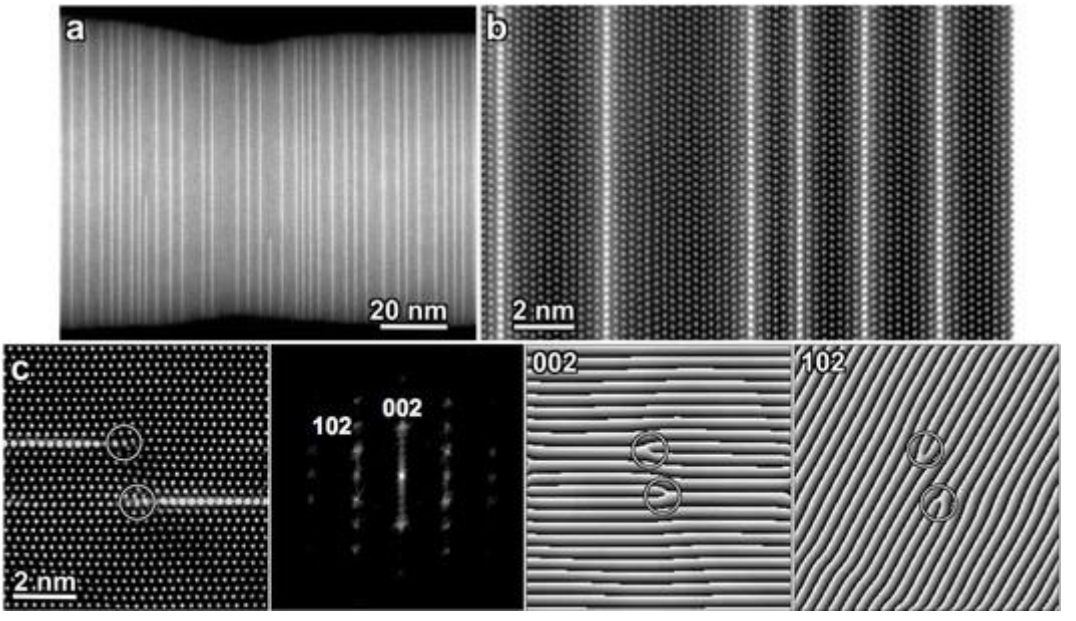

Figure 1. a) STEM image of IGZO nanowire; b) High resolution HAADF image of an IGZO nanowire; c) HR-HAADF image of IGZO oriented on the [010] zone axis with two incomplete MO2- layers and the corresponding FFT; Moiré images taken using the 002 and 102 reflections.

Formin-generated actin filaments in the rear of polarized cells are utilized by myosin II to drive motility

Jan Faix (1)

1) Hannover Medical School, Carl-Neuberg-Str. 1, 30625 Hannover, Germany

Keywords: actomyosin, cell motility, contractility, formin,

Eukaryotic cells can move by distinct modes of action. Fast amoeboid cell migration, as utilized by immune cells or *Dictyostelium* amoebae, is characterized by weak adhesion, formation of actin-rich pseudopods or hydrostatic pressure-driven blebs in their fronts and myosin II driven contractility in the rear. However, it remained poorly understood how the contractile machinery is constituted in the trailing edge to achieve efficient front-back coupling and how this system is localized. Here we identify Diaphanous-related formin A (ForA) from *Dictyostelium discoideum* that nucleates and elongates actin filaments *in vitro*, and show that it acts in concert with IQGAP-related proteins, the anti-parallel actin crosslinker cortexillin (Ctx), and myosin II in the rear to locally increase the mechanical rigidity of the cortical actin meshwork. In repolarizing cells, active ForA invariably relocalized to new prospective ends. Intriguingly, the elimination of ForA markedly increased the speed of randomly migrating cells in unconfined environments that was dependent on myosin II, demonstrating that a more fragile cell cortex can even enhance contractility-assisted cell migration. When compressed under agar, however, ForA-null cells were unable to efficiently migrate, collectively suggesting that myosin II specifically utilizes ForA-generated and Ctx-bundled actin filaments to generate a resilient contractility machinery in the rear. This was further corroborated by imaging of GFP-tagged myosin II in wild-type and forA-null cells in 2D-confined environments, and revealed that in contrast to wild-type cells, the mutant constantly formed blebs in regions with highest myosin II accumulation in the rear. Finally, we show that the localization of ForA abides the established phosphoinositide gradients in polarized cells due to its PI(4,5)P_2-specific C2 domain.

Strategies of imaging low-dimensional electron-beam-sensitive objects with low-voltage aberration-corrected TEM

Ute A. Kaiser (1)

1) Materials Science Electron Microscopy, Ulm University, Albert-Einstein-Allee 11, 89081 Ulm, Germany

Structural and electronic properties of different low-dimensional electron-beam-sensitive crystalline (graphene [1], ion-implanted graphene [2], MoS_2 [3], $MoSe_2$, SiO_2 [4], CN [5], square ice [6] (Fig. 1a), transition-metal clusters [7]) and amorphous (monolayer carbon, SiO2 [8]) objects as well as a new structure of crystalline AuC [9] (Fig. 1b,c) are obtained by analytical low-voltage aberration-corrected transmission electron microscopy following three main strategies: (1) Theory and image processing: For exact calculation of the contrast of dose-limited high-resolution TEM images for low-Z materials at low voltages, image theory and image processing needs to be improved taking into account elastic and inelastic scattering [10-11]. (2) Sample preparation: We demonstrate our method to clean graphene [12]. We show that sandwiching clean radiation-sensitive low-dimensional objects in-between two graphene layers [13] or embedding them into single-walled carbon nanotubes [14] allows to reduce electron-induced damage of the objects. (3) Low-voltage transmission electron microscope: We outline our unique voltage-tunable (20-80kV) spherical and chromatic aberration-corrected TEM and show first results obtained from its prototype [15].

[1] P. Wachsmuth, R.Hambach, G. Benner and U. Kaiser, Plasmon bands in multilayer graphene, PRB 90 (2014) 235434.

[2] O. Lehtinen, I.L. Tsai, R. Jalil, R.R. Nair, J. Keinonen, U. Kaiser, I.V. Grigorieva, Non-invasive transmission electron microscopy of vacancy defects in graphene produced by ion irradiation Nanoscale 6 (2014) 6569.

[3] H.-P. Komsa, S. Kurasch, O. Lehtinen, U. Kaiser and A. V. Krasheninnikov From point to extended defects in two-dimensional MoS2: evolution of the atomic structure under electron irradiation PRB. 88 (2013) 035301.

[4] P. Y. Huang, S. Kurasch, J.S. Alden, A. Shekhawat, A.A. Alemi, P. L. McEuen, J.P. Sethna, U. Kaiser, D. A.Muller Imaging Atomic Rearrangements in 2D Silica Glass: Watching Silica's Dance, Science 342 (2013) 224.

[5] G. Algara-Siller, N. Severin, S. Y. Chong, T. Björkman, R. G. Palgrave, A. Laybourn, M. Antonietti, Y. Z. Khimyak, A. V. Krasheninnikov, J. P. Rabe, U. Kaiser, A. I. Cooper, A. Thomas and M. J. Bojdys Triazine-Based Graphitic Carbon Nitride: a Two-Dimensional Semiconductor Angewandte Chemie 53(29) (2014), 7450.

[6] G. Algara-Siller, O. Lehtinen, F.C. Wang, R. R. Nair, U. Kaiser, H. A. Wu, I. V. Grigorieva, A. K. Geim Nature (2015) accepted.

[7] T. Zoberbier, T. W. Chamberlain, J. Biskupek, N. Kuganathan, E. Bichoutskaia, S. Eyhusen, U. Kaiser, A. N. Khlobystov Interactions and Reactions of Transition Metal Clusters with the Interior of Single-Walled Carbon Nanotubes Imaged at the Atomic Scale J. Am. Chem. Soc. 134(6) (2012) 3073.

[8] P. Y. Huang, S. Kurasch, A. Srivastava, V. Skakalova, J. Kotakoski, A. V. Krasheninnikov, R. Hovden, Q. Mao, J. C. Meyer, J. Smet, D. A. Muller, and U. Kaiser Direct Imaging of a Two-Dimensional Silica Glass on GrapheneNano Lett. 12(2) (2012) 1081.

[9] B. Westenfelder, J. Biskupek, J. C. Meyer, S. Kurasch, X. Lin, F. Scholz, A. Gross, U. Kaiser Bottom-up formation of robust gold carbide, Scientific Reports 5 (2015) 8891.

[10] Z. Lee, H. Rose, R. Hambach, P. Wachsmuth and U. Kaiser The influence of inelastic scattering on EFTEM images - exemplified at 20kV for graphene and silicon Ultramicroscopy 134 (2013) 102.

[11] Z. Lee, H. Rose, O. Lehtinen, J. Biskupek, U. Kaiser Electron dose-dependence of signal-to-noise, atom contrast and resolution in TEM images, Ultramicroscopy 145 (2014) 3.

[12] G. Algara-Siller, O. Lehtinen, A. Turchanin, U. Kaiser Dry cleaning of graphene, APL 104 (2014), 153115.

[13] G. Algara-Siller, S. Kurasch, M. Sedighi, O. Lehtinen and U. Kaiser The pristine atomic structure of MoS2 monolayer protected from electron radiation damage by graphene APL 103 (2013) 203107.

[14] T.W. Chamberlain, J. Biskupek, S.T. Skowron, P.A. Bayliss, E. Bichoutskaia, U. Kaiser, A.N. Khlobystov Isotope substitution extends the lifetime of organic molecules in TEM Small 11 (2014) 622.

[15] U. Kaiser, J. Biskupek, J.C. Meyer, J. Leschner, L. Lechner, H. Rose, M. Stöger-Pollach, A.N. Khlobystov, P. Hartel, H. Müller, M. Haider, S. Eyhusen and G. Benner "Transmission electron microscopy at 20 kV for imaging and spectroscopy" Ultramicroscopy, 111, 8, (2011) 1239.

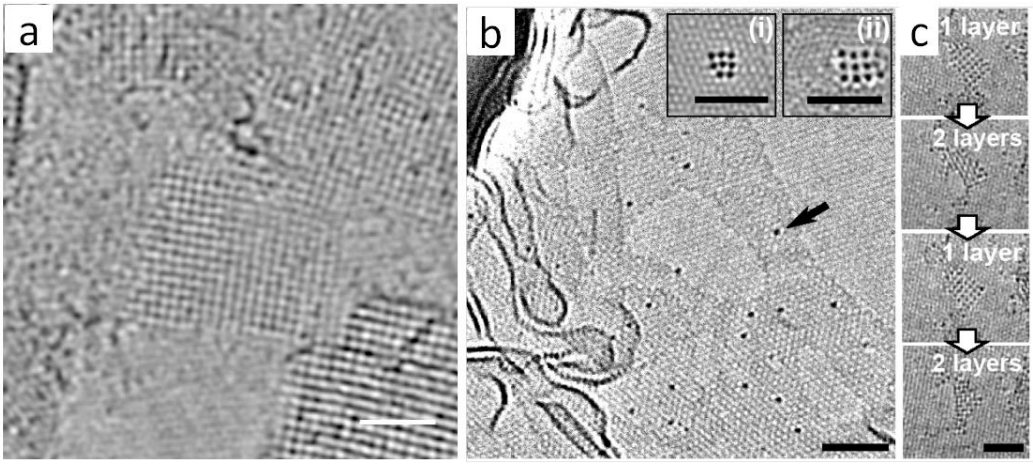

Fig. 1. a) 80 kV HRTEM image of square ice embedded in graphene, (scale bar is 2nm); b) 80kV HRTEM image of graphene at elevated temperature. The arrow marks a mobile Au atom embedded in graphene and the inserts show small Au clusters. (b) HRTEM images of single and double layer of AuC-clusters in a NaCl-crystal structure (scale bars: 1 nm).

Emerging role of extracellular vesicles

Agnes Kittel (1), Xabier Osteikoetxea2 (2), Katalin Szabó-Taylor (2), Andrea Németh (2), Tamás G. Szabó (2), Barbara Sódar (2), Bence György (3), Edit I. Buzás (2)

1) Institute of Experimental Medicine, Hungarian Academy of Sciences, Szigony u. 43. 1083 Budapest,Hungary

2) Department of Genetics, Cell- and Immunobiology, Semmelweis University, Nagyvárad tér 4, 1085 Budapest, Hungary

3) Howard Hughes Medical Institute, Harvard Medical School, 25 Shattuck Street, Boston, Massachusetts 02115, USA

Keywords: microvesicles, exosomes, electron microscopy, therapeutic potential

Release of membrane vesicles is a process conserved in both prokaryotes and eukaryotes. These cell derived extracellular vesicles are submicron structures surrounded by phospholipid bilayer and they represent efficient delivery platforms targeting complex molecular information to professional antigen presenting cells. Compelling evidence supports the significance of this dynamic extracellular vesicular compartment (containing exosomes, microparticles or microvesicles and apoptotic bodies) in a broad range of physiological and pathological processes. These vesicle populations are not only potential biomarkers and possible pathogenic factors in numerous diseases, but they are also considered as emerging therapeutic targets and therapeutic vehicles (1). However, classification of this heterogeneous vesicle population, isolation and detection protocols, and molecular details of vesicular release as well as clearance and biological functions are still under investigation even the nomenclature is still being defined. Our research group has focused on establishing standard methodology of extracellular vesicle purification and characterization. During our work we realized that up till now most published work regarding extracellular vesicles used protein determination or particle enumeration to quantitate extracellular vesicle preparations. As pointed out for the first time by our group (2) protein aggregates share biophysical parameters with extracellular vesicles, and thus, may contaminate extracellular vesicle preparations and falsify experimental results. Furthermore, particle enumeration techniques (such as nanoparticle tracking analysis or tunable resistive pulse sensing) do not distinguish between vesicular and non-vesicular events, and thus, can also often lead to erratic data. In one of our newest studies we combined differential detergent lysis with tunable resistive pulse sensing or flow cytometry and we found that this method may provide a useful simple and fast validation of the vesicular nature of the detected particles. Furthermore, this approach may also provide information about the vesicle subpopulation being studied. Another important step towards improved analysis of extracellular vesicles by enabling a more accurate measurement and providing a novel quality control parameter of them is determining their protein to lipid ratios. This could be a novel parameter which is predictive of the quality of extracellular vesicle preparations (3). However even the most sophisticated combination of different techniques cannot be complete without transmission electron microscopy as the only technique which is able to visualize vesicular and non-vesicular particles in the whole size range of the vesicle population.

References: 1. Géza T Szabó et al., Cell. Mol. Life Sci. (2014) DOI 10.1007/s00018-014-1618-z 2. Bence György et al, Blood (2011) doi:10.1182/blood-2010-09-307595 3. Xabier Osteikoetxea et al., Plos One (2015) in press.

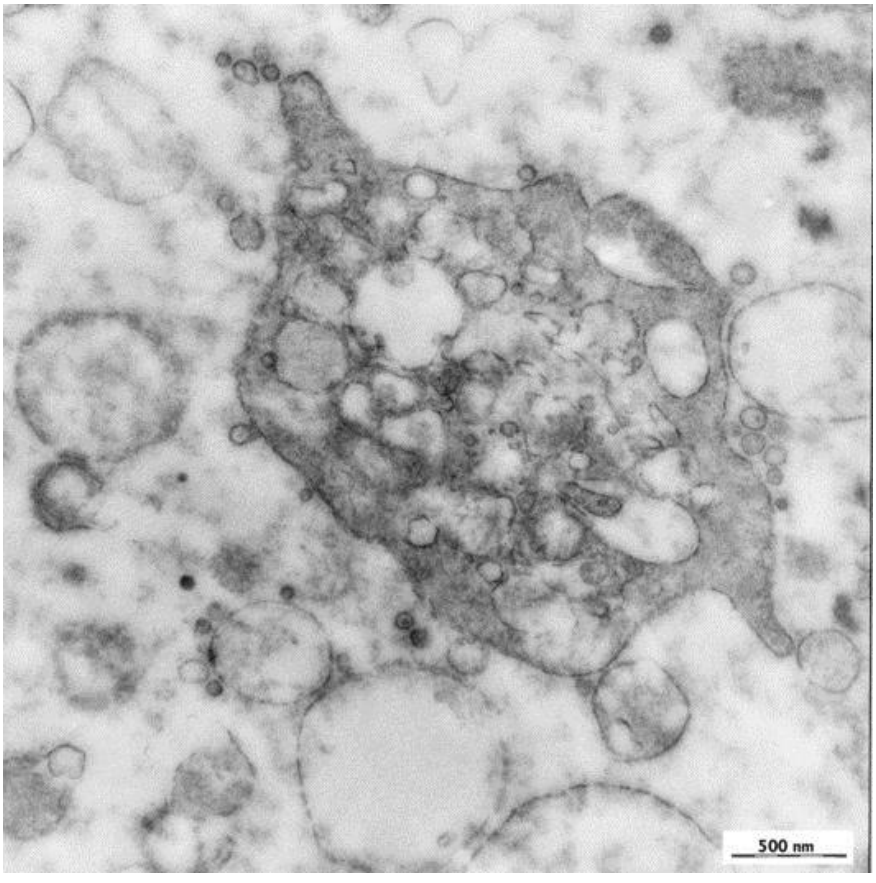

Fig. 1. Different types of vesicles released by human platelet

E3-14.7K peptide that promotes microtubules-mediated transport of plasmid DNA increases polyplexes transfection efficiency

Chantal Pichon (1) and Patrick Midoux (1)

1) Centre de Biophysique Moléculaire, CNRS UPR4301, Inserm and University of Orléans, 45071 Orléans cedex 02, France

Cationic polymers and lipids are promising chemical vectors for gene therapy. However, the limited cytosolic diffusion of plasmid DNA (pDNA) impairs its delivery to the nucleus (Pichon *et al.,* 2010). To improve its intracellular trafficking to the nucleus of the cell, one strategy is to make a pDNA able to interact with cytoskeleton motors, as most viruses do. E3-14.7K early adenoviral protein has been reported to interact with microtubules during adenovirus infection (Li et al., 1998, Lukashok et al. 2000).

We have identified a 20 amino-acids peptide (P79-98) of the E3-14.7K early adenoviral protein interacting with the Dynein light chain TCTEL1 *via* FIP-1 known as RagA. Colocalization experiments and FLIM-FRET experiments were performed to state about the interactions between E3-14.7K, endogenous FIP-1, Dynein light chain TCTEL1 and pDNA. Videomicroscopy and Single Particle Tracking clearly demonstrate that the P79-98/pDNA conjugate exhibits a linear transport with large amplitude along microtubules upon 2h transfection with histidylated polymers whereas pDNA conjugated with a control peptide exhibits short non-directional movements in the cytosol. Remarkably, the link between the pDNA and the peptide is important to improve the transfection efficiency. Optimized condition led to 80% of transfected cells. No improvement was observed with a peptide that interacts directly to dynein. *In vivo* P79-98/pDNA encoding luciferase gene clearly show a 3- to 5-fold transgene expression in skeletal muscles and liver after intramuscular and tail vein hydrodynamic injection in mice, respectively. Comparatively, the transfection efficiency of histidylated liposomes was not improved suggesting that the peptide could be hidden after the multi-lamellar assembly of lipoplexes.

Our results demonstrate for the first time that *in vitro* and *in vivo* non viral gene transfer can be drastically increased when pDNA is conjugated with a FIP-1 interacting sequence allowing its migration on microtubules. This is a real breakthrough in the non viral gene delivery field that opens hope to build artificial viruses.

References

Li, Y. et al.,(1998). *Mol. Cell. Biol.* 18, 1601–1610.

Lukashok, S. A., et al., (2000). *J. Virol.* 74, 4705–4709.

Pichon C. *et al.,* (2010) *Curr Opin Biotechnol.* 21(5):640-645

Pigeon L. *et al.,* (2013) *Small*. 25;9: 3845-3851

PROCEEDINGS OF INVITED TALKS (LIFE SCIENCE)

Imaging chromosome segregation in Streptomyces coelicolor

Graham Falconer (1), (1), Agnieszka Kois-Ostrowska (2), Jolanta Zakrwzeska-Czerwinksa (2), Dagmara Jakimowicz (2), Paul Herron (1)

1) University of Strathclyde, 161 Cathedral Street G4 0RE, Glagsow, United Kingdom

2) University of Wrocław, plac Uniwersytecki 1, 50-137 Wrocław, Poland

Keywords: bacteria, chromosome segregations, time lapse

The reconciliation of mono-directional tip extension with bidirectional chromosome segregation represents a key challenge to organisms that undergo polarized growth such as the filamentous bacterium, *Streptomyces coelicolor*. In order to understand this process, we have developed Fluorescence Reporter Operator Sytem for chromosome segregation in *S. coelicolor*. We used *in vitro* transposon mutagenesis to deliver 120 copies of the *tet* operator (*tetO*) arrayed in tandem to an *oriC*-proximal site within the *S. coelicolor* chromosome. By fusing the cognate repressor protein (TetR) to mCherry and eGFP, we have visualized binding of TetR to the tandem *tetO* array and, as a result, the location of *oriC* during chromosome replication through tip extension, erection of aerial hyphae and sporulation. Using time lapse fluorescence microscopy we have generated a model describing chromosome segregation in this complex filamentous bacterium that permits chromosome colonization of the extending tips as well as apex-distal branches.

Increased uptake by Kupffer cells and reduced liver transduction and toxicity following serotype 5 adenovirus pseudotyping with serotype 3 fiber

N. Raddi (1), F. Vigant (1), C. Bressy (1), J.P. Portela Catani (1), O. Bawa (2), P. Opolon (2), S. Hemmi (3), K. Benihoud (1)

1) Univ Paris-Sud, Laboratoire de Vectorologie et Thérapeutiques Anticancéreuses, UMR 8203, Villejuif, France-94805

2) Unité de pathologie expérimentale de l'IRCIV, Gustave Roussy, 114 rue Edouard Vaillant, Villejuif, France-94805

3) Institute of Molecular Life Sciences, University of Zuerich, Winterthurerstrasse 190, 8057 Zürich, Switzerland

Keywords: Adenovirus, liver, Kupffer, tropism, fiber

The use of adenovirus 5 (Ad5) in gene therapy has been hampered by the strong liver tropism of the virus and associated hepatotoxicity. Mutations of hexon protein ablating Ad interaction with blood coagulation factor X were previously shown to dramatically reduce hepatocyte transduction. Interestingly, pseudotyping Ad5 with a fiber from Ad3 also led to a strong reduction in hepatocyte transduction. We report reduced liver and spleen transduction 2 days after systemic administration of Ad bearing either whole or only the shaft of the Ad3 fiber. Liver transduction by these vectors was further reduced after FX depletion, demonstrating their efficient use of FX for hepatocyte transduction *in vivo*. While both Ad did not show significant difference in initial liver uptake, they were cleared from the liver more rapidly. This phenotype was attributed to an intrinsic property of the Ad3 fiber, since Ad5 pseudotyped with Ad3 fiber as well as Ad3 were strongly taken up by Kupffer cells. Finally, an Ad pseudotyped with Ad3 fiber was shown to efficiently transduce tumors while avoiding hepatocyte transduction after dissemination from tumor site of administration. Taken together, our data demonstrate that the nature of the Ad fiber has a strong impact on *in vivo* Ad behaviour.

Confocal microscopy and DNA repair studies in living cells

Eva Bartova (1)

1) Institute of Biophysics, Academy of Sciences of the Czech Republic, v.v.i.. Královopolská 135 612 65 Brno Czech Republic

Keywords: Confocal microscopy, DNA repair, FRAP, FRET, living cells

The maintenance of genome integrity is fundamental for proper cellular functions. Cells are continuously exposed to genotoxic factors, including UV irradiation or oxidative stress induced by pollutants. Therefore, appropriate DNA repair is more than demanding for genome stability. Genotoxic stress generally leads to induction of DNA lesions that must be repaired in order to avoid deleterious chromosomal translocations. Therefore, in irradiated chromatin of living cells we analyze kinetics and appearance of proteins, involved in DNA repair pathways or proteins recognizing the changes in radiation-caused chromatin conformation. For induction of DNA lesions we are using various sources of radiation, including UVA lasers or gamma-rays. From the view of various types of DNA lesions, by confocal microscopy, we study cell cycle dependent recruitment of selected proteins at radiation-damaged chromatin. We apply local micro-irradiation by 355-nm or 405-nm UVA lasers in order to induce DNA lesions, positive on cyclobutane pyrimidine dimers (CPDs) or phosphorylated histone H2AX (Fig. 1). Our aim is also to study protein-protein or protein-DNA interactions by FRET analysis or protein kinetics by FRAP and bioinformatics approaches. Work was supported by Grant Agency of the Czech Republic, project No.: 13-07822S.

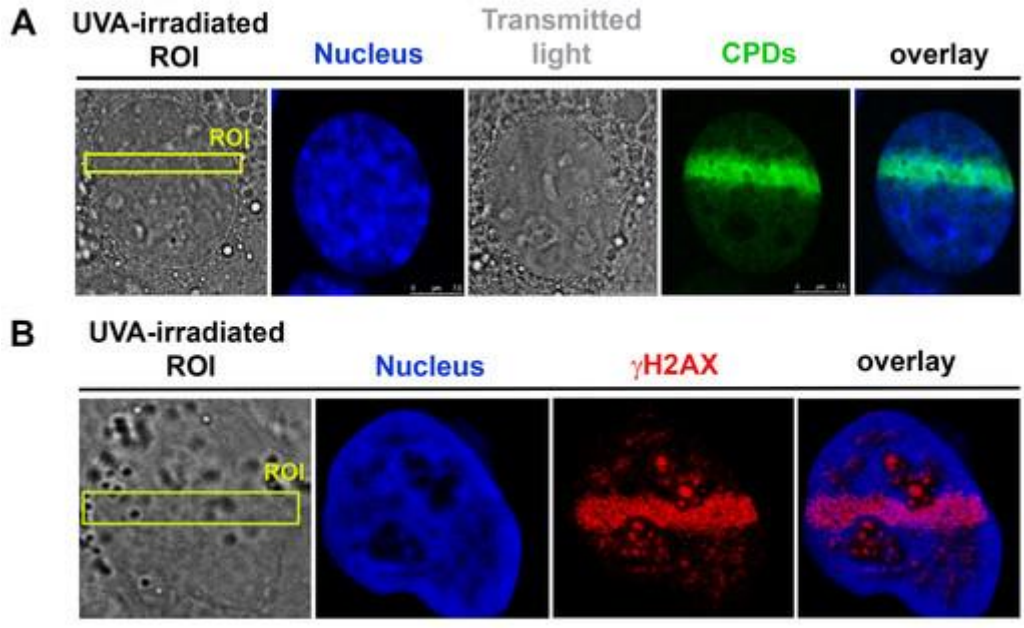

Figure 1. DNA lesions positive on CPDs (A) and gammaH2AX (B). DNA lesions in regions of interest (ROIs) were induced by UVA lasers.

Imaging the Hh-Gli signaling network in various tumor types

Diana Trnski(1), Maja Sabol(1), Petar Ozretić(1), Vesna Musani(1), Lucija Horvat (2), Igor Weber(2), Sonja Levanat(1)

1) Laboratory for Hereditary Cancer, Division of Molecular Medicine, Ruđer Bošković Institute, Bijenička 54, 10000 Zagreb, Croatia

2) Division of Molecular Biology, Ruđer Bošković Institute, Bijenička 54, 10000 Zagreb, Croatia

Keywords: Hh-Gli signaling, confocal microscopy, tumors

In adult organisms, the Hedgehog-Gli pathway contributes to homeostasis and regeneration of certain tissues such as skin and bone, it is active almost exclusively in somatic stem cells, but aberrant activation of the Hh pathway has been linked to tumorigenesis. The pathway activation begins when the ligand Shh binds to its receptor, Patched (Ptch1), resulting in the de-repression of the co-receptor Smoothened (Smo). This triggers a cascade of events in the cytoplasm leading to activation of the transcription factors Gli and transcription of their target genes. The Gli proteins are regulated by the Suppressor of Fused (SuFu), and 3 kinases, including GSK3β, that regulate the processing of Gli proteins. Today it is generally recognized that this pathway is activated in various types of cancer through different mechanisms and it contributes to cancer proliferation, progression and invasiveness. Therefore, this pathway is anticipated to provide a new avenue for cancer therapy.

In our research we used confocal imaging to study the mechanisms of pathway activation in several tumor types. We tracked the changes in localization of pathway components on various levels of the signaling cascade that might indicate pathway modulation. We have observed pathway activation in ovarian dermoids and ovarian carcinomas. We have shown that ovarian dermoid and carcinoma cells respond to pathway activation and inhibition on the upper level of the cascade. On cellular level this can be seen as internalization of the receptor in complex with ligand after pathway activation, and decreasing the localization of the pathway effector Gli1 in the nucleus after pathway inhibition. These results indicate that the Hh-Gli signaling pathway is activated canonically in ovarian tumors (Sabol et al 2012). On the other hand, in breast cancer we observed a cross-talk between Hh-Gli signaling (Shh ligand) and the estrogen receptor, creating a potentially new signaling network (Sabol et al, 2014). Furthermore, in colon cancer cells we observed noncanonical hyperactivation of the pathway caused by the deregulated regulatory kinase GSK3β. Deregulated GSK3β activity leads to overproduction of activator form of Gli3 and to pathway hyperactivation. Inhibition of GSK3β leads to increased co-localization of GSK3β and Gli3 indicating improved regulation of Gli3 processing and results in pathway downregulation (Gojević 2011, Trnski 2015). This suggests a major role for the interplay of GSK3β and Gli3 in the regulation of this pathway in colon cancer (publication in preparation).

The importance of investigating Hh-Gli signaling and its mechanisms of activation is underlined by the estimates that the pathway may be active in one third of all cancers. Better understanding of the modes of Hh-Gli pathway regulation, as well as of interactions of the pathway with other signaling pathways, has an obvious potential for development of better therapies that would be based on combined effects of the Hh-Gli and other pathways inhibitors.

References:

Sabol M, Car D, Musani V, Ozretic P, Oreskovic S, Weber I, Levanat S. The Hedgehog signaling pathway in ovarian teratoma is stimulated by Sonic Hedgehog which induces internalization of Patched. (2012) Int J Oncol. 41: 1411-1418.

Sabol M, Trnski D, Uzarevic Z, Ozretic P, Musani V, Rafaj M, Cindric M, Levanat S (2014) Combination of cyclopamine and tamoxifen promotes survival and migration of MCF-7 breast cancer cells - interaction of Hedgehog-Gli and Estrogen receptor signaling pathways. PLoS One. 9(12):e114510.

Uzarevic Z. (2011) The Hh-Gli signaling pathway activity in estrogen dependent (MCF-7) and estrogen independent (Sk-Br-3) breast cancer cell lines. PhD Thesis University J.J.Strosmayer Osijek, Rudjer Boskovic Institute Zagreb, University of Dubrovnik, University Postgraduate Interdisciplinary Doctoral Study Molecular Biosciences

Gojevic A (2011) Expression of Gli isoforms in sporadic colon cancer. Doctoral Thesis, University of Zagreb

Trnski D (2015) The role of protein kinase GSK3beta in the activation of Hedgehog-Gli signaling in human colon cancer cells. PhD Thesis, J.J.Strosmayer University of Osijek, Rudjer Boskovic Institute Zagreb, University of Dubrovnik, University Postgraduate Interdisciplinary Doctoral Study of Molecular Biosciences

Image-based modelling of cellular blebbing

Richard Tyson (1), Sharon Molyneux (1), Evgeny Zatulovskiy (2), Rob Kay (2), Till Bretschneider (1)

1) Warwick Systems Biology Centre, University of Warwick, Coventry CV4 7AL, United Kingdom

2) MRC Laboratory of Molecular Biology, Francis Crick Avenue, Cambridge Biomedical Campus, Cambridge, United Kingdom

Keywords: cell motility, live-cell fluorescence microscopy, image-based modelling, Dictyostelium, blebbing

Live cell fluorescence microscopy is the method of choice for visualising cellular dynamic processes. A significant bottleneck, however, is extracting quantitative data from time-series image data in order to better understand the complex spatio-temporal regulation of cellular dynamics. For a number of years we have developed software to track cortical fluorescence of proteins involved in cell motility, and correlate their dynamics with that of membrane protrusions and retractions. Recently this has been applied to study blebbing in *Dictyostelium* cells [1]. Blebs form under increased intracellular pressure, mediated by the action of Myosin-II, and occur when the cell membrane rapidly detaches from the actin cell cortex. Blebbing can be efficiently induced by sandwiching migrating cells between a cover slip and an agarose overlay, and are often found in many other cell types moving in 3D environments. It has been a long-standing question how cells could direct blebs to the cell front. Using detailed quantitative analysis of blebs we have identified a so far over-looked mechanism for localising blebs, which is based on inducing negative membrane curvature [2]. In my talk I will present unpublished data showing that a biophysical deformable model of a cell membrane coupled to a static cortex by linkers which break when pulled to hard, can explain a large number of experimentally observed blebs with a sensitivity of more than 70%. Specificity of the minimal model is also greater than 70%. By optimising sensitivity and specificity we can parameterise the intracellular pressure, which is in good agreement with the observed circularity of cells and experimental agarose concentration. Careful studies of situations which lead to true negative blebs in the model help to identify possible mechanisms which prevent blebs to form even when the negative curvature is high. One such case is that of fresh blebs. Although they laterally induce negative curvature, new blebs only form once an actin cortex has been re-established. Work will be presented on how we successively integrate such mechanisms into the model. Our QuimP software for analysing cellular morphodynamics is freely available [3].

References: 1. E. Zatulovskiy et al., J Cell Biol. 204 (2014) 1027-44. 2. R.A. Tyson et al., Proc Natl Acad Sci U S A 111 (2014) 11703-8. 3. http://go.warwick.ac.uk/quimp

Cellular levels of signaling factors are sensed by β-actin alleles to modulate transcriptional pulse intensity

Alon Kalo (1), Itamar Kanter (1), Amit Shraga (1), Jonathatn Sheinberger (1), Hadar Tzemach (1), Noa Kinor (1), Timothee Lionnet (2), Robert H. Singer (3), Yaron Shav-Tal (2)

1) The Mina & Everard Goodman Faculty of Life Sciences & Institute of Nanotechnology, Bar-Ilan University, Ramat Gan 52900, Israel

2) Department of Anatomy and Structural Biology, Albert Einstein College of Medicine, Bronx, NY 10461, USA

3) Howard Hughes Medical Institute, Janelia Farm Research Campus, Ashburn, VA 20147, USA

Keywords: β-actin, SRF, YFP-MS2

Imaging of transcription in living cells using fluorescence microscopy has become an important approach for understanding nuclear gene expression dynamics. The transcriptional response of the β-*actin* gene to extra-cellular stimuli is a paradigm system for transcription factor complex nuclear assembly and regulation. Functional interactions that combine signaling pathways and transcription factors are a mechanism used by cells to govern gene-specific responses to various stimuli. Serum induction leads to a precisely timed pulse of β-actin transcription occurring within minutes of serum addition. We examined how the serum-induction signaling pathway governs the efficacy of the induced transcriptional pulse from several endogenous alleles of β-*actin,* using the MS2-tagging method for following mRNA transcription in single living cells. Our study focused on the nuclear serum response factor (SRF), and the actin protein which regulates the β-*actin* serum response. For instance, we found that lowering SRF levels led to loss of the transcriptional pulse, including a disordered response time, and reduction of activation coordination between the alleles. In contrast, reducing actin protein levels revealed a positive feedback response from the cytoplasm to the nucleus, resulting in stronger allele activation, a prolonged transcriptional response, and increased coordination between the alleles. This study shows that correct amounts of signaling factors are required in order for the cell to achieve a uniform transcriptional pulse from several alleles, otherwise the response is either eliminated or exaggerated. The very rapid timeframes of signal propagation from the cell membrane to the promoter and nucleo-cytoplasmic transport kinetics of mRNAs, as measured in this study, underscore the important timescales of gene expression dynamics revealed from living cell measurements.

References: 1. Yunger, S., Rosenfeld, L., Garini, Y. & Shav-Tal, Y. Nat. Methods 7, 631-633 (2010). 2. Lionnet, T. et al. Nat. Methods 8, 165-170 (2011). This work was supported by the United States- Israel Binational Science Foundation (YST and RHS), the European Research Council (YST), NIH/ NINDS 9R01NS083085-20 (RHS).

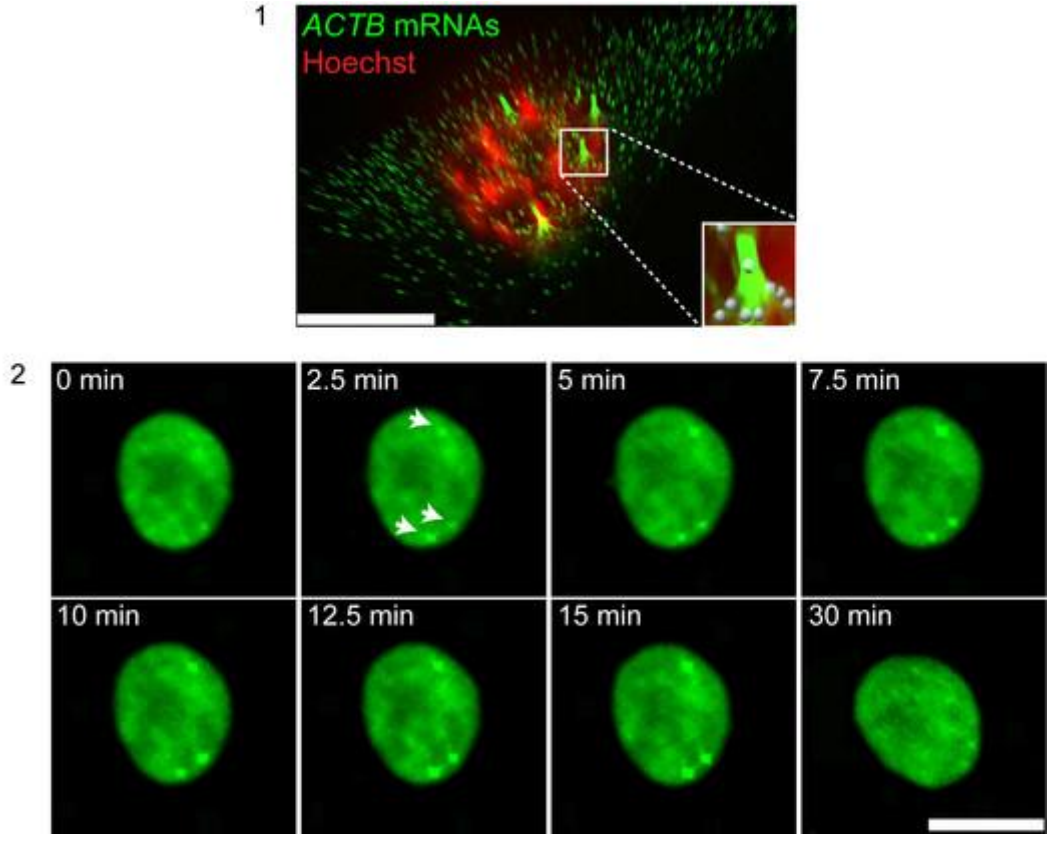

Figure 1. Detection of transcriptionally active endogenous β-actin alleles in MEFs. RNA FISH detects active β-actin-MS2 alleles (strong green dots) and single mRNAs (green dots) in MEFs. Boxed region shows a transcription site (green) and mRNAs (white dots), using Imaris software. DNA is marked in red (Hoechst staining pseudocolored red) Bar 5μm. Figure 2. Transcriptional activity of single alleles in real-time during signal transduction. Frames from live cell imaging showing transcriptional activity of β-actin alleles (arrows) during serum induction (following overnight starvation, time 0). Bar=10μm.

Imaging cathepsins: from cellular processes to *in vivo* diagnostics

Boris Turk (1,2,3)

1) Jozef Stefan Institute, Department of Biochemistry and Molecular Biology, Jamova 39, 1000 Ljubljana, Slovenia

2) Center of Excellence CIPKEBIP, Jamova 39, 1000 Ljubljana, Slovenia

3) Faculty of Chemistry and Chemical Technology, University of Ljubljana, Askerceva cesta 5, 1000 Ljubljana, Slovenia

Cysteine cathepsins are a group of proteases that are normally confined to the acidic vesicles, collectively known as late endocytic compartments. They are normally involved in numerous processes, including in intracellular protein turnover and MHC II- mediated immune response, where they play critical roles. However, they are widely up-regulated in several pathological conditions associated with inflammation, such as cancer, atherosclerosis, rheumatoid arthritis and osteoarthritis. In these inflammatory environments they are secreted to the membrane or into the extracellular milieu by immune cells as well as tumour cells, vascular smooth muscle cells, endothelial cells, synovial fibroblasts and chondrocytes. Cathepsins also have a causal role in these diseases, as they are associated with processing of structural proteins, growth factors and chemokines, thereby promoting cell invasiveness and angiogenesis. Therefore monitoring cathepsin activity *in vivo* has a high diagnostic potential, and can additionally serve as a powerful tool in preclinical research. Development of tools that would allow for selective monitoring of cathepsin activities in cells and *in vivo* goes in several directions, the two main being suicide substrates, known as activity-based probes, and turnover probes. Both have advantages and disadvantages and these will be further discussed.

Microtubule detyrosination guides chromosomes during mitosis

Marin Barisic (1), Ricardo Silva e Sousa (2), Suvranta K. Tripathy (2), Maria M. Magiera (3), Anatoly Zaytsev (2), Carsten Janke (3), Ekaterina L. Grishchuk (2), Helder Maiato (1)

1) Institute for Molecular and Cell Biology, University of Porto, Rua do Campo Alegre, 823, 4150-180 Porto, Portugal

2) Perelman School of Medicine, University of Pennsylvania, 415 Curie Blvd, Philadelphia, PA 19104, USA

3) Institut Curie : 26 rue d'Ulm - 75248 Paris Cedex 05 - France, Centre de protonthérapie (Orsay)

Keywords: Chromosome congression, Tubulin code, Microtubule detyrosination, Kinetochores, CENP-E

Before chromosomes segregate into daughter cells they align at the spindle equator to form a metaphase plate, a process known as chromosome congression. CENP-E/Kinesin-7 is a microtubule plus-end-directed kinetochore motor required for congression of pole-proximal chromosomes in human cells. Because the plus-ends of many spindle microtubules point to the cell cortex, a critical unanswered question is how chromosomes are specifically guided towards the equator. Here we show that chromosome congression depends on post-translational detyrosination of spindle microtubules that point to the equator. CENP-E binds preferentially detyrosinated microtubules in vivo, and CENP-E-dependent transport is strongly enhanced on detyrosinated microtubules reconstituted in vitro from purified components. Blocking tubulin tyrosination in cells causes chromosomes to move away from spindle poles in random directions. Thus, CENP-E-driven chromosome congression is guided by microtubule detyrosination. Our work reveals a critical role for the “tubulin code” as a navigation system for kinetochore-based chromosome motility during mitosis.

PROCEEDING OF INVITED TALKS (MATERIAL SCIENCE)

High-resolution STEM Investigations of SrO-doped Sr(Ti,Nb)O3 and In2O3-doped ZnO oxide thermoelectrics

M. Čeh (1), M. Jerič (1), M. Košir (1), S. Bernik (1), S. Šturm (1), C. Ow-Yang (2), M. A. Gülgün (2)

1) Department for Nanostructured Materials, Jožef Stefan Institute, Jamova 39, 1000 Ljubljana, Slovenia

2) Materials Science and Nanoengineering, Sabanci University, Orhanli - Tuzla, 34956 Istanbul, Turkey

Keywords: Thermoelectrics, HR STEM, HAADF imaging, ABF imaging, EDXS

SrO-doped $Sr(Ti,Nb)O_3$ and In_2O_3-doped ZnO oxide thermoelectrics were investigated by HR-STEM imaging (HAADF, ABF) and EDXS in order to study the chemistry of observed planar faults in these materials, i.e. Ruddlesden-Popper-type (RP) faults[1] in SrO-doped $Sr(Ti,Nb)O_3$ and characteristic inversion domain boundaries (IDB) in In_2O_3-doped ZnO[2]. All results were obtained in a Jeol ARM-200F with a CFEG and Cs probe corrector. HAADF imaging was performed at angles from 70 to 175 mrad, while ABF imaging from 11 to 23 mrad. EDXS spectra were acquired using JEOL Centurio Dry SD100GV SDD Detector. RP planar faults in SrO-doped $Sr(Ti,Nb)O_3$, as viewed along [001] zone axis, are shown in HR STEM micrograph in figure 1a. The commonly observed number of perovskite unit cells between the planar faults is >2, which corresponds to various homologous compounds with the formula $Sr_{n+1}(Ti,Nb)_nO_{3n+1}$. While the measured intensities of individual Sr atomic columns along a single fault do not scatter significantly, the (Ti,Nb)O atom columns exhibit quite large differences in measured intensities, thus indicating significant variation in Nb and Ti content within a single mixed atom column (Fig. 1b). Semi-quantitative analysis of measured HAADF intensities showed that the content of Nb on B sites in perovskite solid solution varies from 5 to 35 at%. The comparison between simultaneously acquired HAADF and ABF images of a single RP fault is shown in figure 1c. While pure oxygen atomic columns cannot be resolved in the HAADF image, they can be readily observed using ABF imaging (Fig. 1d). The positions of oxygen atom columns along the planar faults are in full agreement with the structural model of a RP planar fault. In In_2O_3-doped ZnO ceramics, pure indium monolayers are readily observed by HAADF (Fig. 2a). These basal inversion domain boundaries (IDB's) are parallel to the {0001} ZnO lattice planes and separate domains with different orientation (head-to-head; tail-to-tail). Basal IDB's (b-IDB) are much more clearly resolved by HAADF as opposed to pyramidal IDB's (p-IDB) (Fig 2b). However, by decreasing the inner angle of the ADF detector, the pyramidal IDB's become much more visible, most likely due to an increased contribution of diffraction contrast and/or strain to the image. Indium presence at either b-IDB's and/or p-IDB's can be readily confirmed by the EDXS (Fig. 2c,d).

References: 1. S. Šturm et al., J. Mater. Res. 24(8) (2009) 2596-2604. 2. H. Schmidt et al., Micron 11 (2012) 49-56. 3. The authors acknowledge financial support from the Scientific and Technological Research Council of Turkey (TÜBITAK) under Fellows Program and from EU under Seventh Framework Programme under grant agreement n°312483 (ESTEEM2).

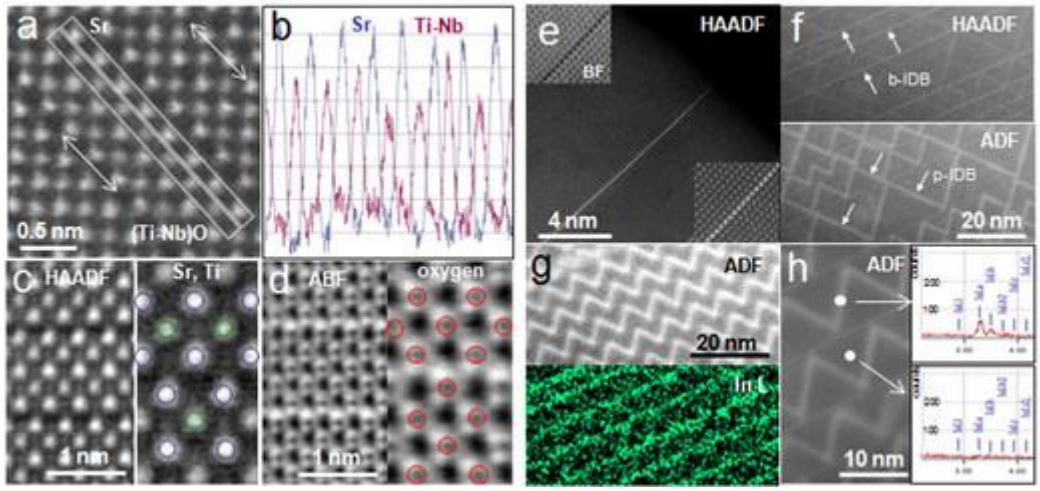

Figure 1. (a) HR HAADF STEM of RP faults in SrO-doped Sr(Ti,Nb)O3 with (b) corresponding intensity profiles. (c) HAADF. (d) ABF. (e) HR HAADF STEM of b-IDB in In2O3-doped ZnO. (f) HAADF and ADF. (g) EDXS mapping. (h) EDXS from ZnO and p-IDB.

Direct correlation between optical properties at sub-nanometer scale and structure at atomic scale, in-situ performance in a STEM

Jordi Arbiol (1,2,3)

1) Institució Catalana de Recerca i Estudis Avançats (ICREA), 08010 Barcelona, Catalonia, Spain

2) Institut Català de Nanociència i Nanotecnologia (ICN2), Campus UAB, 08193 Bellaterra, Catalonia, Spain

3) CELLS-ALBA Synchrotron Light Facility, Campus UAB, 08193 Bellaterra, Catalonia, Spain

Keywords: scanning transmission electron microscopy, chathodoluminescense, nanomaterials, quantum structures

Technology at the nanoscale has become one of the main challenges in science as new physical effects appear and can be modulated at will. Superconductors, materials for spintronics, electronics, optoelectronics, chemical sensing, and new generations of functionalized materials are taking advantage of the low dimensionality, improving their properties and opening a new range of applications. As developments in materials science are pushing to the size limits of physics and chemistry, there is a critical need for understanding the origin of these unique physical properties (optical and electronic) and relate them to the changes originated at the atomic scale, e.g.: linked to changes in (electronic) structure of the material.

During the seminar, I will show how combining advanced electron microscopy imaging with electron spectroscopy, as well as cathodoluminescence in an aberration corrected STEM and ex-situ photoluminescence (PL) will allow us to probe the elemental composition and electronic structure simultaneously with the optical properties in unprecedented spatial detail.

The seminar will focus on several examples in advanced nanomaterials for optical and plasmonic applications. In this way the latest results obtained by my group on direct correlation between optical properties at sub-nanometer scale and structure at atomic scale will be presented. The examples will cover a wide range of nanomaterials: quantum structures self-assembled in a nanowire: quantum wells (2D),[1] quantum wires (1D) [2] and quantum dots (0D) [3] for optical applications (LEDs, lasers, quantum computing, single photon emitters) [3]; as well as metal multiwall nanoboxes and nanoframes for 3D plasmonics.

References: [1] A. Fontcuberta i Morral et al., Small 4 (2008) 899 [2] J. Arbiol et al., Nanoscale, 4 (2012) 7517 [3] M. Heiss et al., Nature Materials, 12 (2013) 439

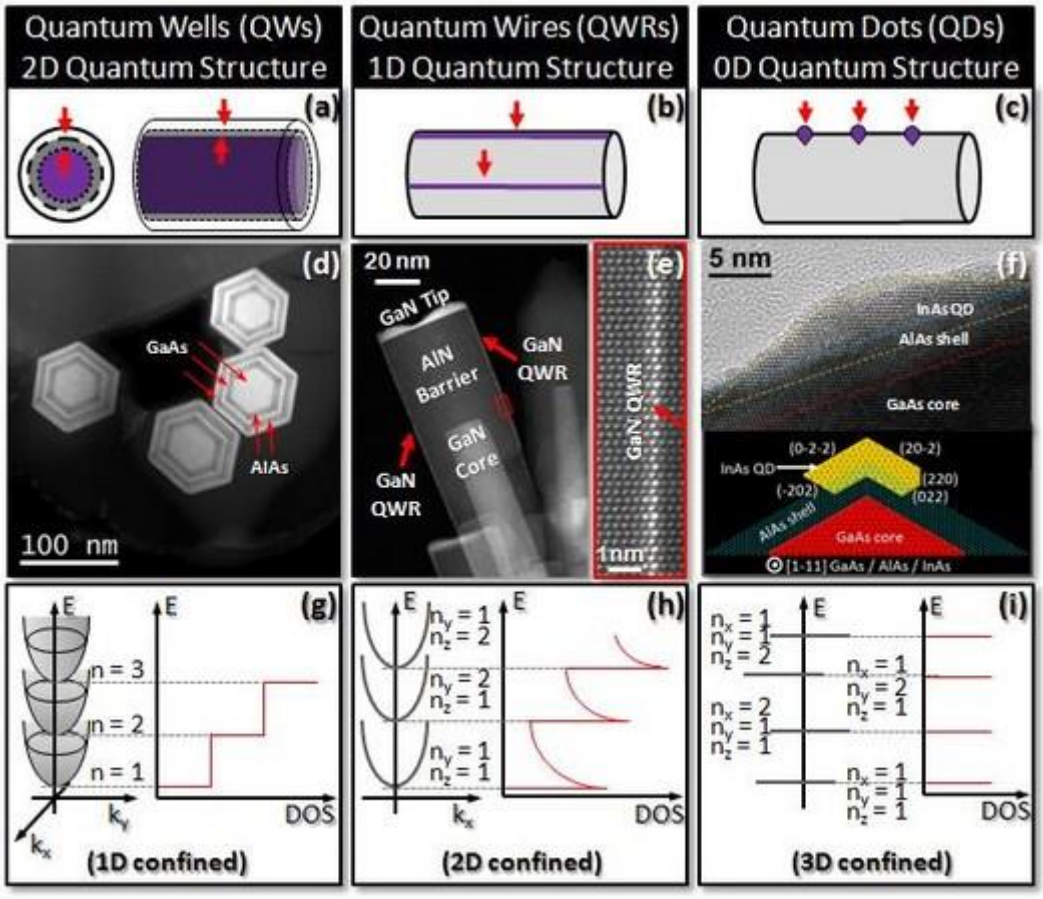

Figure 1. Sketches of different quantum structures classified by their dimensionality: (a) Quantum Wells or 2D structures (QWs); (b) Quantum Wires or 1D structures (QWRs); (c) Quantum Dots or 0D structures (QDs). (d-f) Experimental STEM and HRTEM images of the quantum structures, QWs, QWRs and QDs, respectively

What can electron diffraction tomography do for you?

M. Klementová (1), N. Němec (1), V. Gärtnerová (1), C. A. Corrêa (1), L. Palatinus (1)

1) Institute of Physics of the AS CR, v.v.i., Na Slovance 2, 182 21 Prague 8, Czech Republic

Keywords: diffraction tomography, phase identification, orientation relationship, structure solution and refinement

Electron diffraction tomography (EDT) provides 3D information about the reciprocal space of studied material. It was originally developed for data collection with the aim of structure solution as an analogue of rotation method used in x-ray crystallography. However, the 3D information on reciprocal space can be used in many ways, from simple phase identification to determination of orientation relationship between precipitate and matrix to more complex tasks such as structure solution and refinement. The EDT experiment is quite simple. Starting with a random crystal orientation, the crystal is sequentially tilted in a range (usually 90-120deg), and a diffraction pattern is recorded at every tilt step (usually 1deg). It can be done manually or automatically, possibly with limited input needed from the user to check the sample position during tilting. Sampling of the reciprocal space obtained by EDT is much finer than collecting oriented zone-axis patterns, but one degree step is still quite coarse. If the Bragg condition for a reflection falls between the steps, its intensity may be severely underestimated. This undersampling problem can be solved in two different ways: by precession EDT (PEDT) [1] and rotation EDT (REDT) [2]. The complete 3D diffraction information (even with the missing wedge) allows for measuring all lattice parameters, which together with chemical information obtained by EDS analysis leads to much easier phase identification compared to using oriented diffraction patterns. When more phases are present, their orientation relationship can be determined from the EDT data once the lattice parameters of individual phases are found. Orientation of the basis vectors of the reciprocal lattice with respect to the orthogonal system of the microscope is given by orientation matrix. Therefore, from two orientation matrices the orientation relationship between two crystals can be calculated. As an example, orientation of $MgZn_2$ precipitate in Mg matrix is shown in Fig. 1b. Structure determination and refinement from EDT data has made an enormous progress over the past few years. At present, complex structures with hundreds of atoms in the unit cell can be solved. As an example, structure of $MgZn_2$ precipitate is shown in Fig. 1c,d. The initial model for the refinement is typically optimized using the kinematical approximation for the calculation of model diffracted intensities. This approximation is quite inaccurate for electron diffraction and leads to high figures of merit and inaccurate results with unrealistically low standard uncertainties. The obvious remedy to the problem is the use of dynamical diffraction theory to calculate the model intensities in structure refinement. This technique can be used not only on oriented zone-axis patterns [3] but also on non-oriented patterns acquired by PEDT.

References: 1. Enrico Mugnaioli et al., Ultramicroscopy 109 (2009) 758-765. 2. Daliang Zhang et al., Z. Kristallogr. 225 (2010) 94-102. 3. Lukas Palatinus et al., Acta Cryst. A69 (2013) 171–188.

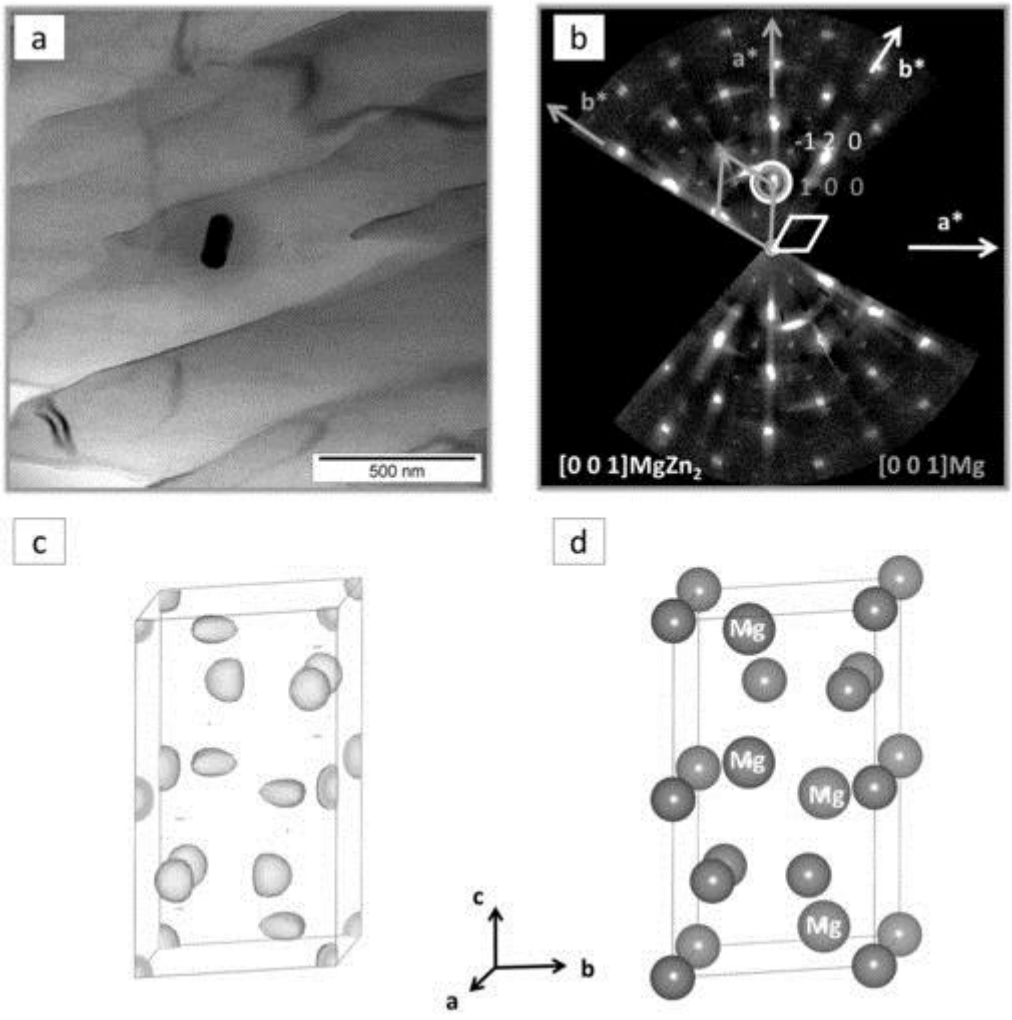

Figure 1. MgZn2 precipitate in Mg-matrix. (a) BF image, (b) section through the experimental 3D reciprocal map showing orientation relationship, (c,d) results of structure solution (c) map of electrostatic potential (d) structural model.

Quantitative element/site-selective microanalysis using high-angular resolution electron channeled x-ray/electron spectroscopy

Shun Muto (1), Kazu Tatsumi (1), Masahiro Ohtsuka (2)

1) EcoTopia Science Institute, Nagoya University, Nagoya 464-8603, Japan

2) Graduate Scool of Engineering, Nagoya University, Nagoya 464-8603, Japan

Keywords: scanning transmission electron microscopy, electron energy-loss spectroscopy, energy-dispersive x-ray spectroscopy, beam-rocking, electron channeling

The current state-of-the-art scanning transmission electron microscope (STEM) equipped with aberration correctors allows us handy for atomic scale imaging and elemental/electronic structural analysis, due to its high-brightness electron source and highly focused subatomic probe size available. The technique inevitably leads to a drawback associated with a high density of focused electron probe and its small illuminating area (i.e., a small number of sampling points), so that the probe can drill the sample or otherwise the obtained data may contain high level noise accordingly. We have hence been engaged in an alternative microanalysis method, instead of exploiting the atomic resolution in real space, using inelastic scattering by channeled electrons in a crystal. The method takes advantage of the high angular resolution intrinsic to TEM, and we have developed an 'integrated electron spectroscopic STEM', where electron energy-loss spectroscopy (EELS), energy/wavelength dispersive x-ray spectroscopy (E/WDXS) and cathodoluminescence (CL) are implemented in a single STEM.

The concept of the present element/site selective microanalysis is schematically shown in Fig. 1, where the incident electron beam is rocked about a pivot point on a sample, acquiring the spectroscopic data as functions of the diffraction condition (and the momentum transfer vector in EELS) with respect to the incident beam direction. The sample orientation and diffraction condition is monitored by the beam rocking pattern recorded by the ADF detector. The present method is an extension of high-angular resolution electron channeled X-ray (electron) spectroscopy (HARECX(E)S) [1,2], thereby exploiting element/site selective chemical information of the material associated with the different electron densities propagating along the specific atomic planes/columns by varying Bloch wave symmetry excited in the crystalline sample even from nanoscale areas. The acquired datasets of fluorescent x-ray intensities, core-loss spectra and light intensities bear information on the local spatial/electronic structures around the excited elements of interest, which can be quantitatively analyzed by comparing with theoretical simulations, based on the dynamical elastic/inelastic electron diffraction theories [3].

We have analyzed rare earth dopants in a metal oxides for a novel red light-emitting material (Eu/Y co-doped Ca_2SnO_4) as one of the representative applications of the present method: the occupation sites of Eu and Y were quantitatively determined by EDXS, the valence states of the rare earths by EELS. Another application is to elucidate the site occupancies of a trace element in M-type strontium ferrite, where doped Co occupies 5-different Fe sites to improve the cohesive force of the material.

References: 1. K. Tatsumi, S. Muto and J. Rusz, Microsc. Microanal. 19 (2013) 1586-1594. 2. K Tatsumi and S. Muto, J. Phys.: Condens. Matter 21 (2008) 104213. 3. J. Rusz, S. Muto and K. Tatsumi, Ultramicrosc. 125 (2013) 81-88.

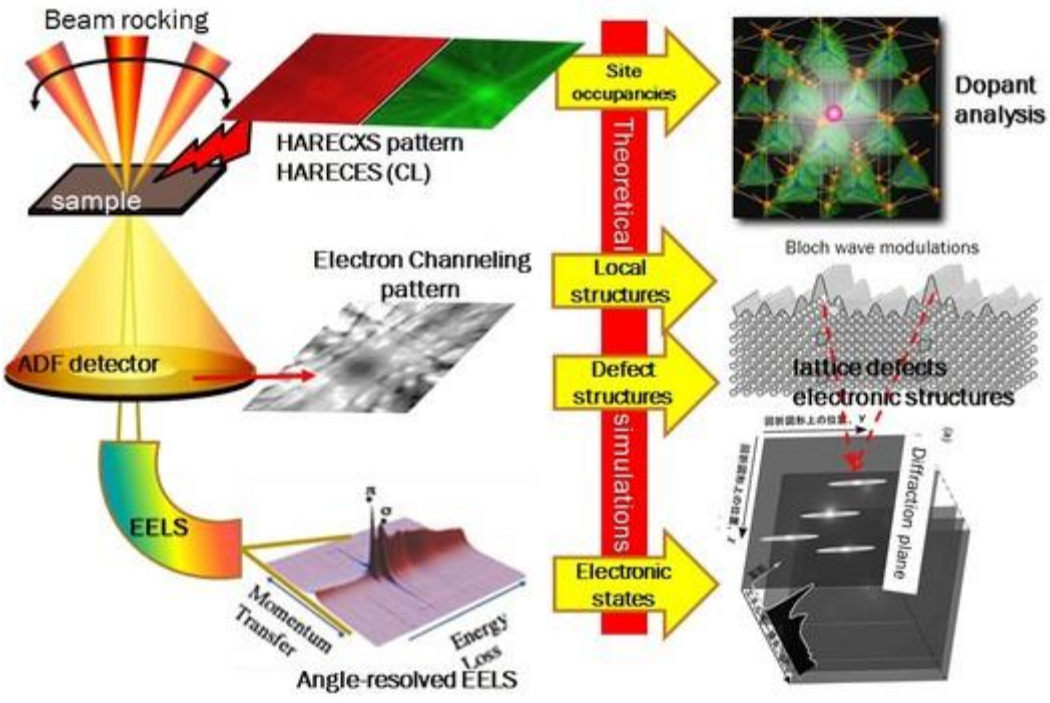

Figure 1. Schematic diagram of element/site selective microanalysis using integrated spectroscopic STEM.

Variation of energy density of states in quantum dot arrays due to interparticle electronic coupling

Manca Logar (1)

1) Laboratory for chemistry of materials, National Institute of Chemistry Slovenia, Hajdrihova 19, 1000 Ljubljana, Slovenia

Keywords: Energy density of states; STEM-EELS; electronic coupling; quantum dot; superlattice

Ordered arrays of colloidal quantum dots (superlattices) exhibiting collective optical and electrical phenomena have gained considerable interest among the scientific community, with promising applications in photovoltaics, optoelectronics, information technology, and catalysis. Mediated by capping ligands, the quantum dots (QDs) can be treated as artificial atoms and assembled into higher order nanostructures such as metamaterials and supraparticles. These structures have programmable physical and chemical properties, widening the array of available functional materials for relevant applications.Gaining in-depth insight into the electronic coupling phenomena among the QD arrays is of great importance for the precise engineering of superstructures. Most work in the area is presently focused on the effect of different capping ligands on electron energies. On a macroscopic level, the effect is seen as a red shift of the optical absorption peak as the interparticle distance decreases in thin films of monodisperse QDs.[1] However, such red shifting can be caused by changes in the dielectric environment in addition to changes in electronic coupling between the dots.[2] It is difficult to isolate these factors when examining the macroscopic optical transition energies of the arrays, especially considering the inhomogeneity in the dielectric environment introduced by the inevitable size and shape variation of the QDs in the sample. On the microscopic level, scanning tunneling microscopy and spectroscopy (STM-STS) have been used to investigate the electronic local density of states (LDOS) of single nanoparticlesand their superlattice films. Band gap reduction was verified by comparing the density of states in isolated and arrayed QDs. We present localized measurements of the electronic energy structure of lead sulfide (PbS) QD pairs, as well as spatial variation in the lowest available electron transition energy (LATE) in a set of monodisperse QD superlattices capped with different size ligands. Sub-nanometer resolved local electron energy structure was measured in PbS quantum dot superlattice arraysby using electron energy-loss spectroscopy in a (scanning) transmission electron microscope [(S)TEM-EELS].[3] The spatial resolution of this technique allows independent measurement of the joint local density of states (JLDOS) inside of and between individual QDs. We found an increased density of electronic states in the space between quantum dots with shorter interparticle spacing, indicating extension of quantum dot wavefunctions as result of interparticle electronic coupling. In addition to reproducing previously observed changes in the macroscopic band gap of the lattices, our results reveal changes in the local electronic structure in between QDs as their spacing is diminished, providing direct experimental observation of electronic coupling of the dots.

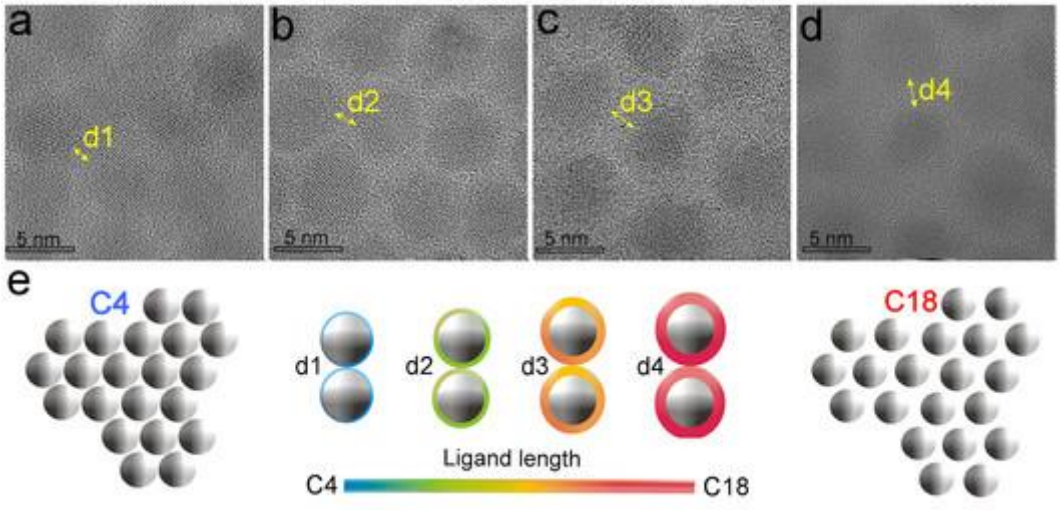

Figure 1. HRTEM images of of PbS quantum dot arrays capped by (a) butylamine (C4), (b) octylamine (C8), (c) dodecylamine (C12), and (d) oleic acid (C18). (e) Schematic showing variation in spacing of QDs as a function of ligand length. Average values of d1, d2, d3, and d4 are 0.6 nm, 1.0 nm, 1.5 nm, and 2.0 nm. Figure 2. Variations in the lowest available electron transition energy (LATE) across neighboring PbS QDs with different interparticle spacings. LATE line profiles across QDs capped by (a) butylamine, (b) octylamine, (c) dodecylamine, and (d) oleic acid. Figure 3. 2D maps of integrated EELS signal intensity over the energy range 0.9-2 eV and EELS spectra taken at the locations of the white dots over PbS QDs capped by (a) butylamine, (b) octylamine, (c) dodecylamine, and (d) oleic acid.

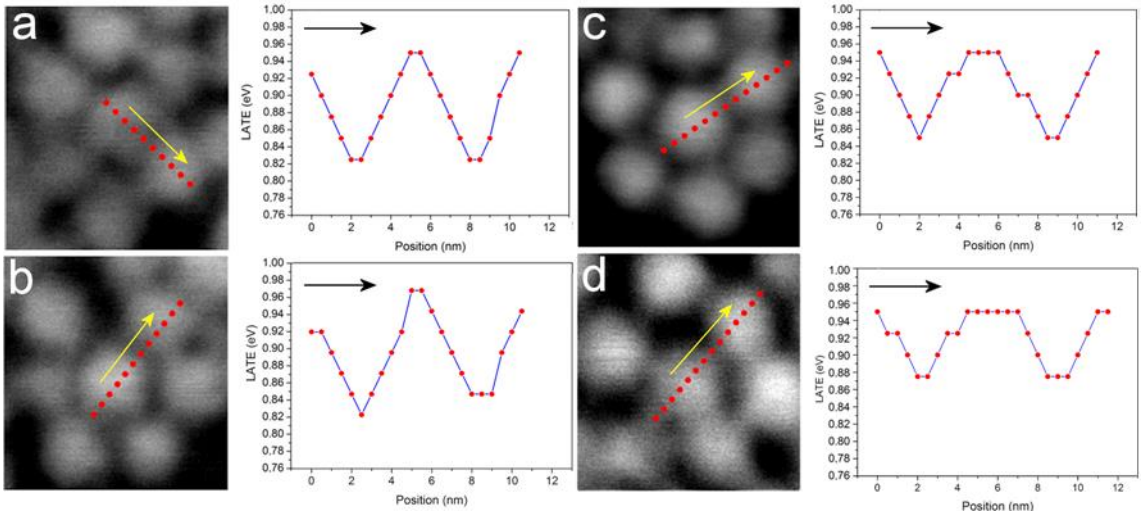

Figure 2. Variations in the lowest available electron transition energy (LATE) across neighboring PbS QDs with different interparticle spacings. LATE line profiles across QDs capped by (a) butylamine, (b) octylamine, (c) dodecylamine, and (d) oleic acid.

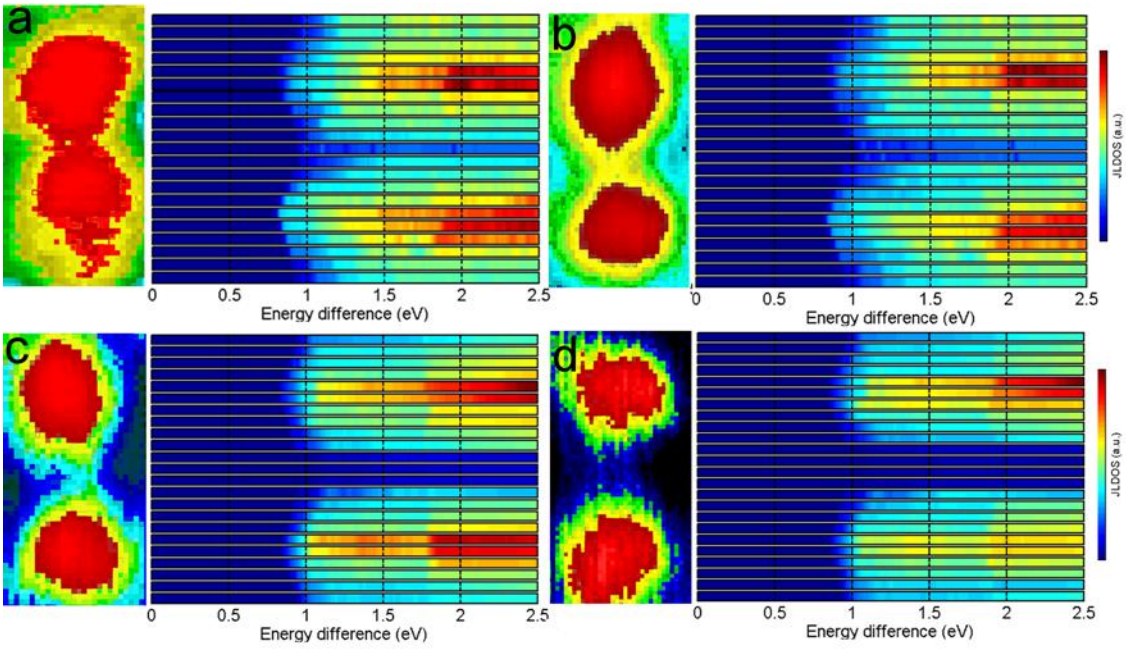

Figure 3. 2D maps of integrated EELS signal intensity over the energy range 0.9-2 eV and EELS spectra taken at the locations of the white dots over PbS QDs capped by (a) butylamine, (b) octylamine, (c) dodecylamine, and (d) oleic acid.

References: 1 Mikhail Artemyevet al., Phys. Rev. B 60 (1999) 1504–1506. 2 Abraham Wolcott et al. J. Phys. Chem. Lett. 2 (2011) 795–800. 3 Hee Joon Jung et al. Nano Lett. 13 (2013) 716–21.

In-situ observation of graphene growth dynamics by environmental scanning electron microscopy

Marc Georg Willigner (1), Zhu-Jun Wang (1), Gisela Weinberg (1), Robert Schlögl (1)

1) Fritz-Haber-Institut der Max-Planck-Gesellschaft, Faradayweg 4-6, 14195 Berlin Germany

Keywords: In-situ SEM, catalyst dynamics, graphene growth

As opposed to conventional electron microscopy, where materials are mostly studied in vacuum and close to ambient temperature, *in*-situ electron microscopy enables the investigation of materials under an external physical (mostly mechanical, electrical, or optical) or chemical stimulus. Especially in the field of heterogeneous catalysis, observations of dynamic processes that are induced by the chemical potential of a gas phase are a key for a mechanistic understanding.

In recent years, the potential of *in-situ* transmission electron microscopy has widely been recognized. Commercially available instruments as well as dedicated *in-situ* sample holders have further contributed to an increased availability of the technique and its growing popularity.

In my presentation I will demonstrate the potential of *in-situ* scanning electron microscopy. Although that instrument does not provide comparable resolution, it has quite a potential for the study of dynamics that are either too fast for the temporal resolution of most TEMs or for observations at a length scale and lateral resolution that is similar to that obtainable with other techniques such as *in-situ* XPS, Raman or XRD.

Using a modified environmental scanning electron microscope (ESEM) we have studied the metal catalyzed chemical vapor deposition (CVD) growth of graphene under relevant low-pressure CVD conditions. It will be shown that *in-situ* SEM allows visualizing structural dynamics of the active catalyst at temperatures of 1000°C while simultaneously the formation and growth of atomically thin single layer graphene can be studied in an unparalleled way. The experiments inside the chamber of the ESEM enable the observation of a complete CVD process from substrate annealing through graphene nucleation and growth and, finally, substrate cooling in real time and nanometer-scale resolution without the need of sample transfer. A strong dependence of surface dynamics such as sublimation and surface pre-melting on grain orientation is demonstrated, and the influence of substrate dynamics on graphene nucleation and growth is presented. Insights on the growth mechanism are provided by a simultaneous observation of the growth front propagation and nucleation rate. Furthermore, the role of trace amounts of oxygen during growth is discussed and related to graphene induced surface reconstructions during cooling.

References: Z.J. Wang et al., ACS Nano 2015, in print (DOI: 10.1021/nn5059826)

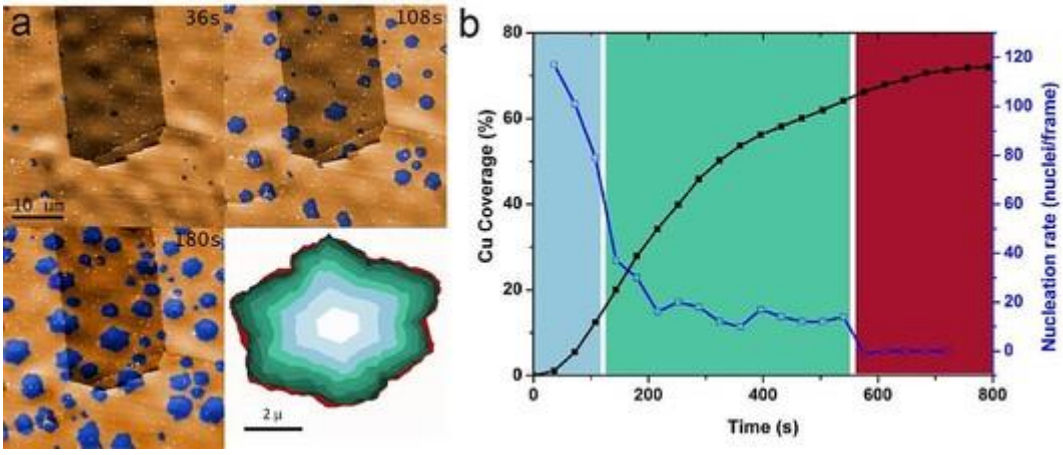

Figure 1. (a) Snapshots recorded during in-situ SEM imaging of graphene growth. (b) Nucleation and growth behavior versus time.

Structural diversity of thermoelectric cobaltates

Boštjan Jančar (1), Damjan Vengust (1), Goran Dražič (2), Medeja Gec (3), Manca Logar (2), Ioannis Petousis (4), Danilo Suvorov (1)

1) Jozef Stefan Institute, Advanced Materials Department, Jamova 39, 1000 Ljubljana, Slovenia

2) National Institute of Chemistry, Laboratory for Materials Chemistry, Hajdrihova 19, 1000 Ljubljana, Slovenia

3) Jozef Stefan Institute, Department for Nanostructured Materials, Jamova 39, 1000 Ljubljana, Slovenia

4) Stanford University, Department of Mechanical Engineering, 452 Escondido mall Stanford, CA 94305, USA

Keywords: oxide thermoelectrics, layered cobaltates, intergrowth structures, probe-corrected microscopy, electron energy-loss spectroscopy

Materials based on layered cobaltates $Na_xCoO_{2+\delta}$ and $Ca_3Co_4O_{9+\delta}$ have been identified as potential candidates for p-type legs in high-temperature thermoelectric modules. These materials exhibit a combination of high Seebeck coefficient, high electrical conductivity and low thermal conductivity, which are believed to stem from a combination of electronic correlations, spin-state degeneracy and layered crystal structure. In terms of coordination polyhedra the $Na_xCoO_{2+\delta}$ crystal structure consists of sheets of edge-sharing CoO_6 octahedra with sodium in two different prismatic sites between the layers. For $x<1$ the prismatic layers are partially filled which results in ordering of sodium ions and vacancies leading to a variety of incommensurately modulated structures. In $Ca_3Co_4O_{9+\delta}$ the edge-sharing CoO_6 layers are separated by a triple rock-salt-type structure consisting of a CoO and two CaO layers or alternatively the crystal structure of $Ca_3Co_4O_{9+\delta}$ can be interpreted as a misfit compound of rock salt Ca_2CoO_3 and CdI_2-type CoO_2 systems. Electrical conductivity in layered cobaltates takes place in the plane of CoO_2 layers, which as a consequence of charge transfer between the layers contain a high concentration of electron holes.[1] In the case of ceramics a high degree of texturing is thus required in order to achieve high conductivity in the direction parallel to CoO_2 layers. The relatively high Seebeck coefficient is interpreted as a consequence of high spin entropy arising from crystal-field splitting of energy levels in CoO_2 layers. It has recently been shown, utilizing EELS, that stacking faults in the $Ca_3Co_4O_{9+\delta}$ structure result in local increase of spin states of cobalt ions within the CoO_2 layers which in combination with low spin states within the CoO layers results in an increased Seebeck coefficient.[2] In terms of thermoelectric figure of merit zT the materials based on $Na_xCoO_{2+\delta}$ with $0.66<x<0.75$ are superior to materials based on $Ca_3Co_4O_{9+\delta}$, however, high mobility of interlayer sodium ions renders $Na_xCoO_{2+\delta}$ prone to reaction with atmospheric water and carbon dioxide.[3] We have found that intergrowth of both structural types leads to atmosphere-resistant materials with high degree of spontaneous texturing, exhibiting moderate electrical conductivity and enhanced Seebeck coefficient. STEM reveals structural diversity between CoO_2 layers of intergrowth structures. Individual grains contain both the $Ca_3Co_4O_{9+\delta}$ and the $Na_xCoO_{2+\delta}$ structural types with respect to the distance between CoO_2 layers. The interlayer space, however, can, apart from $Ca_3Co_4O_{9+\delta}$ type rock-salt sequence and disordered sodium ions characteristic for $Na_xCoO_{2+\delta}$ structural type, contain ordered

calcium ions. The observed structural diversity was investigated using EELS and DFT calculations.

References: 1. G. Yang, Q. Ramasse and R. F. Klie, Phys. Rev. B, 78 15 (2008) 153109. 2. R.F. Klie, Q. Qiao, T. Paulauskas, et al., Phys. Rev. Lett,108 19 (2012) 196601. 3.D. Vengust, B. Jancar, A.Sestan, et al., Chem Mater 25 23 (2013) 4791.

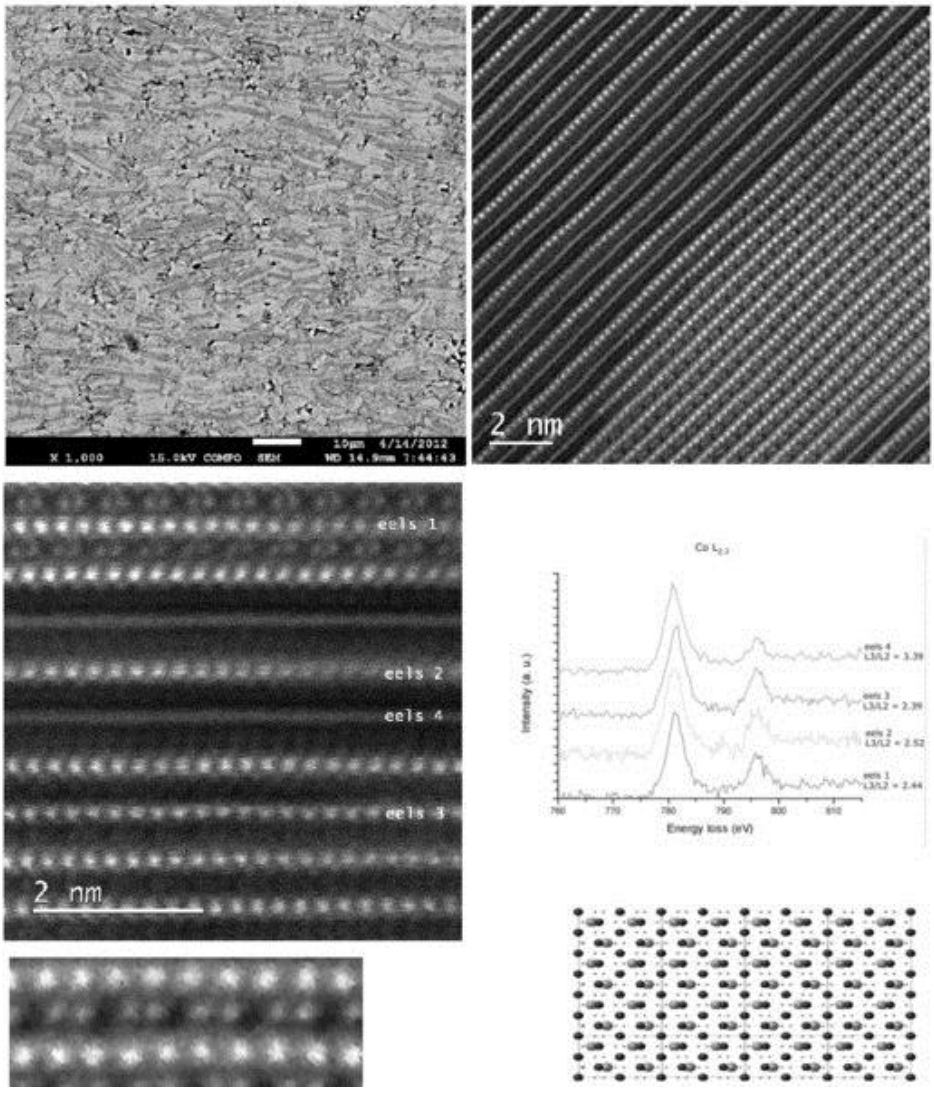

Figure 1. SEM-BSE image of textured integrowth microstructure, structural diversity within individual grain, EELS spectra collected from diffrenet Co-containing planes and calculated structural model of ordered Ca ions in sodium cobaltate structural type

Microscopy of GaN devices beyond the blue LED

B. Pecz (1)

1) Institute for Technical Physics and Materials Sci., Centre for Energy Research, Hungarian Academy of Sciences, P.O.B. 49, H-1525 Budapest, Hungary

Keywords: GaN transistors, diamond, graphene

GaN together with the related materials (AlN and InN) is a group of materials widely used by now for optoelectronic purposes, as well as for lighting. Ternary alloys can be grown and the bandgap can be tuned with their composition. This layers can be used not only in optoelectronics, but also in high power devices.

Self-heating of high power devices is a major problem in GaN high electron mobility transistors (HEMT), in which the power reached the values of 10 W/mm (the length of the gate in mm). Therefore the heat dissipation became one of the major issues and substrates with high heat conductivity are needed. Apparently there are two kinds of materials with excellent thermal conductivity which can be used as a heat sink: diamond and graphene.

Two examples using diamond are shown. In the first one GaN layers (device structures) were grown on diamond substrates by molecular beam epitaxy and the deposition process was optimised using transmission electron microscopy (TEM). The grown GaN layers are free of inversion domains and are of high quality [1].

The second example is a polycrystalline diamond coating layer which covers the grown HEMT transistor [2] and provides a heat sink for the high power devices close to the active region. This method is more general, than the former one and can be applied on various semiconductors.

The third example shows how one can grow GaN over a graphene/SiC substrate [3]. TEM investigations are used to determine the dislocation density in grown GaN and to explore the nanoscale details of the grown structure.

References: 1. B. Pécz et al. Diamond and Related Materials, 34 (2013) 9-12. 2. M. Alomari et al., Diamond and Related Materials, 20 (2011) 604-608 3. A. Kovács et al., Advanced Materials Interfaces, published online: 22 DEC 2014 DOI: 10.1002/admi.201400230

PROCEEDINGS OF ORAL PRESENTATIONS (LIFE SCIENCE)

Nanoparticle clustering within lipid membranes induced by surrounding medium. nanomechanical and thermotropic study on model lipid membranes

Suzana Šegota (1), Danijela Vojta (1), Dania Kendziora (2), Ishtiaq Ahmed (2), Ljiljana Fruk (2), Goran Baranović (1)

1) Ruđer Bošković Institute, Bijenička 54, 10000 Zagreb, Croatia

2) Center for Functional Nanostructures, Karlsruhe Institute for Technology, Wolfgang-Gaede-Str. 1a, 76131 Karlsruhe, Germany

Keywords: Force spectroscopy; IR spectroscopy; Membrane electrostatics; Nanomechanics; Nanoparticles

The research of the nanoparticle (NP) delivery systems and the use of NPs both for diagnostic and therapeutic purposes have created a need for understanding the complex interactions of NPs with cells. Membrane-NP interactions are of crucial importance both for the cell uptake and toxicological investigations. For that reason, lipids that are the cell membrane building blocks, have been used as simplified model systems to study not only the mechanical properties of the membranes and their interactions with different molecular species, but also their structural organization in, for example, marine ecosystems, which are particularly sensitive to the toxicological environmental effects [1].

The interactions between hydrophobic or semihydrophobic gold and silver NPs and a dimyristoylphosphatidylcholine (DMPC) bilayer as a model cell membrane in two ionic solutions result in the structural reorganization within the bilayer manifested as locally increased nanomechanical compaction in the vicinity of NP clusters as well as changed overall thermotropic properties. The reorganization was investigated by AFM imaging, force spectroscopy and IR spectroscopy. The effects of NP surface charge and hydrophobicity were examined by using two different dithiole ligands. First, hydrophobic stearyl amine was coupled to lipoic acid coated gold and silver NPs. Second, newly synthesized positively charged semihydrophobic ligand containing additional amine group was used to functionalize gold and silver NPs by ligand exchange method. The mean diameter of the NPs estimated from the mean heights as observed by AFM imaging was 3 nm, i.e. small enough to enable embedding of NPs within the bilayer. The ligand effect of NPs on a non-local level of the bilayer phase change (bulk property) has been recorded as lowering of the phase transition temperature at the most by 1.0 °C in PBS and as increasing of the phase transition temperature at the most by 0.5 °C in seawater. The force spectroscopy results, on the other hand, indicated that (semi)hydrophobic NPs increased the bilayer density around NP clusters and thus locally increased lateral compaction of the bilayer. The strengthening effect was observed for both the silver and the gold NPs in a high ionic strength solution such as seawater (SW), while it was absent under physiological conditions. The local lipid rearrangement induces the long range lipid reorganization resulting in the bilayer phase transition shifting towards lower or higher temperatures depending on the solution ionic strength.

References: [1] S. Šegota , D. Vojta, G. Pletikapić, G. Baranović, (2014) Chem. Phys. Lipids 186 (2015) 17–29.

Biomineral structures of aragonite in marine mollusks at the nanoscale: FESEM and AFM studies

Vida Čadež (1), Srečo D. Škapin (2), Suzana Šegota (1), Branka Salopek-Sondi (1), Ivan Sondi (3)

1) Ruđer Bošković Institute, Bijenička 54, 10000 Zagreb, Croatia

2) Jožef Stefan Institute, Jamova 39, 1000 Ljubljana, Slovenia

3) Faculty of Mining, Geology and Petroleum Engineering, University of Zagreb, Pierottijeva 6, 10000, Zagreb

Keywords: biomineralizaton, FESEM, AFM, aragonite, nanostructure

Marine mollusks produce complex aragonite biomineral forms that have unique structural and morphological properties in comparison with abiotic analogues, especially because they are formed at ambient pressure and temperature. This research studies the formation, structural and morphological properties of aragonite biomineral occurring in Noah's ark (*Arca noae*), noble fan mussel (*Pinna nobilis*) and common cuttlefish (*Sepia officinalis*). Morphology of aragonite in these organisms was examined by field emission scanning electron microscopy (FESEM) and atomic force microscopy (AFM). Results obtained showed that aragonite structures are composed of well defined and uniform nanoparticle building blocks formed through the oriented aggregation processes of the initially formed nanosized aragonite crystallites. These findings confirm the hypothesis that the non-classical nanoscale aggregation route is a common mechanism in the formation of the hierarchically organized aragonite forms in marine organisms.

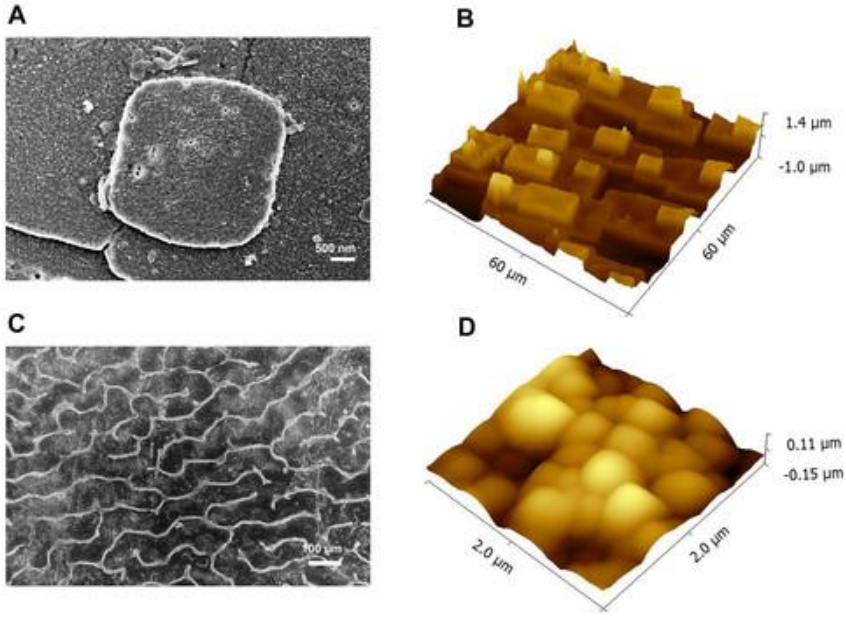

Figure 1. Inner shell surface from Pinna nobilis; FESEM microphotograph of aragonitic tablet (A) AFM surface topography images presented as a 3D – view of height data (B) and cuttlebone from Sepia officinalis; FESEM microphotograph of ventral surface (C) with AFM surface topography images of aggregated nanoparticles presented as a 3D – view of height data (D)

Once upon a time, there were women in microscopy sciences in Croatia

Danijela Poljuha (1) and Barbara Sladonja (1)

1) Institute of Agriculture and Tourism Poreč, Karla Huguesa 8, 52440 Poreč, Croatia

Keywords: Ailanthus altissima, history of microscopy, Vjera Petaj, extrafloral nectaries

It was not easy to be a scientist a century ago, and it was certainly even more challenging to be a woman scientist. There are just a few Doctors of Philosophy from early years of the 20th century. One of those is Vjera Petaj, a passionate botanist who achieved a PhD degree with a thesis based on microscopy science. She studied at the Faculty of Philosophy at the Royal University of Francis Joseph I in Zagreb as one of the first female students, and in her Doctoral Thesis entitled „Extrafloral nectaries on the leaves of Tree oh Heaven (*Ailanthus glandulosa* Desf.)" she used microscopy techniques for the investigation of morphology, anatomy, microchemistry and biology of extrafloral nectaries of this ornamental tree. All her results were later confirmed by modern microscopy techniques and this topic is still actual, since Tree of Heaven, *A. altissima* (Mill.) Swingle, is a highly invasive tree, present on the IUCN list of 100 worst invasive species, and today widespread on all continents, with the highest abundancy in Europe and North America. Its allelopatic, as well as medicinal effects are widely investigated. In this presentation results of this early microscopic work will be presented, moreover an insight into a social element, particularly on the status of women in the Croatian academic community in the early 20th century will be given. In fact, legal rights of men and women in Croatia became equal only after 1905, but many years and efforts were needed to lessen differences between men and women scientific career opportunities. This presentation is also a tribute to Vjera Petaj and other highly educated female scientists through an overview of their achievements a century ago. Through dr. Petaj's research special emphasis on the relevancy of microscopic analysis and achieved results as well as on the actuality of this topic in modern science will be given.

References: 1. Vjera Petaj, University of Zagreb, 1916, pp23. 2. Ferdaous Albouchi et al., S. Afr. J. Bot. 87 (2013) 164–174. 3. Tihana Luetić, Povijesni prilozi, 22 (2002) 167-208. The aid of Dr. Nikola Ljubešić and Dr. Tihana Luetić is gratefully acknowledged.

Exploring protein-protein interactions of S-adenosyl homocysteine hydrolase (SAHH) using bi-molecular fluorescence complementation (BiFC)

Adriana Lepur (1), Lucija Kovačević (1), Robert Belužić (1), Ivana Grbeša (1), Pau M. Muñoz Torres (1), Jelena Trmčić-Cvitaš (1), Oliver Vugrek (1)

1) Division of Molecular Medicine, Translational Medicine Laboratory, Ruđer Bošković Institute, Bijenička cesta 54, 10000 Zagreb, Croatia

Keywords: S-adenosyl homocysteine hydrolase, bi-molecular fluorescence complementation, cell imaging, interactome, Adenosylhomocystein hydrolase-Like 1

S-adenosyl homocysteine hydrolase (SAHH) is the only mammalian enzyme capable of hydrolyzing S-adenosyl homocysteine – a byproduct in cellular methylation reactions. Thus, SAHH is crucial for maintaining the cellular methylation potential, indirectly impacting methylation of DNA, mRNA, tRNA, lipid and protein (1). SAHH deficiency leads to serious developmental defects - muscular hypotonia, brain white matter atrophy and liver inflammation. SAHH interacting partners could help elucidate the regulation of its expression, enzymatic activity and intracellular dynamics. In search for SAHH interactors we used a bi-molecular fluorescence complementation (BiFC) approach. To do so, we cloned proteins of interest into suitable host vectors and fused them to fluorescent Venus protein that is split into two parts. Subsequently, we expressed the fused proteins in either bacteria or in cultured human cells. Detection of fluorescence indicates reassembly of split-Venus, hinting at protein-protein interactions between proteins of interest.

Using BiFC we confirmed SAHH self-association in human kidney cell line Hek293T. SAHH mutant that lacks C-terminal region necessary for SAHH multimerisation, served as a negative control. We also observed SAHH interaction with Adenosylhomocystein hydrolase-Like 1 (AHCYL1), a protein closely related to SAHH (2). This interaction plays a role in SAHH shuttling between the cytoplasm and the nucleus, where SAHH contributes to DNA methylation. Also, we found a few unexpected SAHH interactions, e.g. with TLR7. TLR7 mediates a response to viral single-stranded RNA after macrophages internalize it in endosomes.

This interaction is less surprising if we know that the elements involved in TLR-mediated RNA responses are controlled by modifications such as methylation. Dysregulation of SAHH can also change DNA methylation pattern - a hallmark of malignant lesions, which are regularly coupled with progressive inflammation (3). To explore this further, we assessed SAHH and/or AHCYL1 levels in lung cancer samples and human monocytes, and compared it to the expression of an inflammatory marker Galectin-3.

Immunocytochemistry showed that monocytes down-regulate SAHH after differentiation, but preserve AHCYL1 expression. When we used LPS to induce pro inflammatory macrophage phenotype, the cells stopped expressing AHCYL1 protein completely. Next, we aim to study how SAHH influences the immune function of monocytes and macrophages, while exploring its interactome using bi-molecular fluorescence complementation. Since SAHH dysfunction leads to numerous pathologies

including cancer, hepatitis, neurological and vascular disorders, it is crucial to dig deeper into its regulation and intracellular functions.

References: 1. Oksana Tehlivets et al, Biochim Biophys Acta. Jan 2013; 1832(1): 204–215 2. Benoit Devogelaere et al, Bioessays. Jul 2008; 30(7): 642-52 3. JF Leal et al, Carcinogenesis. Aug 2008; 29 (11): 2089-2095.

Living cells viability study after 200 kHz laser illumination in a wide-field two-photon microscope

Vitalijs Zubkovs (1), Carlos Macias-Romero (1), Aleksandra Radenovc (2), Sylvie Roke (1)

1) Laboratory for fundamental BioPhotonics, Institute of Bioengineering, École Polytechnique Fédérale de Lausanne (EPFL), 1015, Lausanne, Switzerland

2) Laboratory of Nanoscale Biology, Institute of Bioengineering, École Polytechnique Fédérale de Lausanne (EPFL), 1015, Lausanne, Switzerland

Keywords: two-photon microscope, photodamage, living cells, endogenous fluorescence, near infrared laser

Light microscopy retains its strong position as the main tool for studying living cells on a sub-micrometer scale. One of advanced light microscopy techniques is two-photon excitation fluorescence imaging. A typical two-photon fluorescence microscope operates with a pulsed laser illumination source. In order to reach a good signal-to-noise ratio image acquisition procedures require high illumination fluence that could be damaging for living cells and tissues. Photodamage is an important issue in light microscopy and it cannot be avoided but can be minimized by optimizing the imaging parameters. It is possible to reduce photodamaging effects in living cells by decreasing the illumination fluence and keeping at the minimum light absorption by intrinsic chromophores. We have developed a wide field two-photon excitation and Second Harmonic Generation microscope with a pulsed laser source at 1028 nm with 200kHz repetition rate and 190 fs pulse duration. The setup has advantages for living cells imaging in comparison with commercial scanning two-photon microscopes. First of all, a wide field illumination and full-frame iCCD image recording significantly reduces the image acquisition speed [1]. Secondly, linear absorption of endogenous chromophores is insignificant at 1028 nm wavelength and it lowers cytotoxicity. Last but not the least, reduction of the pulse repetition rate allows raise the illumination power without pronounced living cell damage.

In this work we preset living cells viability studies and characterization of photo damaging effects cased by near infrared laser light illumination at 1028 nm. The viability test is based on analysis of cultured human embryonic kidney 293 (HEK) cells cloning efficiency after illumination with the laser light. The results show that the illumination with the laser light fluence below 6 mJ/cm2 doesn't induce significant changes in living cells cloning efficiency that permits long-term imaging with minimal photodamage. The fluece above 20 mJ/cm2 induces direct damage of the living cells that is visually observable after several minutes of illumination.

Our results confirm the general assumption that the tolerable illumination light fluence is approximately half of the direct photodamage threshold [2]. As well we present the advantages of using a low repetition rate near infrared laser for in vitro studies.

References: 1. Carlos Macias-Romero, et al., Nano Let. 14 (2014) 2552–7. 2. Roberta Galli, et al., PloS One. 9 (2014) e110295.

Near-field optical (SNOM) nanoimaging for glia-synapse correlations and functions

Masaru Sakai(1), Kazuharu Uchiyama(1), Hirokazu Hori(1), Kiyoshi Kobayashi (1), Youichi Shinozaki (2), Keisuke Shibata (2), Eiji Shigetomi (2), Schuichi Koizumi (2)

1) Department of Science for Advanced Materials, Interdisciplinary Graduate School of Medicine and Engineering, University of Yamanashi, Yamanashi 409-3898, Japan

2) Department of Neuropharmacology, Interdisciplinary Graduate School of Medicine and Department of Liaison Academy, Faculty of Medicine, University of Yamanashi, Yamanashi 409-3898, Japan

Keywords: super-resolution, SNOM, bioimaging, topography and fluorescence, astrocyte microprocess

A nanophotonic logic device consisting of three quantum dots based on excitation (energy) transfer and control via optical near fields under the presence of both excitation in the control dot and phonon environment has been proposed and experimentally verified[1], while in brain system Ca^{2+} imaging have revealed that glial cells dynamically control neuron activities via releasing gliotransmitters such as ATP[2]. Among glial cells, astrocytes participate in this process by intimately associating with synapses, where chemical neurotransmission between two neurons in the neural network is executed. Analogies between semiconductor nanostructures and living brain cells both of which are surrounded by the environmental systems, and furthermore importance of environmental roles themselves have been recognized, but it is still open to clarify fine structures and functions of astrocyte and synapse correlations as a fundamental unit for brain activities, mainly because of the diffraction limit. Towards deep understanding of astrocyte-synapse interactions and correlations (i.e. tripartite synapse) in a microscopic, level, which might be a fundamental building block of a glia-type nano device with brain-like spontaneous functions, it is crucial from spatial and temporal viewpoints to noninvasively investigate the astrocyte-synapse interactions and correlations, as a basic unit, with the help of microscopy and spectroscopy. Several super-resolution imaging methods have been developed to achieve sub-hundred nano meters in resolution using visible light, and among them, SNOM based on the near-field optical interactions between probe and sample, is a promising method[3] for our study to give sub-ten-nanometer lateral resolution with visible excitation light whose resolution limit essentially depends on the smallness of probe tip and the sharpness of probe taper angle. By considering the current technological infrastructure, even if the visible light is used, a single nanometer in resolution will be expected, in combination with software techniques used in the other methods. To investigate basic processes responsible for brain functions by nano-imaging of fine structures of the tripartite synapse, we have successfully developed a homemade SNOM, extendable for measurements *in vitro*, combined with an inverted optical microscope providing nanoscopic views as well as macroscopic ones. Comparing with the zoom-in SNOM images and the zoom-out images obtained from the conventional microscope, we have found new fine structure that can be identified only in the zoom-in SNOM images, while the SNOM images of synapses indicate that those near the surface are represented more precisely. We are now ready for discussing the fine structures and snapshot of differences of the sample states with/without stimulation of astrocytes due to their interactions and correlations in spatial resolution of *lambda*/10. The system is

expected to be a useful tool for the discussion. The details will be given in the presentation.

References: 1. T. Kawazoe, K. Kobayashi et al., Appl. Phys. Lett., 82 (2003) 2957-2959. 2. S. Koizumi, Proc. Natl. Acad. Sci. 100 (2003) 11023-11028. 3. M. Sakai, Nanotechnology 15 (2004) S362-S364.

Multiple imaging modalities to assess the mouse brain after stroke

Srećko Gajović (1), Dora Polšek (1), Marina Dobrivojević (1), Dunja Gorup (1), Dinko Mitrečić (1)

1) University of Zagreb School of Medicine, Šalata, 10000 Zagreb, Croatia

Keywords: mouse, brain, stroke, bioluminiscent imaging, microCT, immunohistochemistry

The visualization of molecular events in the experimental animals represents a constant challenge for researchers. The classical approaches include a postmortal analysis of fixed specimen representing a single time point. Although morphologically very precise, this approach requires animals to be sacrificed in order to obtain specimens for analysis and each time point is represented by the group of animals, which should be compared to each other. As an innovative complementary approach, in vivo imaging offers the insight in molecular events in the living animals enabling to follow the changes in the same animal in different time points. Moreover, the possible translation of the in vivo approaches on the laboratory animals, to the possible diagnostic procedures in humans is desirable.

To analyze the consequences of the ischemic lesion on the mouse brain as a model of the human ischemic stroke, the animals were subjected to medial cerebral artery occlusion (MCAO) for 60 minutes and subsequent reperfusion (1). The procedure resulted with ischemic lesion, covering part of the cortex, hippocampus, and striatum. The extent of the lesion and the process of recovery was monitored in these animals, and putative therapeutical approaches were tested. Two in vivo imaging modalities were applied to analyze the consequences of the stroke in the living animals, microCT (μCT), and bioluminescent imaging (BLI). The μCT is based on X-ray imaging and enables easy visualization of hard tissues as bones and teeth. Brain as a soft-tissue is in general considered not adequate for μCT imaging. BLI as imaging modality requires a presence of transgene in the mouse genome. The transgene is luciferase gene from firefly, and it should be controlled by promoter of the gene of interest. The transgenic mouse line used for this study was Tlr2-luc mouse line, where luciferase gene was driven by Tlr2 promoter. Tlr2 is a receptor involved in innate immunity, and its expression reflects the extent of inflammation after the stroke (2). The histological analysis was used as a control of the obtained in vivo images. To enable the brain imaging with μCT different contrast agents were used, and subsequently the non-ionic contrast agent Omnipaque was selected with the best gray/white matter contrast (3). The imaging was performed on postmortal brains immersed in the contrast agents. As a result the morphology of the brain was visible and the extent of the ischemic lesion was measured, and 3D reconstructions obtained (Figure 1). The lesion size was confirmed subsequently by histology (Figure 2). The imaging was applied not only to assess the stroke, but as well to monitor the labeled stem cells transplanted to the brain.

Bioluminescent imaging visualized brain molecular reaction to the stroke and the reaction was followed through the time (Figure 3). The 3D reconstruction of the image was possible although the resolution of the signal allowed to locate it only in the particular parts of the brain. The extent of neuroinflammation was monitored in the mice

after stroke in particular after stem cell transplantation, where it was shown that mesenchymal stem cells modify the brain response.

In conclusion, the diverse in vivo imaging modalities are complementary to microscopy modalities and enable the insight in molecular events in the living animals to be used as a model for human disease.

References: 1. Winters L et al. Neuroscience 2013;238:87-96 2. Dobrivojević M et al. Croat Med J 2013;54:3-11. 3. Bohaček I et al. J Neuoinflammation 2012, 9:191. We acknowledge the support of EU FP7 Project GlowBrain (REGPOT-2012-CT2012-316120).

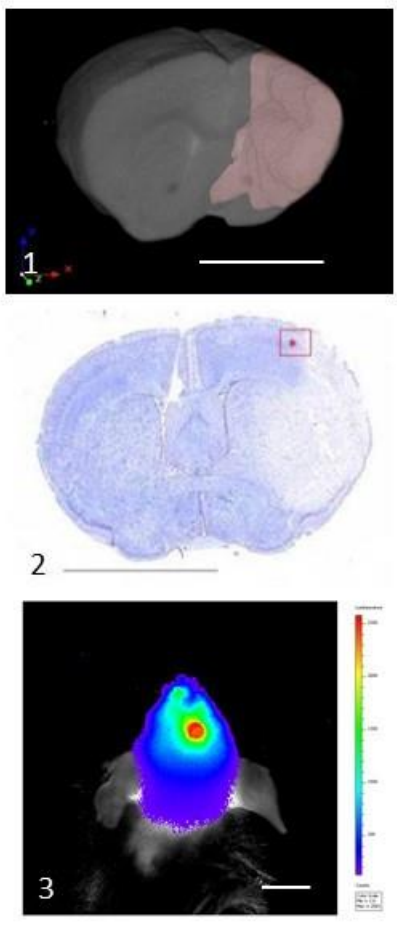

Figure 1. 3D reconstruction of the mouse brain visualised by microCT, stroke area visible as a lighter region. Bar 1 mm. Figure 2. Histological section of the mosue brain with ischemic lesion seen as a lighter region. Red dot - place of transplantation of mesenchymal stem cells. Staining - cresyl violet. Bar 1 mm. Figure 3. Bioluminescent imaging of Tlr2 signal after ischemic lesion superimposed to the mosue head. Bar 1 mm.

PROCEEDINGS OF ORAL PRESENTATION (MATERIAL SCIENCE)

Increased photoconductivity in BaTiO3/TiO2 composites

Milivoj Plodinec (1), Andreja Gajović (1), Ana Šantić (1), Janez Zavašnik (2), Miran Čeh (2)

1) Ruđer Bošković Institute, Bijenička 54, HR-10002 Zagreb, Croatia

2) Jožef Stefan Institute, Jamova 39, SI-1000 Ljubljana, Slovenia

Keywords: heterojunctions, nanotubes, photoconductivity, vacancies, surface conductivity

$BaTiO_3$ (BTO), is a well-known and widely investigated dielectric material. It is mainly used in capacitors due to its high dielectric constant. The dielectric properties of BTO are controlled by purity and microstructure which are dependent on the methods of preparation. Recent advances in nanotechnology such as MLCC, MEMS, DRAM have resulted in miniaturization of devices [1, 2].

In this work barium titanate TiO_2 nanostructured arrays (BTO-TiO_2 NT) were synthesized by hydrothermal processing of titanium based precursor (TiO_2 nanotube arrays prepared by anodisation of titanium foils) in aqueous solution of $BaCl_2$ and NaOH (Fig. 1.).

Structural and compositional properties were investigated by XRD, SEM, EDX, TEM, HRTEM, SAED and Raman spectroscopy (ex–situ and in-situ), while electric measurements were studied by impendence spectroscopy.

The persistent photoconductivity (PPC) effect in nanotube arrays of barium titanate and TiO_2 (BTO/TiO_2NT) was studied at room temperature under daylight illumination. The BTO/TiO_2NT heterostructures exhibited a giant PPC effect that was six orders of magnitude higher than the dark conductivity, followed by a slow relaxation for 3 hours . The PPC effect in this material was explained by the existence of defects at the surfaces and the interfaces of the investigated heterostructures. The sample was prepared using a two-step synthesis: the anodization of a Ti-foil and a subsequent hydrothermal synthesis.

References: [1] N. A. Hill, J. Phys. Chem. B, 2000, 104, 6694–6709. [2] M. A. Pena and J. L. G. Fierro, Chem. Rev., 2001, 101, 1981–2018.

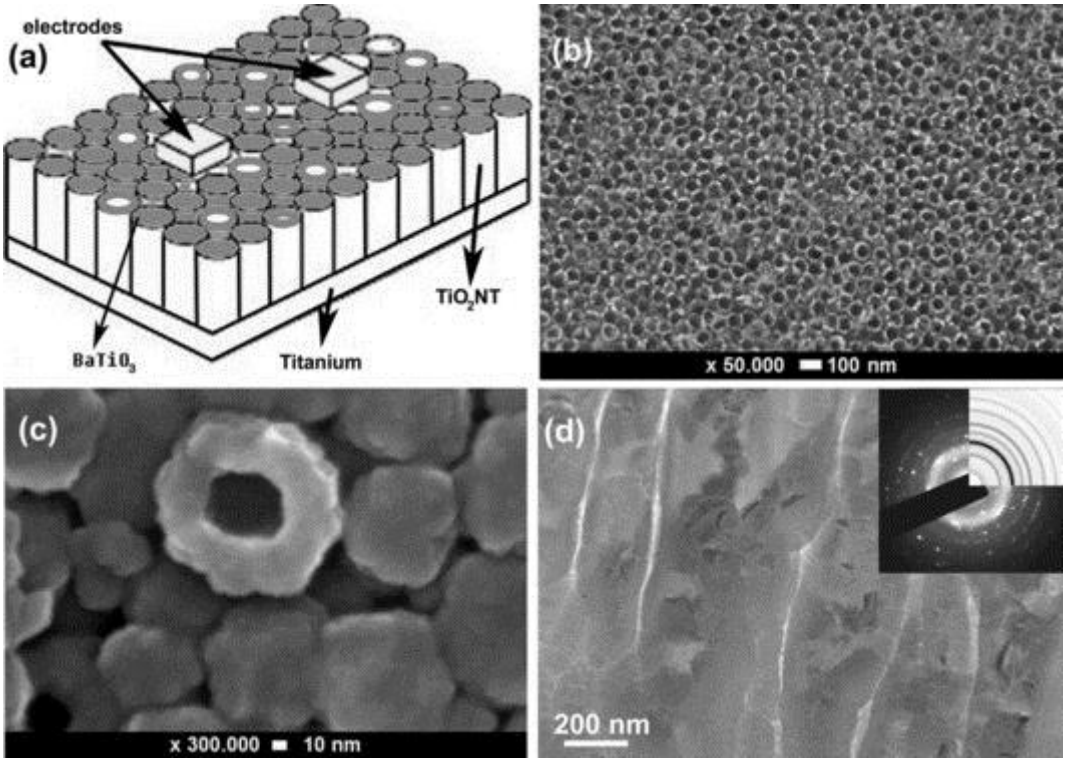

Figure 1. (a) Schematic view of the electrodes for electric measurements, (b) SEM of TiO2 nanotube array, and (c) BaTiO3 surface, (d) TEM of cross-section of BTO/TiO2NT heterostructure, inset SAED with simulated pattern of tetragonal BaTiO3

Novel mixed phase sno2 nanorods for enhancing gas-sensing performance towards isopropanol gas

Igor Djerdj (1)

1) Ruđer Bošković Institute, Bijenička 54, 10000 Zagreb, Croatia

Keywords: Gas-sensing, mixed phase, SnO2

The synthesis and the gas sensing properties of a novel mixed phase (i.e., tetragonal and orthorhombic phase) coexistence SnO_2 nanorods is presented. The mixed phases SnO_2 nanorods were obtained by calcinations of SnC_2O_4 synthesised with a chemical precipitation method using $SnCl_2 \cdot 2H_2O$ and PEG 400 as precursors. The resulting nanorods appear as polycrystalline composed of spherical mixed phases SnO_2 nanocrystals and have a high surface area. It was observed that the calcination temperature was the key parameter determining the content of the orthorhombic phase. The as-synthesized compounds were used as sensing materials of the sensors of indirect heating structure and tested for their ability to detect volatile organic compounds (VOCs), such as isopropanol, acetone, alchohol, and formaldehyde. Gas sensing tests showed that these mixed phases SnO_2 nanorods are highly promising for gas sensor applications, as the gas response for isopropanol was significantly enhanced by the presence of orthorhombic phase (S=61.5 to 1000 ppm isopropanol and response time and recovery time of 4 and 10 s). The as-prepared two phases SnO_2 nanorods with the highest content of the orthorhombic phase exhibit excellent gas response, selectivity, and stability toward isopropanol gas at the optimized operating temperature of 255 °C. The enhancement in sensitivity is attributed to the presence of small orthorhombic SnO_2 crystals with average radius shorter than the Debye screening length of 7 nm for SnO_2.[1]

References: 1. Dan Hu, Bingqian Han, Shaojuan Deng, Zhipeng Feng, Yan Wang, Jasminka Popovic, Marko Nuskol, Yude Wang and Igor Djerdj, J. Phys. Chem. C 118 (2014) 9832-9840.

Four-dimensional crystallography of Ca.83CuO2 composite crystal; an electron and X-ray diffraction study

Ognjen Milat (1)

1) Institute of Physics, Bijenička 46, 10000 Zagreb, Croatia

Keywords: Electron crystallography, composite crystal structure

Composite structure of $Ca_{.83}CuO_2$ crystal was studied using methods of four dimensional crystallography. Structure solution and refinement were done using electron diffraction patterns on single crystals, and Rietweld method on powder X-ray diffraction data; JANA2006 software package is applied for analysis in terms of four dimensional crystallography.

The $Ca_{.83}CuO_2$ crystal belongs to a class of composite crystals consisting of two subsystems: „CuO_2-chains“ and „M_x-cations“; the subsystems are interpenetrated, mutually modulated, and usually incommensurate along the chain direction (1). Lattices of these subsystems have common $\boldsymbol{a}$ and $\boldsymbol{b}$ parameters while the ratio of parameters along the “chains” $\boldsymbol{c_M/c_{Ch}}$ varies with 1/x. This holds for $M_x = Ca_{.83}$, $Sr_{.73}$, and $Ba_{.67}$, and in particularly for the $M_x = [(Sr/Ca)_2Cu_2O_3]_{.70}$. In this latest case, the crystal is known as a “chain – ladder compound” with formula $(Sr/Ca)_{14}Cu_{24}O_{41}$. It is well known because of exotic interaction, ordering, and dynamics of electron holes and spins within either of the two constituting subsystems. In case of La for Sr substitution the charge distribution and spin depletion in CuO_2-chains are strongly affected. On the other hand, electron diffraction studies reveal that it is only the amplitude of displacive modulation of the basic crystal structure that is slightly influenced by the charge and spin ordering (2).

This analysis of the structures of the $[M]_xCuO_2$ crystals with x neither integer nor a rational number (of the form: p/r in general), reveals that one needs four Miller indices for assigning the Bragg spots in the diffraction patterns. The Bragg spots do not belong to a single lattice but have to be assigned to two reciprocal lattices with a common central plane, and two generally non-collinear rows of nodes running out of plane with two mutually incommensurate spacings. The conjugated lattices in direct space define two incommensurate subsystems: “CuO_2-chains”, and “Ca-strings”. Such a composite crystal structure can be adequately characterised only by using contemporary methods of four-dimensional crystallography.

References: (1) O. Milat et al., Acta Cryst. A48 (1992), 618-625 (2) V. Ilakovac et al., Phys. Rev. B85 (2012) 075108

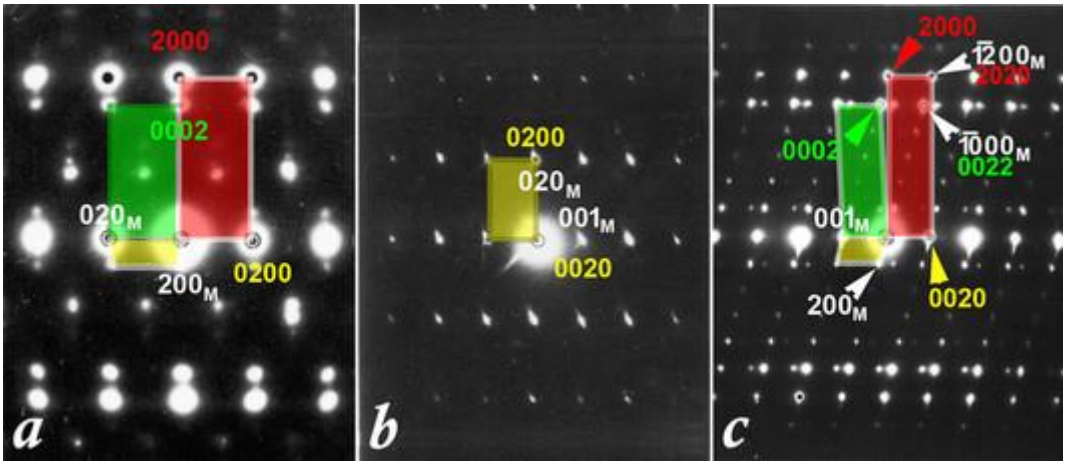

Figure 1. Diffraction patterns of Ca.83CuO2 composite crystal along the zones: (a) [0011]*; (b) [1000]*; (c) [0100]*. Bragg spots of „CuO2-chains“ and „Ca-strings“ subsystems and their reciprocal lattice cells are colored red and green, while the yellow indices are for the common spots. Cell of the 3-dim periodic monoclinic superlattice is colored yellow, while indices of the superlattice nodes are marked in white with subscript M.

Microscopic and micro-spectroscopic techniques for pigment and binder investigation on the „Crucifixion“ of Gianfrancesco da Tolmezzo

Tea Zubin Ferri (1)

1) METRIS Materials Research Centre, Zagrebačka 30, 52100-Pula, Croatia

Keywords: optical microscopy, SEM/EDS, μFT-IR, pigments, binder

Since analyses related to cultural heritage materials are performed using the smallest possible amount of sample, microscopy and micro-spectroscopic techniques are essential and are becoming more and more accurate while reducing the required sample amount with new and improved technological features. As regards the analyses performed on samples prepared as cross-sections and taken in minimum quantities from a painting, a multidisciplinary approach represents an important precondition. The correct results interpretation, as well as the setup of the right methodology, requires a knowledge background of each expert included in the research. As an example of good practice, the analyses performed in the framework of the altarpiece „Crucifixion“ of Gianfrancesco da Tolmezzo restoration, carried by Croatian Conservation Institute, will be presented. The analyses performed on cross-sections prepared from samples taken from a painting whose surface exceeds two square meters, consisted of the investigation of chemical composition of the original pigments and binders as well as of materials applied later, during past interventions, more or less documented (Figure 1). Observation by optical microscope using visible, UV and polarized light was done first, in order to define the paint layers and their function and decide which strata to focus the chemical analysis on. Chemical composition analyses on the cross-sections were carried out by field emission scanning electron microscope with energy dispersive spectroscopy device (FEI Quanta 250 FEG) for elemental characterization. In order to determine the organic compounds present in the painted strata, a FT-IR microscope with ATR objective, Hyperion 1000 Bruker, was used. Each analyzed cross-section contains several strata, so the research was first directed toward differentiation of the original and the strata added successively, as well as to a detailed chemical characterization of the original materials (pigments and binder). The application of polarized light in optical microscopy observation is useful for thin metal layer identification (Figure 2), while UV light permits immediate response by some synthetic resins, binders or pigments, which absorb UV light. SEM analysis were performed by back scattered electrons which emphasize compositional differences on the sample surface, allowing instantaneous distinction of strata composition and individuation of details, particles or damages among layers (Figure 3). ATR micro FT-IR spectra collected on different samples and layers, do not show stretching vibration of the C=O bond, usually found at 1740 cm-1 and typical for oils, indicating that the altarpiece was painted in tempera technique, as it was initially assumed by the restorers. The correct arrangement and sequence of microscopic and micro-spectroscopic techniques applied and a multidisciplinary approach that takes into account the history and dating of the artifact, could enable a fast and relatively inexpensive palette identification, crucial data for adopting an appropriate restoration methodology.

References: 1. Rosu M.C. et al.: Materials Science in Semi-conductor Processing (16) 1554 (2013) 2. Vlachos N. et al.: Analytica Chimica Acta 461, 573–574 (2006) 3. Church A.H.: The chemistry of paints and painting, 4th edition, London, 148 (1915)

Figure 1. Gianfrancesco da Tolmezzo's "Crucifixion", ca. 1505 (Nikolina Oštarijaš, Croatian Conservation Institute).

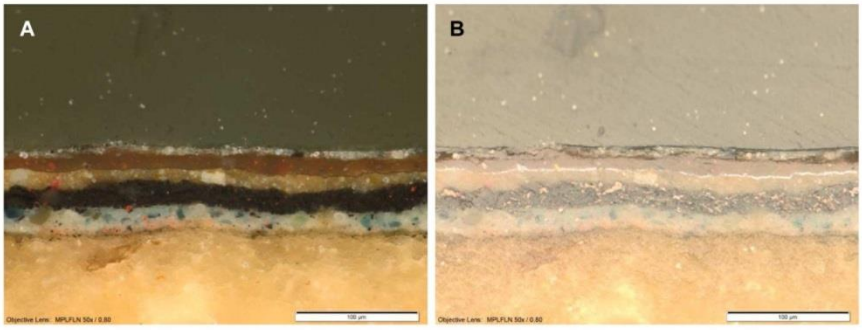

Figure 2. Sample cross-section observed by optical microscope in visible light (A) and polarized reflected light (B).

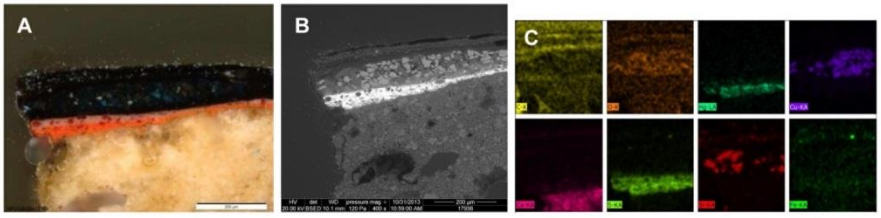

Figure 3. Sample cross-section observed in visible light (A), SEM BSE image (B) and EDS elemental maps (C).

Micro- and nano-features of kaolin aggregates as a result of weathering processes

V. Bermanec (1), A. Botha (2), N. Tomašić (1)

1) Division of Mineralogy and Petrology, Faculty of Science, University of Zagreb, Horvatovac 95, HR-10000 Zagreb, Croatia

2) Laboratory for Microscopy and Microanalysis, University of Pretoria, Private bag X20, Hatfield 0028, Pretoria, South Africa

Keywords: kaolin, stacking, nanowhiskers

Kaolin is a member of kaolin-serpentine group. It is a sheet silicate, and is found to be a result of hydrothermal alteration, weathering processes or even combination of it. Kaolin is found in different environments such as tropical soils, sedimentary deposits, hydrothermal mineral deposits, and even on the Mars surface.

As a clay mineral, kaolin displays various particle sizes, layer stacking defects, and consequently different models of its real crystal structure (1, 2).

Kaolin samples from various localities in tropical areas in Brazil and Africa. X-ray diffraction and high-resolution scanning electron microscopy (Zeiss Gemini Ultra microscope with in-lens detectors) were employed.

Microscopic examinations revealed existence of defects between the layers in layered crystal structure which are observed as divergent crystals resembling half open books (Fig. 1a). The size of such crystals varies from a few hundred nanometers up to 10 or 15 micrometers. A distinguishable thickness of layers within the crystals can vary from 10 to 150 nm. The book-like texture of kaolin crystals is due to deformation of crystal structure, i.e. because of filling two-thirds of octahedral sites with aluminum (or other trivalent cation), and because of lateral misfit between octahedral and tetrahedral sheets. Accumulation of these misfits in the crystal structure results in defects easily observable on high resolution scanning electron images.

The second micro-feature of the kaolin samples was observed at the edges of crystals. The edges are frequently found undefined, and look like lace. It is obvious that such an edge is a result of growing, and it can be easily recrystallized even through a simple process like lyophilization.

Low magnification and high electron energy used in conventional scanning microscopy do not allow an observation of real hexagonal shapes of small kaolin crystals or even layers. By applying low voltages and in-lens detectors the hexagonal symmetry of single layers of kaolin becomes clearly visible. The observed stacking is responsible for lowering the symmetry, what is obvious from different elongation for the duration of growing, and three types of crystal growth can be recognized. The first one is more common stacking of layers, layer by layer. The second one is skeletal growth of kaolin like snowflake.The third type of crystal growth is screw-like. Every investigated sample of kaolin has cracks between the blocks or layers within the big crystals. Inside the cracks/defects within the crystals nanowhiskers were found (Fig. 1b). They are randomly distributed, sometimes very often. The size of whiskers varies between 100 and 200 nm in length and about 20 nm in width. Some of whiskers are broken. These nanowhiskers could influence to mechanical properties of clay containing kaolin.

References: Etienne Balan et al., Elements 10 (2014) 183-188 Rossman F. Giese, Reviews in Mineralogy 19 (1991) 29-62

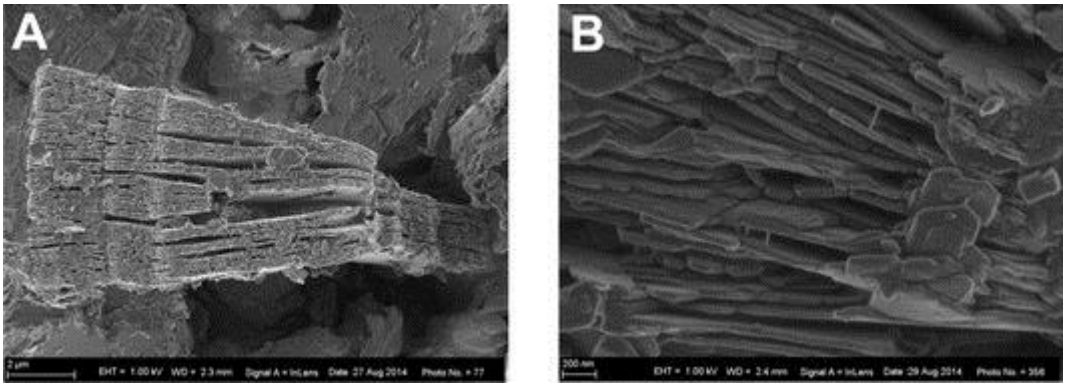

Fig. 1. A. Divergent crystals resembling half open books. B. Kaolin crystal from Jacu pegmatite near Equador, Brazil, with nanowhiskers up to 200 nm long and 15 to 25 nm thick.

The influence of grain size of waste foundry sands on removal percentage of Copper ions

Lj. Slokar (1), A. Štrkalj (1), Z. Glavaš (1), K. Maldini (2), D. Hršak (1)

1) University of Zagreb Faculty of Metallurgy, Aleja narodnih heroja 3, 44103 Sisak, Croatia

2) Croatian Waters, Central Water Management Laboratory, Vukovarska 220,10 000 Zagreb, Croatia

Keywords: microstructure, grain size, waste foundry sands, adsorption, heavy metals

Foundry sand is used during the metal casting production. It consists of quartz sand (>90 %), binders (chemical or clay) and additives. Waste foundry sand (WFS) may be used in constructions and in recently for heavy metals removal from aqueous solutions by adsorption [1, 2]. Heavy metals, e.g. copper, may cause many diseases and for this reason they must be controlled in waste water [3].

In this research the influence of grain size of chemical bonded (sodium-silicate) waste foundry sand (WFS-CHB) and clay bonded (bentonite) waste foundry sand (WFS-CB) on removal percentage of Cu(II)-ions was examined. Adsorption was performed with 1 g of WFS-CHB, as well as WFS-CB, and 50 ml Cu(II)-ions solution of concentration 100 mg/l at 25 °C until equilibrium state (20 min). Sediments in form of discs were prepared with binder KBr for microscopic examination. Microstructure was observed by stereo microscope equipped with digital camera. Grain size was determined by Olympus GX51-Analysis software according to ASTM standard E112-96 and its effect on efficiency of adsorption was established as well.

Validation of ions removal in this research was performed using light microscopy, as a part of adsorption research which is in a progress.

Light micrograph of WFS-CHB (Fig. 1a) shows that the mixture of binder and sand is not homogenous and on Fig. 1b it can be seen that the adsorption occurred (blue color of adsorbed Cu(II)-ions).

Figure 1c shows that a mixture of clay and sand is much homogenous than chemical bonded sample (Fig. 1a). Figure 1d shows WFS-CB after adsorption.

The smallest average grains size was in sample of WFS which is clay bonded (203.26 μm). After adsorption, diameter of grains was increased for 9.42%. Among the all samples the largest grains are in the sample of waste foundry sand - chemical bonded after adsorption (379.00 μm). The increase is 71.99% compared to the initial state (220.36 μm) indicating that the adsorption was take place in large extent. Sediment on the sand grains increased their average size.

The percentage of Cu(II)-ions removal from solution is higher for sample of chemical bonded waste foundry sand (98.32 %) compared to this for clay bonded sample (72.94 %) probably due to simultaneously sedimentation and adsorption and assuming that in latter sample only adsorption is taken place.

Microscopical observations in this research were proved removal potential of waste foundry sand. Since the difference in initial grains size in WFS-CHB and WFS-CB samples was measured as negligible, it is not a crucial for a good adsorption. According to grain size after bonding, Cu(II)-ions removal is better with chemical bonded than clay bonded WFS.

Obtained results show that waste foundry sand is suitable for removal of Cu(II)-ions from aqueous solutions. Since there is a lack of literature data, this research will contribute to new insight of using the waste foundry sand as a quality and low-cost agent for removal of Cu(II)-ions.

References: [1] Yogesh Aggarwal et al., Constr Build Mater, 54 (2014), 210-223. [2] Anita Štrkalj et al., Chem Biochem Eng Q, 27 (2013) 1, 15-19. [2] Gunnar Nordberg et al.,Handbook of Toxicology of Metals, European Environment Agency, Copenhagen, 2005.

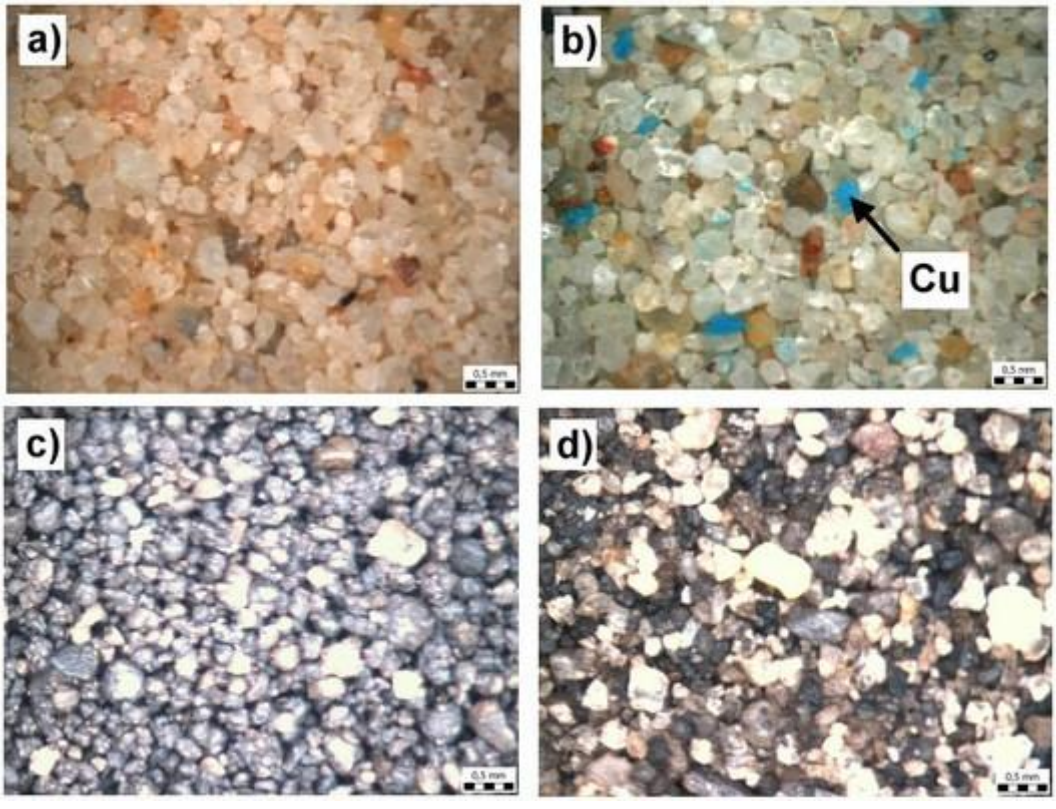

Fig. 1. Light micrograph of a) WFS-CHB, b) WFS-CHB+Cu(II)-ions, c) WFS-CB and d) WFS-CB+Cu(II)-ions

Porous yttria-stabilized zirconia for bone implants

Jelena Macan (1), Andreja Gajović (2), Marco Deluca (3), Raul Bermejo (3)

1) University of Zagreb, Faculty of Chemical Engineering and Technology, Marulićev trg 19, HR-10001 Zagreb, Croatia

2) Ruđer Bošković Institute, Bijenička 54, HR-10002 Zagreb, Croatia

3) Institut für Struktur- und Funktionskeramik, Montanuniversitaet Leoben, Peter Tunner Straße 5, A-8700 Leoben, Austria & Materials Center Leoben Forschung GmbH, Roseggerstraße 12, A-8700 Leoben, Austria

Keywords: yttria-stabilised zirconia, bone implants, strength, hardness, porosity

Zirconia is a biocompatible and hypoallergenic ceramic material with established use in implants, especially in dental medicine. In order to produce bioactive bone implants, it can be modified by application of bioactive calcium phosphate (CaP) coatings. Resulting composite ceramic implant would derive its bioactivity from the CaP coating, and mechanical and chemical stability from the zirconia scaffold. Porous zirconia stabilised with 10 wt% yttria was prepared by sol-gel process from zirconium butoxide and yttrium acetate. The resulting dry gel was sieved to particle size < 80 μm, calcined at 300 °C / 2 h and then milled at 500 rpm / 2 h. Obtained powder was uniaxially pressed (180 MPa) into tablets and sintered at 900-1400 °C / 8 h. For comparison, unpressed calcined powder was sintered in same conditions. XRD analysis has shown that zirconia crystallizes in tetragonal form, but since tetragonal and cubic zirconia structures have similar lattice parameters, Raman spectroscopy was used to distinguish the two phases and confirm the tetragonal structure of stabilised zirconia. Structure and porosity of obtained ceramics was examined by SEM (Fig. 1). Since higher sintering temperatures lead to denser ceramics, samples for mechanical characterization were sintered at 1400 °C and polished. Porosity of obtained ceramic was investigated by BET and calculated from theoretical and true density as determined by Archimedes principle. Density was determined to be 4.34 g cm^{-3}, which is 76.4 % of theoretical density. Pore volume as determined by BET was 8.80 cm^3 g^{-1}, which upon calculation gives apparent porosity of only 0.7 %. This is due to closed porosity of obtained ceramics, since only surface pores are available for adsorption/desorption during BET analysis. Hardness of the samples was measured by Vickers indentation test under two different loads, 5 and 20 kg. Vickers hardness was determined to be 3.8 ± 0.2 GPa, and true hardness 4.1 ± 0.3 GPa, for both loads. Under 5 kg load the samples showed no cracking, and a limited cracking (~450 μm total crack length for ~380 μm diagonal) at 20 kg load. Lack of cracking is an indication of material's toughness. The strength was measured using ball-on-3-balls test method on 20 samples, and the results were analysed by Weibull statistical analysis. The strength was determined to be 257.7 MPa (with 90 % confidence interval 240.00 – 277.06 MPa). Fractographic analysis of samples was performed on a stereoscopic microscope and SEM. It showed possible surface crack origins, but the analysis was difficult on most samples. Both strength and hardness are lower than expected values for zirconia due to samples' porosity, but sufficient for bone implants (bone strength ranges 4 – 24 MPa [1]).

References: 1. J. Wang et al., Bone 72 (2015) 71-80. This research was supported by Croatian-Austrian bilateral project entitled „Design, physical-chemical and mechanical characterization of innovative ceramic composites for bone implants“, and Croatian

Academy of Sciences and Arts support for project „Optimiranje priprave porozne ZrO2 keramike sol-gel postupkom“. The authors are grateful to Dr. K. Žižek for BET analysis.

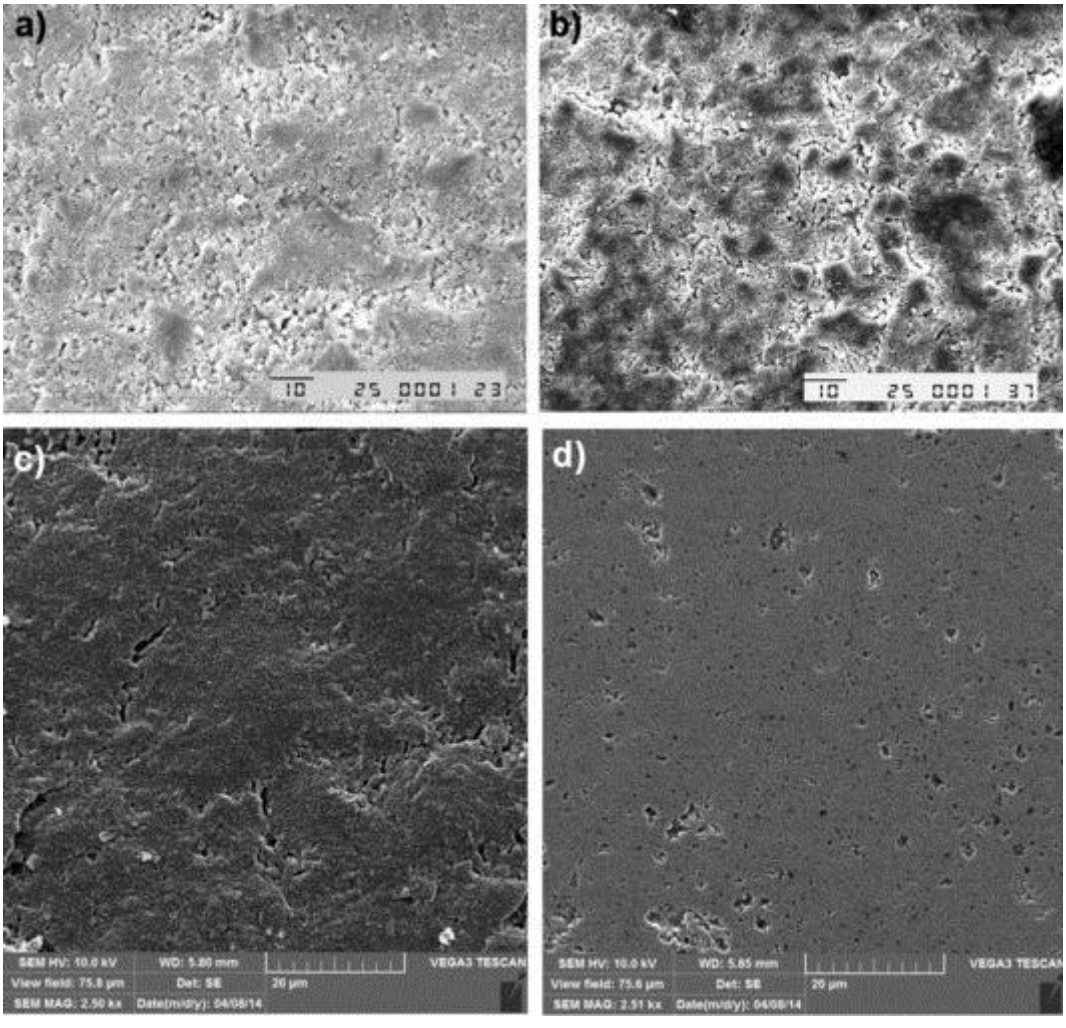

Fig. 1. SEM micrographs of zirconia tablets sintered at: a) 900 °C, b) 1200 °C and c) 1400 °C; d) polished surface of tablet sintered at 1400 °C.

POSTERS

P1 Expression pattern of phox2b, NF200 and IB4 markers in the developing human spinal ganglia

Ivana Dujmović (1), Katarina Vukojević *(2), Ivana Bočina (3), Natalija Filipović (2), Mirna Saraga-Babić (2)

1) Faculty of Philosophy, University of Split, Teslina 12, 21 000 Split, Croatia

2) School of Medicine, University of Split, Šoltanska 2, 21 000 Split, Croatia

3) Faculty of Science, University of Split, Teslina 12, 21 000 Split, Croatia

*Corresponding author: Katarina Vukojevic, Department of Anatomy, Histology and Embryology, School of Medicine, University of Split, Šoltanska 2, 21000 Split, Croatia;

Keywords: spinal ganglia, human embryo, phox2b, IB4, NF200

In this study we investigated developmental pattern of the neural crest cells towards first appearing of the neuronal subtypes in the spinal ganglia. The aim of the study was to estimate the spatial and temporal appearance of the neural crest cells in the spinal ganglia and their differentiation into neuronal subtypes. Expression of the neural crest cells and neuronal subtypes markers were studied in 10 human embryos and fetuses, ranging in age between the 5th and 10th developmental week. The differentiation of the neurons was analysed using immunohistochemistry and immunofluorescence methods on paraffin sections. Quantification of positive cells was performed counting the ratio of positive cells in the total cell number in squares of 50μm × 50μm at 40× magnifications. Data were expressed as mean ± SD and the difference between dorsal and ventral part of the spinal ganglia were analysed by the Mann-Whitney test and t-test. The phox2b marker (for early differentiated neurons) had the strongest expression in the 5/6th developmental week (73% of positive cells), gradually decreasing to 59% in the 9/10th developmental week. The number of phox2b positive cells was higher in the dorsal parts of the spinal ganglia than in the ventral parts, especially in the 7/8th week (t-test, p=0.007). First NF200 (mechanoreceptors) and IB4 positive neurons (nociceptors), appeared already in the 5/6th developmental week (9% and 7%, respectively). Their number subsequently increased to 22% and 24% in the foetal period. The number of NF200 positive cells was higher in the ventral parts of the spinal ganglia than in the dorsal parts especially during 5/6th and 9/10th developmental week (Mann-Whitney, p=0,040 and p=0,003 respectively). Our results indicate the high potential of early differentiated neuronal cells, which slightly decreased with progression of spinal ganglia differentiation. On the contrary, the number of neuronal subtypes displayed increasing differentiation at later developmental stages. The great diversity of phenotypic expression found in the spinal ganglia neurons is the result of a wide variety of influences, occurring at different stages of development in a large potential repertory present in these neurons.

References: Katarina Vukojevic et al., J. Mol. Histol.3 (2008) 339-49 Alison Hall et al., J. Neurosci., 8 (1997) 2775-84

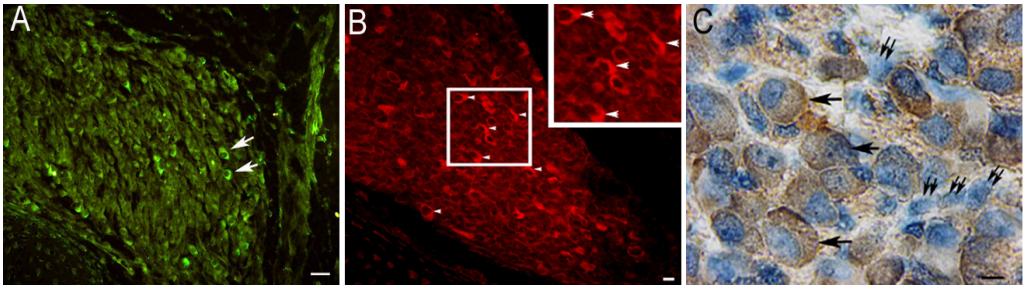

Fig.1. Transversal section through spinal ganglia in 5 and 10-week old human embryo. A NF200 positive cells (arrows). B IB4 positive cells (arrows). C Phox2b-positive (arrows) and negative cells (double arrows). Immunostaining to NF200, IB4 and phox2b. x40, x40, x100. Scale bar 10μm, 20μm,10μm.

P2 Occurrence of radiating Fe-oxides and Fe-oxyhydroxides crystal groups in the rocks of cores from the borehole Bunjani-59, Croatia.

M. Matošević (1), R. Slavković (1), N. Tomašić (2)

1) E&P Laboratory Department, Exploration Sector, Exploration & Production BD, INA – Oil Industry Plc, Lovinčićeva 4, 10000-Zagreb, Croatia

2) Division of Mineralogy and Petrology, Faculty of Science, University of Zagreb, Horvatovac 95, 10000-Zagreb, Croatia

Keywords: Fe-oxides, borehole, alteration, radiating aggregates

The borehole Bunjani-59 is located in the Sava Depression in the Republic of Croatia, drilled about 10 km SE from the city of Ivanić Grad. The deepest cored rock material from the borehole, at a depth of 715 m, is made of igneous and metamorphic rocks like granites, gneisses and schists which belong to the crystalline basement of the Pannonian Basin. In addition to the major minerals such as quartz and feldspar, the bedrock is also made of iron-rich minerals like biotite, amphibole belonging to the hornblende group, chlorite, cordierite, pyrite and magnetite. The igneous and metamorphic rocks continue vertically in shallow intervals of the borehole in the form of drifted and subsequently processed gravel fragments of rocks, separate sand grains, and minerals in younger sediments like conglomerates, gravelly sandstones and sandstones from 681 to 615 m in depth. By macroscopic examination of cores, reddish, brownish-red and yellow blotchy parts of rocks that occur along the continuously cored intervals of the borehole were observed. With a more detailed study of the rocks, by using the polarizing microscopes Olympus BX51 and Zeiss Axiolab, as well as a scanning electron microscope JEOL JSM-6510 LV, a presence of hematite and goethite was confirmed in these blotchy areas. These are formations of Fe-oxides and Fe-oxyhydroxides in the form of massive earthy coatings and globular clusters and in particular, in the form of the subhedral to euhedral crystals radially arranged like blades and needles. Such different aggregates fill up fractures within the minerals, the interstices among the grains within the gravelly and sandy rock fragments of the basement, and they permeate together with clay minerals within the matrix. The microcrystalline radiating occurrences of hematite and goethite are generally observed directly related to the minerals such as biotite, chlorite, chloritized biotite and hornblende, and are located on the surface of minerals, especially on planes {001} of mica and chlorite (Fig. 1a). The individual crystals as blades and needles have a length of 2 to 15 μm, while they are 0.30 to 1.25 μm in width (Fig. 1b). They often form snowflake forms. The occurrence of Fe-oxides and Fe-oxyhydroxides is a result of the subsequent chemical changes in the environment caused by weathering of primary rocks and alteration of iron-rich minerals (1) of the crystalline basement of the Pannonian Basin. Their exposure to the air in the zone of weathering crust, i.e. the action of meteoric water, leads to oxidation and leaching of metals (Fe ions) from the rock. Further water fluctuations in eroded and drifted rocks, formed soils and sediments deposited away from their source material, that are found in shallower intervals of the borehole, favor the acidity changes of the environment and additional transitions of hematite to goethite and vice versa.

References: 1. Goss, C.J. (1987), Mineral. Mag., 51, 437-51

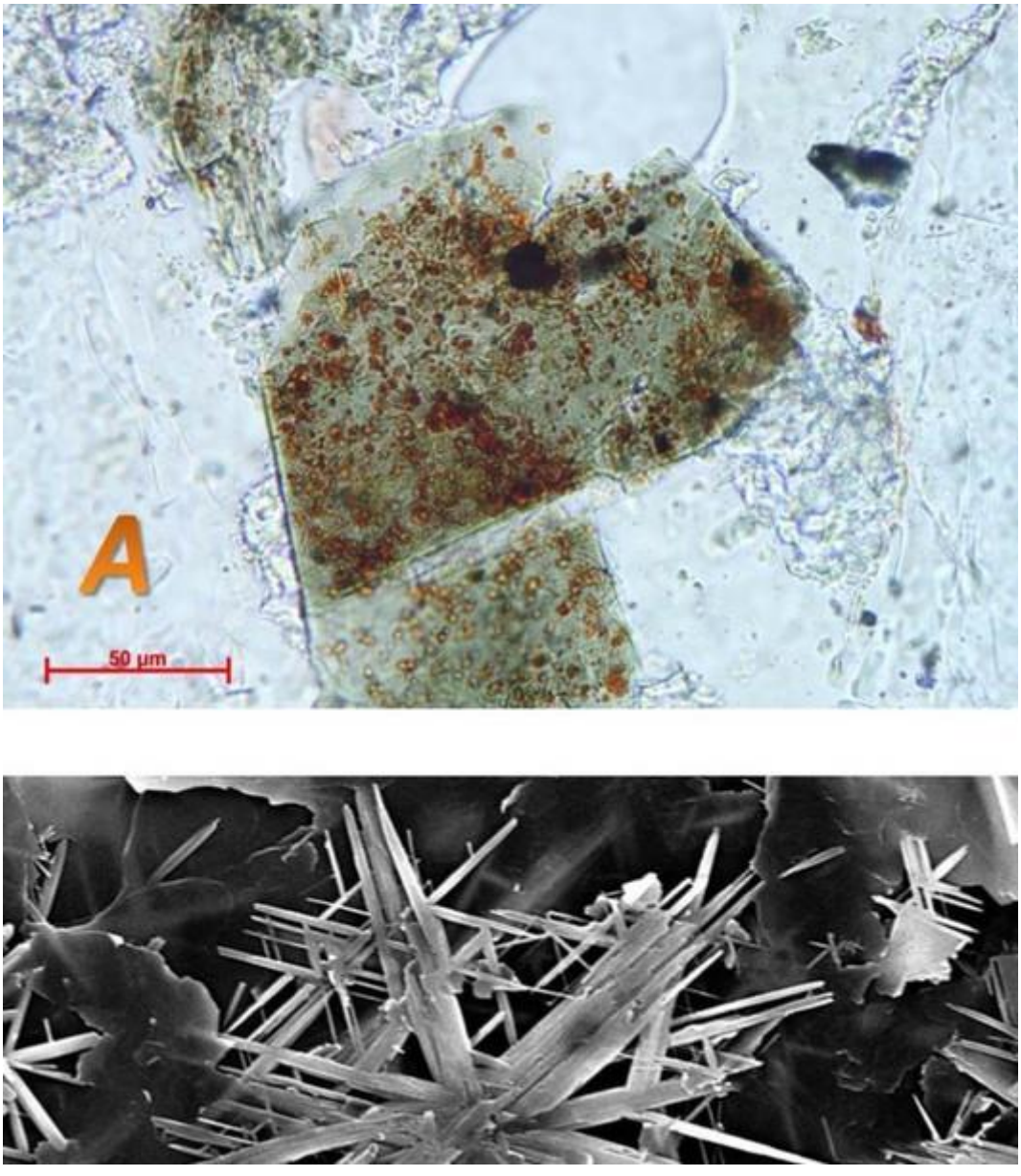

Fig. 1. Occurrence of Fe-oxides in the borehole rock samples: a) hematite aggregates on chlorite flakes observed by polarizing microscope, b) SEM image of the acicular Fe-oxide crystal aggregates.

P3 Determination of normal glomerular basement membrane thickness at Department of Pathology and Cytology, Dubrava University Hospital, Zagreb

P. Šenjug (1), A. Krištić (1), A. Bauer Šegvić (1), S. Bulimbašić (1), D. Galešić Ljubanović (2)

1) Department of Pathology and Cytology, Dubrava University Hospital, Zagreb

2) Department of Pathology and Cytology, Dubrava University Hospital, Zagreb, Institute of Pathology, School of Medicine, University of Zagreb, Zagreb

Keywords: kidney, electron microscopy, glomerular basement membrane, GBMN thickness

Electron microscopy (EM), along with light microscopy and immunofluorescent analysis, represents key method in renal biopsy specimen analysis. EM is crucial for diagnosing disorders that directly influence structure of glomerular basement membrane (GBM) such as Alport's syndrome (AS), thin glomerular basement membrane nephropathy (TBMN) and diabetic nephropathy. Thickness of GBM depends on multiple factors. It is age and sex dependent, but it is also influenced by methodology of tissue preparation and processing. Referential span of normal GBM thickness varies in different centers of proficiency and in multiple research papers. Following previously mentioned, many authors emphasize need for referential span of normal GBM thickness for each laboratory.[1,2] Orthogonal intercept/mean harmonic thickness measurement is considered the most precise method of GBM thickness measurement. Due to complexity of described method, most frequently used is alternative method of direct measurement of GBM thickness. In this research we have applied modification of the direct measurement / arithmetic mean method to measure GBM thickness in Laboratory for Nephropathology and Electron Microscopy at Dubrava University Hospital, Zagreb. Digital EM photographies with magnification of 4000-8000x were selected from our database of EM pictures of kidney biopsy samples. Pictures were taken on multiple capillaries from 1-3 glomeruli. A total of 30 GBM measurements were taken on 10 randomly selected capillaries to determine an average GBM thickness for each biopsy. Position of measurements in capillary loops were determined similarly as described by Haas.[1] Direct measurements were made using iTEM software (Olympus Soft Imaging Solutions GmbH), with digital zoom of 150-400% to measure the distance between the endothelial and podocyte plasma membranes. Using this method we obtained mean ±SD values for the normal GBM thickness of adult males and females of 340±36 nm and 301±44 nm. These values were based on average GBM thickness for each of 23 males and 22 females, aged from 19 to 84 years, with minimal change nephropathy, acute interstitial nephritis, normal renal parenchyma or acute tubular injury. Exclusion criteria were hematuria and diabetes mellitus. We defined normal ranges for each gender (268-412 nm for males, 213-389 for females), as being within 2 SD of these means. With this research we have standardized method for GBM thickness measurement for Laboratory for Nephropathology and Electron Microscopy at Dubrava University Hospital and defined referential span of normal GBM thickness for our laboratory. Our research results are crucial for more accurate diagnosis of disorders characterized with structural changes of GBM such as AS and TBMN.

References: 1. M. Haas, Arch Pathol Lab Med, 133 (2009) 224-232. 2. K. Tryggvason, J. Patrakka, J Am Soc Nephrol, 17 (2006) 813-822.

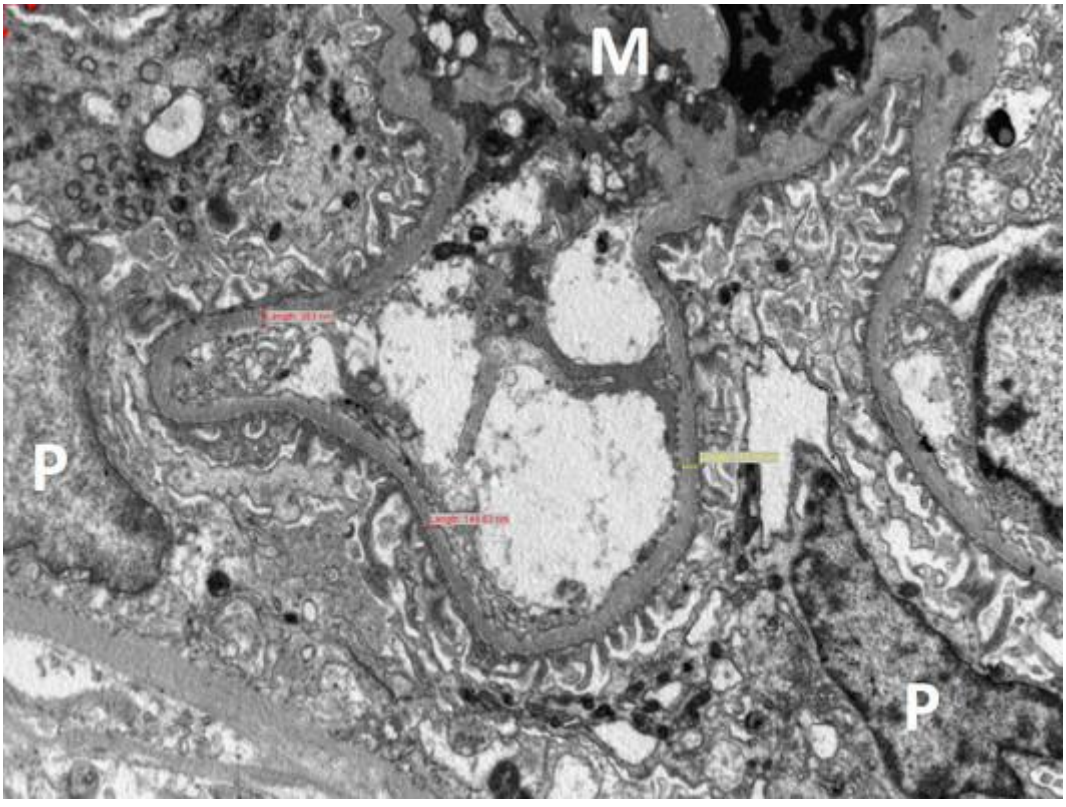

Fig. 1. Full glomerular capillary loop with mesangium (M), 3 measurements of GBM thickness and podocytes (P). Magnification x8000.

P4 Phytoplankton cells as seen under the light microscope

Mia Bužančić (1)

1) Institute of Oceanography and Fisheries, Šetalište I. Meštrovića 63, 21000 Split, Croatia

Keywords: Light microscopy, Epifluorescence, Lugol's iodine, Formaldehyde

Microscope counting of the cells requires fixation and available techniques for optimal preservation and enumeration of nano- and microplankton are taxon specific. The most widely used fixatives for phytoplankton are formaldehyde and potassium iodide plus iodine known as Lugol's iodine solution. In addition, many phytoplankton species are partially transparent or cryptic when viewed under the light microscope, so different techniques are needed to improve contrast or to highlight important features of the certain taxons.

The light microscopy

Lugol's iodine is a widely used fixative and is commonly recommended for preserving ciliates and flagellates. The advantage of Lugol's iodine solution is that it has an instant effect and increases the weight of the organisms reducing sedimentation time. However, it has been shown to introduce artifacts, including changes in cell size and shape, reduction in the abundance of detected cells, especially nanoplankton fractions. Furthermore, it can stain the cells and give them an unnatural color that makes them more difficult to identify, or a failure to preserve certain taxa. Samples preserved in Lugol's iodine should be kept in the dark and checked periodically for light tea coloration, adding more fixative if needed. If samples are stored for long periods, they should be preserved with neutral formaldehyde, which keeps samples viable for a long time. **Formaldehyde** is a good fixing and preserving agent for most species, except the "naked" flagellates because some naked algal forms may disintegrate, or the cell shape is distorted and flagella are lost. In addition, the cell content is bleached, making it very difficult to distinguish between pigmented and non-pigmented cells. Formaldehyde is suitable for preserving algae with a more rigid cell wall, as it keeps cell wall structures and other characteristics like eye spots remain visible for a long time.

The epifluorescence microscopy

Autofluorescence of the phytoplankton can easily be detected by epifluorescence microscopy, an effective method to enhance detection and identification of certain organisms. In formalin fixed samples, autofluorescence in the phytoplankton cells is obtained from photosynthetic and other pigments and can be used to differentiate between heterotrophic and autotrophic organisms, or to significantly facilitate the identification of phytoplankton to the species level. Epifluorescence is especially important among dinoflagellates and euglenids, in which both phototrophic and obligate heterotrophic genera/species are present. Phycobilins of cyanobacteria, rhodophytes and cryptophytes have a special autofluorescence, thus this method is particularly suited to detect and count cryptophytes and small coccoid cyanobacteria. Epifluorescence microscopy is significantly helpful in taxonomy, by adding a specific stain to the sample that causes cellulose to fluoresce. **Calcofluor** is a specific stain, which acts by binding to the cellulose theca in armored organisms and allows a detailed examination of the plate structure and sutures. The stain does not dye structures in most other pelagic organisms

including the diatoms therefore, it can help to enhance counting effort and identification of other organisms like armored dinoflagellates. Staining will give dinoflagellate theca a clear intensive blue epifluorescence including the sutures of the plates, making it easy to recognize the thecal plates of taxonomic importance, thereby facilitating the taxonomic identification to species level. That cannot always be done by the Utermöhl method using formaldehyde or Lugol's iodine preservation. It is also important to monitor the pH in samples, as the intensity of epifluorescence is pH dependent and in acidic samples, epifluorescence is absent or poor.

The images in this poster presentation will show the difference between formalin preservant and Lugol's solution on phytoplankton cells under the light microscopy. Some typical phytoplankton species of Adriatic coastal waters will be presented and the comparison of the same phytoplankton cells will be done on the images under the bright field and epifluorescence.

References: 1. Intergovernmental Oceanographic Commission of ©UNESCO. 2010. Karlson, B., Cusack, C. and Bresnan, E. (editors). Microscopic and molecular methods for quantitative phytoplankton analysis. Paris, UNESCO. (IOC Manuals and Guides, no. 55.) (IOC/2010/MG/55) 110 pages. 2. Fritz, L., Triemer, RE 1985. A rapid simple technique using calcofluor White M2R for the study of dinoflagellate thecal plates. J. Phycol. 21: 662-664.

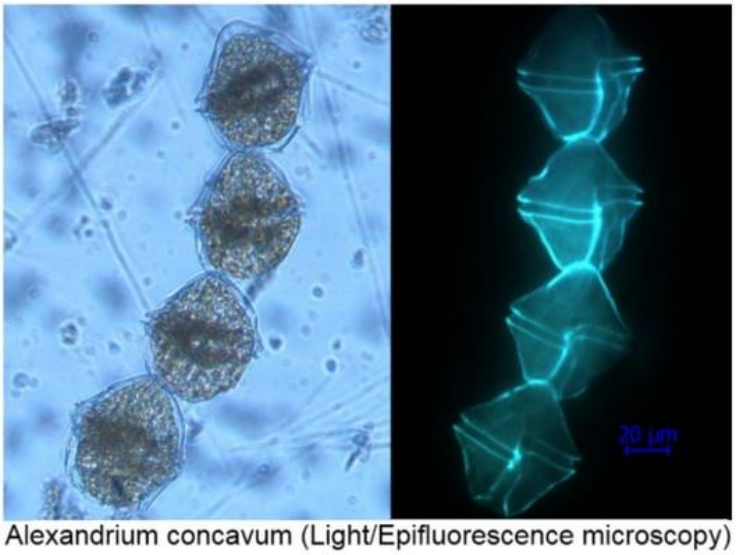

Alexandrium concavum (Light/Epifluorescence microscopy)

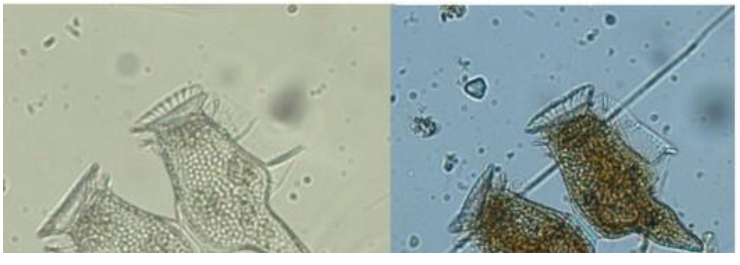

Fig 1. Phytoplankton cells as seen under the light microscope

P5 Lost without the host: isolated endosymbiotic algae in a toxic environment

Goran Kovačević (1), Martina Ivšić (2)

1) Faculty of Science, University of Zagreb, Department of Biology, Division of Zoology, Rooseveltov trg 6, HR-10000 Zagreb, Croatia

2) Vidrićeva 32, HR-10000 Zagreb, Croatia

Keywords: isolated endosymbiotic algae, green hydra, Chlorella test, morphometry, iron

Symbiosis is ubiquitous in terrestrial, freshwater and marine communities. It has played a key role in the emergence of major life forms on Earth and in the generation of biological diversity (Moran 2006). As microalgae are significant as primary producers in aquatic ecosystems and are the basis of many food chains it is important to understand the processes that can enable them better survival in a potentially toxic environment.

The aim of this work was to research advantages and disadvantages of forming a symbiotic relationship - in this research of photoautotrophic endosymbiotic algae and green hydra host. Comparative toxicity test of iron (iron dextran) was performed on endosymbiotic algae isolated from green hydra, species *Desmodesmus subspicatus* (Chodat) Hegewald and Schmidt and *Mychonastes homosphaera* (Skuja) Kalina and Punčochářová (*Chlorella zagrebiensis* group Kovac. and Jelen.) and on related free-living species *Chlorella kessleri* Fott and Novak. [K&H, 1992] strain LARG/1 and *Chlorella vulgaris* Beij. [K&H, 1992] strain SAG 211 - 11b in three concentrations (1 mg Fe/L H_2O, 400 mg Fe/L H_2O and 1400 mg Fe/L H_2O) compared with control samples (Kovačević et al. 2010).

Six tubes per concentration and control sample for each species of algae were used. The experiment was performed in duplicate. The results were observed macroscopically in tubes during 21 days as well as microscopically in relation to many parameters: cell viability, division and shape, and size of cells, chloroplasts and nuclei, the level of damage, intensity of green colour of cells in relation to the concentrations of the toxicant and evaluated by the use of Chlorella test (Kovačević et al. 2008), light microscopy and morphometry. Light microscope Nikon Eclipse E600 was used in the experiment and micrographs were made by digital camera Nikon DXM1200. Preliminary results showed that higher concentrations of iron caused higher rate of mortality, which was visible as a formation of white dotted clusters of dying cells in tubes, described as “dried cells”. Morphological observations showed that at higher concentrations of iron (Figure 1) all algal species had bleached cells, growth inhibition and cell enlargement. However, the divisions were unfinished and the cells deformed. It was found that the free-living algal species were less sensitive to the toxic effect of iron than the isolated endosymbiotic algae from green hydra. The research revealed that isolated algal species *Mychonastes homosphera* proved to be better adapted to a toxic environment than isolated algae species *Desmodesmus subspicatus*.

The isolated endosymbiotic algae from green hydra host appeared to be less adapted to unfavourable microenvironmental conditions than their free-living relatives. Symbiosis of algae and green hydra could present the best way for these algae to survive extreme situations in the environment and after having lost that advantage they become more vulnerable.

References: 1. Kovačević G. et al., Folia. Biol. (Kraków) 58/1-2 (2010) 57-63. 2. Kovačević G. et al., Period. Biol. 110/4 (2008) 373-374. 3. Moran N.A., Curr. Biol. 16 (2006) 866-871.

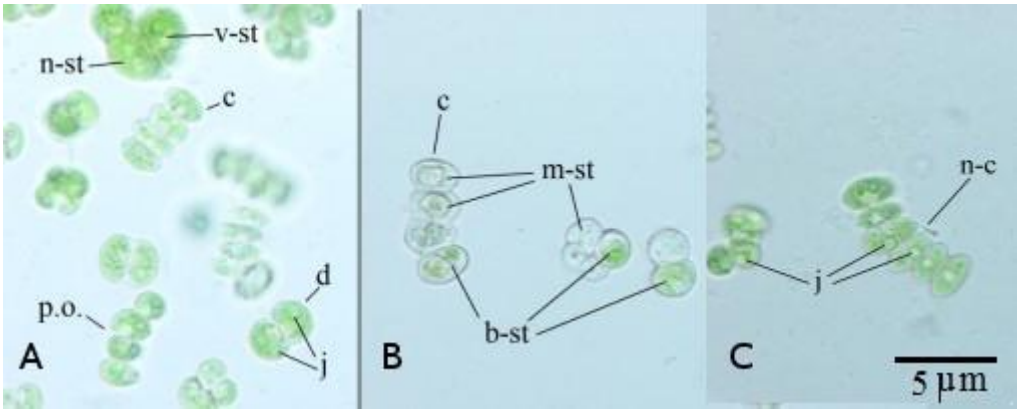

Fig. 1. Desmodesmus subspicatus. Control (A). The highest concentration of iron (B, C). Regular cell (n-st), enlarged cell (v-st), regular forms (c, p.o.), division (d), nuclei (j), bleached cell (b-st), dead cell (m-st), irregular forms (n-c).

P6 Structural studies of biomineralization in the sea hare aplysia punctata by electron microscopy and diffraction

A M Tonejc (1), D Medaković (2), S Popović (1), A Jaklin (2)

1) Faculty of Science, Dept. of Physics, Bijenička 32, 10000 Zagreb, Croatia

2) Center for Marine Research, Ruđer Bošković Institute, G. Paliaga 5, Rovinj, Croatia

Keywords: HRTEM, SAED, ESEM, EDS, biomineralization

X-ray diffraction (XRD), transmission electron microscopy (TEM), selected area electron diffraction (SAED), high resolution transmission electron microscopy (HRTEM), environmental scanning electron microscopy (ESEM) and energy dispersive X-ray analysis (EDS) were used in study of starting biomineralization processes in embryos of the sea hare species Aplysia punctata. 10 days old embryos (sample C4) appeared amorphous according to XRD patterns. TEM of the same sample showed that first grains of nanocrystalline dolomite began to form in the amorphous area. The identification of dolomite was confirmed according to TEM dark field images and SAED (Fig. 1.). SAED was taken with (104) diffraction spot of dolomite, D. Grains of dolomite have sizes about 10 nm. In Fig. 1. corresponding SAED pattern shows that the strongest diffraction spots of dolomite D(104) form nanocrystalline diffraction ring. In HRTEM (Fig. 2.) the lattice fringes of dolomite D(104), spacing d_{104} =0.289 nm, and aragonite A(110), spacing d_{110} = 0.421 nm, are marked. In Fig. 2. the corresponding SAED pattern in [010] D orientation of dolomite from an area 100x100 nm^2 is shown. In further development stages of the embryos very faint aragonite rings became visible by SAED (Ref. 1.). It was shown that the biomineralization process in Aplysia punctata started by formation of the dolomite nanograins which served as centers of crystallization for further aragonite deposition in the larval shell. The accepted theory dealing with the starting biomineralization in marine invertebrates is based on the fact that, during the embryonic development, amorphous calcium carbonate (ACC) precedes the first crystal formation, thus ACC being the precursor phase for further mineralization of the skeleton (Ref. 2.). In the present study we have used the combination of biological and instrumental methods with an aim to register and describe the formation of the first biominerals in the marine gastropod Aplysia punctata (Cuvier, 1803). ESEM with energy dispersive X-ray analysis (EDS) was used in order to find appearance of crystallographic phases in the particular periods of growth and development of Aplysia punctata, found in adult shells by X-ray diffraction (Ref. 1.). The idea of the combined ESEM and EDS investigation was to observe the beginning of appearance of calcium and magnesium as constituents of crystallographic phases observed in embryo in the early phases of shell morphology formation. Magnesium, the constitutive element of dolomite, was observed in a very small amount in sample C4 (Fig. 3. 7b) before the appearance of calcium. That confirms the results obtained by HRTEM and SAED that dolomite is the first crystalline phase in Aplysia punctata embryos precipitated from amorphous calcium carbonate. Also, these results are in accordance with the general model of initial biomineralization processes referred to in the relevant literature (Refs. 2. and 3.).

References: 1. Anđelka Tonejc et al., Croat. Chem. Acta 87 (2014) 143-152. 2. Ingrid Maria Weiss et al., J. Exp. Zool. 293 (2002) 478-491. 3. Lia Addadi et al., Chem. Eur. J. 12 (2006) 980-987.

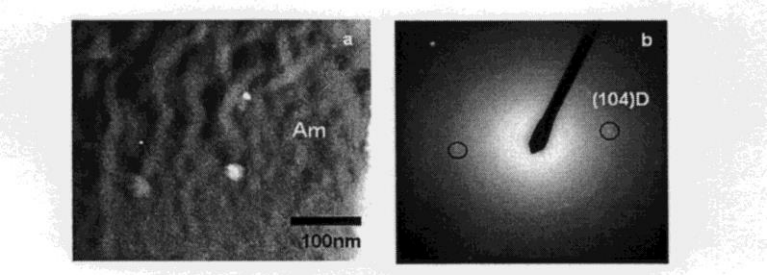

Figure 1.

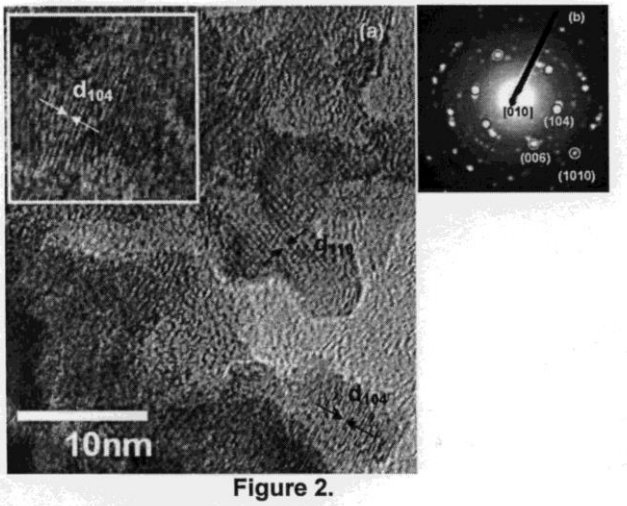

Figure 2.

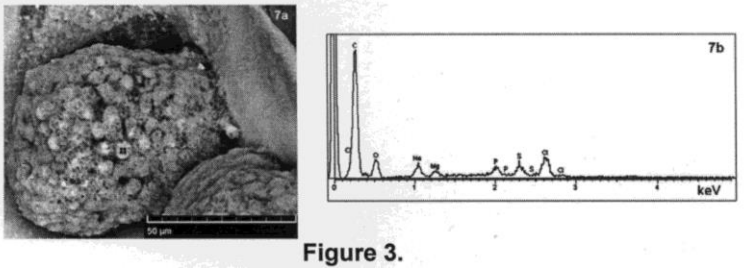

Figure 3.

Fig.. 1., 2., and 3. represent 10 days old embryos of sea hare Aplysia punctate examined by DF, SAED, HRTEM, ESEM and EDS showing initial biomineralization process.

P7 Monograph „Electron Microscopy in Croatia”

D. Bauman (1), S. Gajović (2)

1) Croatian Microscopy Society, Šalata 12, 10000 Zagreb, Croatia

2) School of Medicine, University of Zagreb, Šalata 3, 10000 Zagreb, Croatia

Keywords: monograph, electron microscopy, technological development

Electron microscopy is an example of superior technology whose implementation laid the groundwork for development of science in Croatia. It has been 59 years since the first electron microscope in Croatia was bought and installed at the Ruđer Bošković Institute in Zagreb, and 36 years since the first scanning electron microscope in Croatia was obtained at the “Željezara Sisak” Institute of Metallurgy in Sisak. Landmark events in the development of electron microscopy in Croatia are depicted in Monograph „Electron Microscopy in Croatia”. The concept and the content of this Monograph allow one to travel through time by presenting written and pictorial documents related to the development of electron microscopy in Croatia based on the words and memories of eminent experts in this field, doyens of Croatian microscopy scene. Written in an approachable way, this Monograph is expected to become an educational tool for students, future engineers, researchers and scientists.

P8 Single-stranded DNA binding protein has a key role in chromosome segregation during sporulation of Streptomyces coelicolor

T. Paradžik (1), Ž. Filić (1), N. Ivić (2), A. Bielen (3), B. Manjasetty (4), P. Herron (5), D. Jakimowicz (6), M. Luić (2), D. Vujaklija (1)

1) Division of Molecular Biology, Ruđer Bošković Institute, Bijenička 54, 10 000 Zagreb, Croatia

2) Division of Physical Chemistry, Ruđer Bošković Institute, Bijenička 54, 10 000 Zagreb, Croatia

3) Department of Biochemical Engineering, Faculty of Food Technology and Biotechnology, Pierottijeva 6, 10 000 Zagreb, Croatia

4) European Molecular Biology Laboratory, Grenoble Outstation and Unit of Virus Host-Cell Interactions, UJF-EMBL-CNRS, Grenoble CEDEX 9, 3265, France

5) Strathclyde Institute of Pharmacy and Biomedical Sciences, University of Strathclyde, 161 Cathedral Street, Glasgow G4 0RE, UK

6) Department of Molecular Microbiology, University of Wroclaw, Joliot Curie 14A, 50-383 Wroclaw, Poland

Keywords: Streptomyces coelicolor, SSB protein, chromosome segregation

Single stranded DNA binding proteins (SSB) proteins are essential in all domains of life. These proteins bind ssDNA with a high affinity and in a sequence independent manner. Thus SSB proteins protect transiently formed ssDNA during DNA replication, recombination and repair and prevent formation of unproductive secondary structures. In addition, SSB proteins interact and modulate the functions of various proteins involved in all aspects of DNA metabolism. Our recent analysis of all available bacterial genomes revealed the presence of multiple copies of SSB proteins in many bacteria indicating that evolution of these proteins in Eubacteria is highly dynamic. However, the role of duplicated SSB proteins is poorly studied. We have selected multicellular prokaryote, bacterium *Streptomyces coelicolor* with mycelial life style which also possesses two SSBs, as a good model system to study biological role(s) of paralogous SSB proteins. Differential regulation of paralogous *ssb* genes in *S. coelicolor* also suggested that their products have different biological roles. Expression of *ssbA* is constant and high during life cycle, decreasing towards late stationary phase, while the expression of *ssbB* is at all-time low. In minimal medium the *ssbB* is significantly upregulated. Promoters for both genes are determined. Surprisingly, promoter of *ssbB* possesses unusual features and is active in taxonomically distant *Escherichia coli*. Results of the gene disruptions strongly indicated that SsbA is essential for survival while SsbB is important during the sporulation process. To get a better insight into the biological role of SsbB and the complex mechanism of cell division in *Streptomyces* we have constructed double (*ssbBparB; ssbBsmc)* and triple (*ssbBparBsmc*) mutant strains carrying mutations in *ssbB* gene and in the genes reported previously to be important for the chromosomal segregation. By fluorescence microscopy we examined the effect of these mutations on chromosome segregation during reproductive phase of *S. coelicolor.*

P9 Morphology investigation of electrospun nanostructured composites and metal oxides

Marijan Marciuš (1), Mira Ristić (1), Željka Petrović (1), Svetozar Musić (1)

1) Ruđer Bošković Institute, Bijenička 54, 10000 Zagreb, Croatia

Keywords: NiO, ZnO, RuO2, electrospinning, nonfibers

In the past several decades nanostructured materials have become a cornerstone of modern high-tech industry, wherein not only their chemical composition, but also their size, shape and structure at the microscopic level have become increasingly important. Regardless of application, size and morphology of these nanomaterials have led to a discovery of their astonishing new chemical and physical properties, fueling the development of vast modern synthesis methods. Electrospinning is one such method that enables production of down to a few *nm* thin nanofiber materials from a viscous solution. Delicate experimental conditions which include electrostatic field configuration and atmospheric conditions, as well as solution properties such as composition, density, surface tension, conductivity and viscosity represent key elements for a successful synthesis of desired nanostructured fiber materials. In order to confirm the size and morphology of synthesized materials, as well as consistency of electrospinning process, scanning electron microscopy (SEM) has proven to be irreplaceable imaging characterization method combined with EDS spectroscopy. Nanofibers containing metal oxides are usually electrospun as composite materials in combination with polymer materials, and therefore require a thermal postprocessing treatment in order to get pure metal oxide nanostructures. In present works influence of experimental conditions on synthesis of three metal oxide composites was investigated. Nickel oxide (NiO) due to its specific electro-chromic, thermoelectric and semiconductor properties presents a very challenging industrial material. Additional, NiO is antiferromagnetic material at room temperature, but at relatively low Neél temperature of 523 K exhibits a transition to a paramagnetic state. In contrast, pure Nickel is strong ferromagnetic material which exhibits transition to a paramagnetic state at 627 K (Currie temperature). Ni/NiO composite was prepared from viscous solutions containing nickel nitrate ($Ni(NO_3)_2$), polyvinylpyrrolidone (PVP), ethanol (C_2H_5OH), and H_2O. At a lower $Ni(NO_3)_2$ concentration, a porous microstructure consisting of interconnected fibers was obtained, whereas at a higher $Ni(NO_3)_2$ concentration, a laminar microstructure was obtained. In a similar experiment, composite nanofibers were prepared by electrospinning from a solution containing ruthenium nitrosyl nitrate ($RuNO(NO_3)_3$), PVP and C_2H_5OH/H_2O, whereas depending on concentration of $RuNO(NO_3)_3$ ribon-like fibers were produced. The surface of ribbon-like RuO_2/Ru fibers, remaining upon calcination, showed a porous nano/microstructure. For preparation of long composite zinc based nanofibers, a viscous solution containing PVP, zinc acetate and C_2H_5OH/H_2O mixture was used. Nanofibers upon calcination at high temperature transformed into zinc oxide (ZnO) nanoparticles retaining original nanofiber structure. ZnO is extremely versatile industrial material being used as additive in production of ceramics, glass, cement, pigments, even in food industries, as well as in production of semiconductor devices and various gas sensors.

References: 1. Ristić, M., Marciuš, M., Petrović, Ž., Ivanda, M., Musić, S. (2014). The influence of experimental conditions on the formation of ZnO fibers by electrospinning. Croatica Chemica Acta, 87(4), 315-320. 2. Ristić, M., Marciuš, M., Petrović, Ž., Musić, S. (2014). Dependence of NiO microstructure on the electrospinning conditions. Ceramics International, 40(7 PART A), 10119-10123. 3. Ristić, M., Marciuš, M., Petrović, Ž., Ivanda, M., Musić, S. (2015). Formation and characterization of ribbon-like RuO2/Ru fibers. Mat. Lett, submitted.

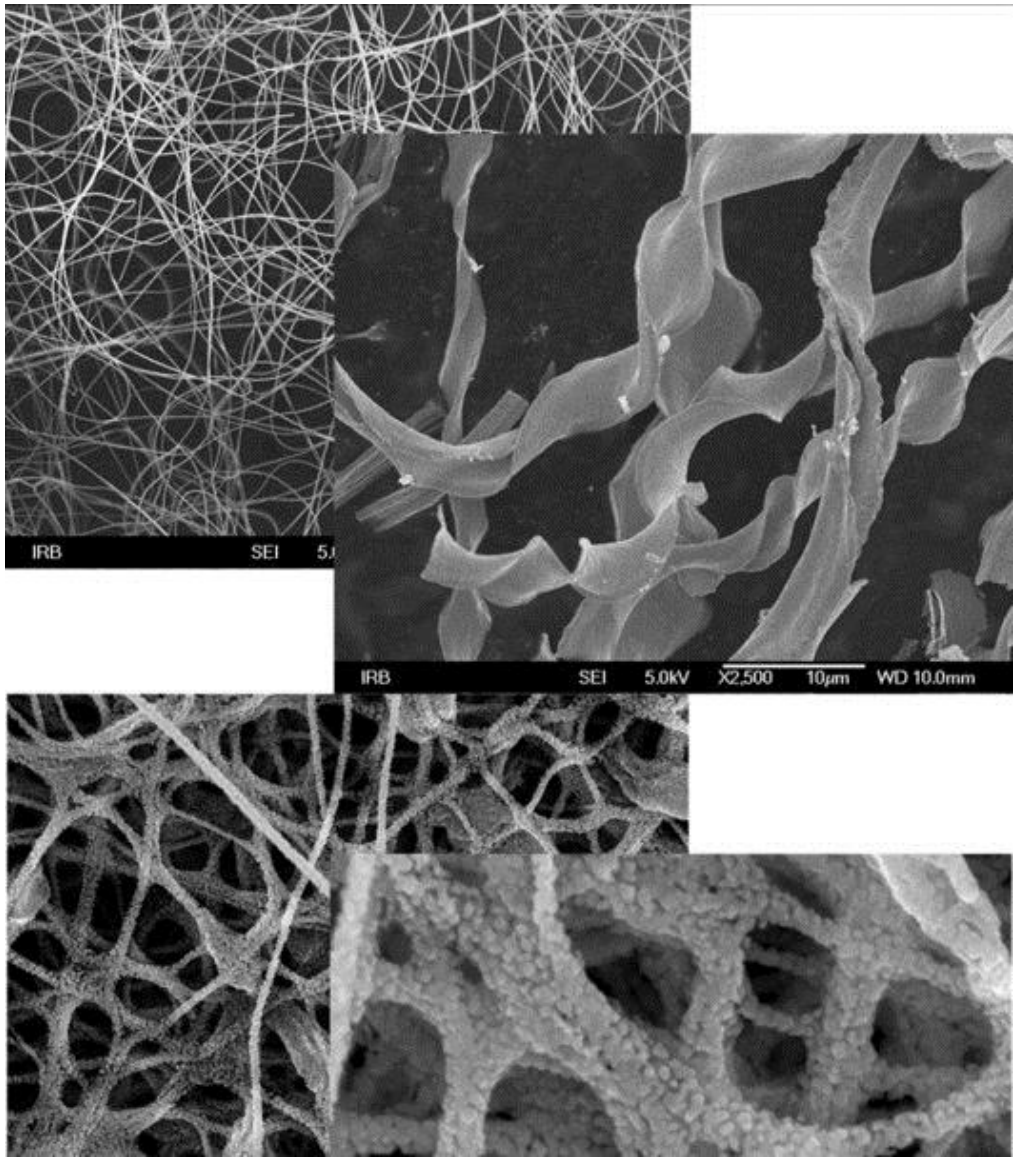

Fig. 1. FE-SEM images of nanofibers produced by electrospinning

P10 The fabrication of ZnO microrods on monolayer graphene and their photocatalytic application

Jincheng Fan (1), Tengfei Li (2), Heng Hang (3), Berislav Marković (4), Igor Djerdj (5)

1) Ruđer Bošković Institute, Bijenička 54, 10000 Zagreb, Croatia

2) School of Materials Science and Engineering, Anhui University of Technology, Maanshan 243002,China.

3) Center for Analysis and Testing, Nanjing Normal University, Nanjing 210097, China.Department of Physics, Nanjing Normal University, Nanjing 210097, China.

4) Department of Chemistry, University of Osijek, Cara Hadrijana 8A, HR-31000 Osijek, Croatia.

5) Ruđer Bošković Institute, Bijenička 54, 10000 Zagreb, Croatia

Keywords: ZnO microrods; rhodamine B; photocatalysis

Zinc oxide microrods were fabricated on graphene/SiO_2/Si substrate by a simple hydrothermal route. The obtained products were characterized using X-ray powder diffraction, scanning electron microscopy, energy dispersive X-ray spectrometry, photoluminescence and UV–visible spectrometry. Microrods exhibits hexagonal wurzite structure. Some ZnO clusters and twinned ZnO structures were found spread on the microrod array layer. The formation mechanism of ZnO microrods is discussed, emphasizing the formation mechanism of isolated clusters and twinned ZnO structures. Furthermore, microrods demonstrated a good photocatalytic performance towards rhodamine B degradation as ascribed to oxygen vacancies and interstitials considered as the photocatalytical active sites.

P11 Elucidation of NR – Filler Interactions in aqueous condition by Multi-Modal Microscopy

A.J. Chan (1), K. Steenkeste (1), M. Eloy (2), A. Canette (3), F. Gaboriaud (2), M.P. Fontaine-Aupart (1)

1) Institut des Sciences Moléculaires d'Orsay (ISMO), CNRS, Université Paris-sud, Orsay-Cedex, France

2) Michelin, 23 Place des Carmes, Clermont-Ferrand Cedex 9, France

3) Micalis, UMR 1319, INRA AgroParisTech, Massy, France

Keywords: Natural rubber latex, Silica, Rubber – filler interaction, Confocal microscopy

Natural rubber (NR) is an indispensable raw material used in manufacturing of over 40,000 products in various industrial sectors. Primarily due to its excellent physical properties such as elasticity, resilience, flexibility, mechanical strength, and renewability that cannot be easily mimicked by synthetically produced polymers. However, NR is seldom used in its raw state because it needs to be reinforced with particulate fillers to further improve its physical strengths and processability necessary for most applications. Two of the most widely used fillers nowadays are carbon black and silica.

Natural rubber reinforcement has been the research focus for decades, yet the fundamental nature of reinforcement is still not satisfactorily explained. It is however, generally accepted that this phenomenon is largely dependent on NR particle – filler interaction and filler dispersion in the rubber matrix. Several techniques exist in mixing and dispersing NR particles and filler e.g. conventional solid/melt mixing and an alternative approach liquid mixing that is anticipated to provide better filler dispersion. However, the microscopic mechanisms involving interactions between the NR particles and the fillers in liquid blending are still unknown and literature available is very limited.

In this context, properties pertaining to the filler such as charge and surface activity, composition of the solution (ion valence and ionic strength) and NR particle properties were investigated in aqueous condition to describe the mechanism behind the NR particle – filler interaction and visualize the resulting structure. The originality of our approach was to use combined methods of fluorescence correlation spectroscopy, fluorescence intensity imaging and transmission electron microscopies to elucidate the NR-filler interaction

References: 1. S.S. Sarkawi et. al., (2014), Eur. Polym. J., 54, 118-127. 2. K. Cornish, Nat. Pod. Rep., (2001), 18, 182-189. 3. A. Bridier et. al., (2011), Adv. Exp. Med. Biol., 715, 333-349.

P12 Direct observation of graphene growth and associated substrate dynamics by in situ scanning electron microscopy

Zhu-Jun Wang (1)

1) Fritz-Haber-Institut der Max-Planck-Gesellschaft, Faradayweg 4-6, 14195 Berlin, Germany

Keywords: In situ, Graphene growth, Electron microscopy, Catalysis

Most promising approaches for industrial scale production of graphene are based on metal catalysed chemical vapour deposition (CVD). Although improvements in graphene quality and yield have been achieved, there remains a lack in the mechanistic understanding of graphene formation. This lack of understanding is due to the fact that most insights on graphene growth have been derived from post growth characterizations, which are in principle incapable of capturing the dynamics of a CVD process. As we have learned from heterogeneous catalysis, a mechanistic insight can (in most cases) only be obtained on the basis of in-situ techniques that are capable of capturing the interaction of the catalyst with the environment while the product is formed. Here we report on in-situ graphene growth on nickel, copper and platinum catalysts inside a modified environmental scanning electron microscope. Using this method, we are able to visually follow the complete CVD process involving substrate annealing, graphene nucleation and growth and finally, substrate cooling. Due to the high sensitivity of the secondary electron signal to changes at the surface, we are able to visualize the formation and growth of single atom thick graphene sheets. The in-situ experiments presented here reveal the dynamic nature of the process in an unparalleled way and provide important insights on the growth kinetics and the substrate-film interactions at the micron to nanometer scale (Figure 1). In the case of growth on nickel, temperature and atmosphere induced dissolution and precipitation dynamics can be observed. For the case of copper, it is found that graphene growth.

The nucleation and growth behaviour will be discussed and the influence of grain dependent surface dynamics presented. Furthermore, we show that graphene induced copper surface reconstructions occur during cooling.above 850°C occurs on a pre-melted, highly mobile surface.

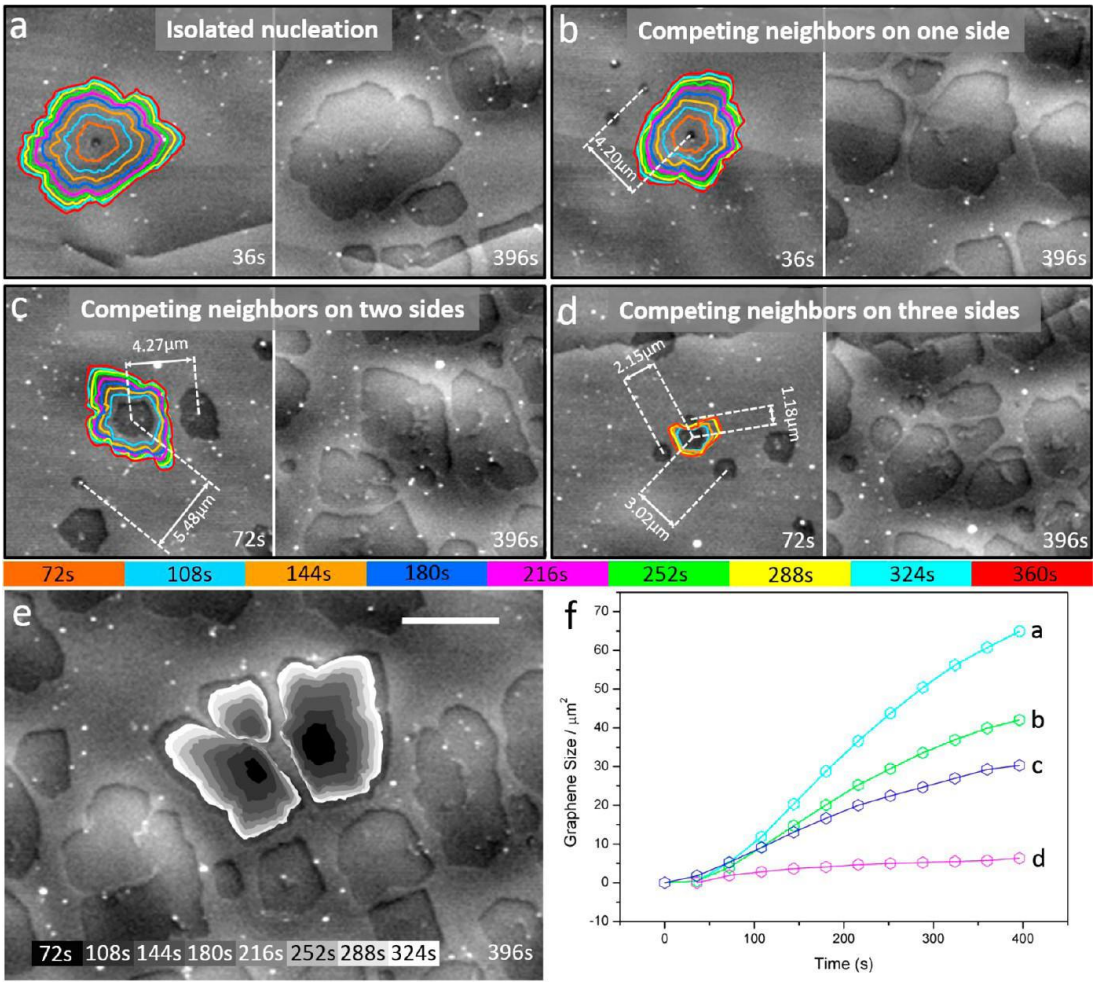

Figure 1: (a-d) Shape evolution of growing graphene sheets as a function of the local surrounding. The outlines of growing sheets are color coded according to the growth time provided in the color legend. Surface diffusion and growth competition within the capture layer influence growth shape and rate as shown in (e) and (f). Scale bar in (e) measures 5 μm.

P13 Study of thermal stability of (3-aminopropyl)trimethoxy silane-modified titanate nanotubes for application as nanofillers in polymers

Milivoj Plodinec (1), Andreja Gajović (1), Damir Iveković (2), Jelena Macan (3), Tatjana Haramina (4), Marc Willinger (5)

1) Ruđer Bošković Institute, Zagreb, Bijenička 54, HR-10000 Zagreb, Croatia

2) Faculty of Food Technology and Biotechnology, University of Zagreb, Pierottijeva 6, HR-10000 Zagreb, Croatia

3) Faculty of Chemical Engineering and Technology, University of Zagreb, Marulićev trg 19, HR-10000 Zagreb, Croatia

4) Faculty of Mechanical Engineering and Naval Architecture, University of Zagreb, Ivana Lučića, HR-10002 Zagreb, Croatia

5) Fritz-Haber-Institute der Max-Planck-Gesellschaft, Faradayweg 4-6, 14195 Berlin, Germany

Keywords: titanate nanotubes surface modified by (3-aminopropyl) trimethoxy silane; thermal stability; epoxy-based nanocomposites

Titanate nanotubes (TiNT) [1] are a mesoporous TiO2-based nanomaterial extensively studied over the last decade. In comparison to other nanotubular materials, TiNT exhibit some distinct advantages, including the ease with which they can be prepared in high purity and high yield, a low cost, a high specific surface area, a high density of surface OH-groups, and ion-exchange and semiconducting properties [1]. Due to the high density of surface OH-groups (in average, 5.8 OH-groups per nm2 [2]), TiNT are a promising material for surface modifications, particularly with functionalized alkoxysilanes, (RO)3Si−R'X, where R'X denotes an alkyl chain terminating with a functional group X. Depending on the nature of the group X, the physical and chemical properties of the TiNT surface can be varied and a range and the potential field of application of TiNT can be greatly expanded. Titanate nanotubes are a promising nanofiller for polymer composite materials. Their modulus is comparable to that of carbon nanotubes, they can be produced in large quantities, and the chemistry of their surface modification is the same as for conventional inorganic fillers. In this work [3], chemically modified TiNTs were studied. The aim was to prepare TiNT-H surface-modified with (3-aminopropyl)trimethoxy silane (APTMS) that can be further used for strengthening of polymers. Usage of prepared nanotubes for polymer reinforcement was also studied. Protonated titanate nanotubes (TiNT-H) were surface-modified with APTMS by novel method suitable for syntheses of large amounts of materials with low costs. Transmission electron microscopy was used for the investigation of the prepared nanotubes, while the polymer nanocomposite were examined by scanning electron microscopy (SEM) measuremets working in STEM mode. Since the thermal stability of nanofiller was important to preserve their functional properties, stability was studied by in situ high temperature Raman spectroscopy before inbuilt in polymer. The most temperature stable sample, 20 min silanized nanotubes, was used for preparation of epoxy-based nanocomposites (Fig. 1 a). All the APTMS modified titanate nanotubes were bond well with the epoxy matrix (Fig. 1 b) since amine groups on the TiNTs surface can react with epoxy group to form covalent bonds between the matrix and the nanofiller. This nanofiller form smaller (few hundreds of nm) and larger (few μm) aggregates in polymer (Figs. 1 c and d), where the amount of aggregates increase with addition of

nanofillers. Very small addition (0.19 – 1.52 wt%) of nanotubes significantly increased the glass transition temperature and the modulus in rubbery state of the epoxy based polymer. A smaller amount of added nanofiller provide larger increase in these parameters and therefore better dynamic mechanical properties due to the smaller amount of large aggregates. In this work APTMS modified tianate nanotubes were proved as promising nanofiller in epoxy based nanocomposits.

References: 1. H. H. Ou and L. S. Lo Sep. Purif. Technol. 58 (2007) 179-91 2. V. D. Bavykin and C. F. Walsh, Titanate and Titania Nanotubes Synthesis, Properties and Applications, RSC Nanoscience & Nanotechnology Cambridge (2009) 100-1. 3. M. Plodinec et. al. Nanotechnology 25 (2014) 435601-435614.

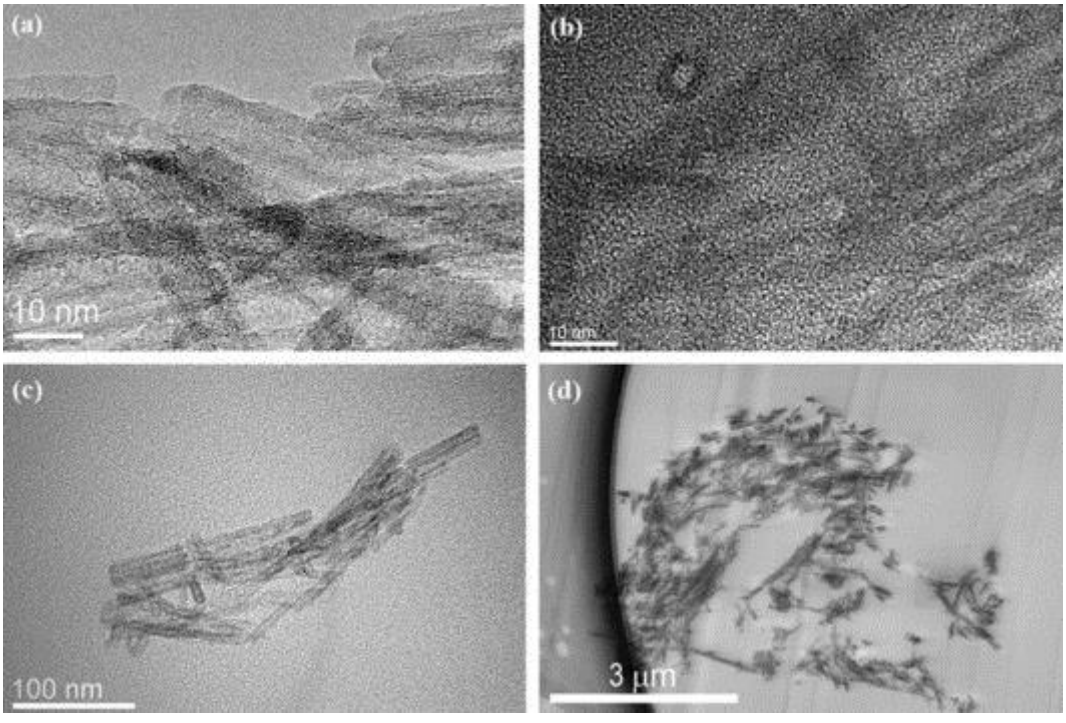

Figure 1: (a) Titanate nanotubes modified with (3-aminopropyl)trimethoxy silane, (b) APTMS modified nanotubes inbuilt in polymer, (c) smaller and (d) larger nanotube aggregates of nanofiller in polymer.

P14 Imaging the behaviour of silver nanoparticles in biological media

Marija Ćurlin (1), Darija Jurašin (2), Srećko Gajović (1), Ivana Vinković Vrček (3)

1) Croatian Institute for Brain Research, School of Medicine, University of Zagreb, Šalata 12, 10000-Zagreb, Croatia

2) Ruđer Bošković Institute, Bijenička cesta 54, 10000-Zagreb, Croatia

3) Institute for Medical Research and Occupational Health, Ksaverska cesta 2, 10000-Zagreb, Croatia

Keywords: silver nanoparticles, biologic media, BSA, aggregation, TEM

Research and development in the area of nanoscience and nanotechnology offer new opportunities for making superior nanomaterials (NMs) having an enormous economic potential for new drugs and medical treatments, electronics, environmental remediation. Due to the large production volume of NMs, manufactured nanoparticles (NPs), the primary building blocks of NMs, may be released into the environment during handling, washing, disposal or abrasion, thus, raising concerns about potential toxic effects of NMs on the environment and human health. Despite a number of biological studies on the toxicity of various NPs in vitro or in vivo, strict physicochemical data on the primary steps of their stability and behaviour in biological media are still missing. In order to draw valid conclusions from the evaluation of the cellular influences of NPs, we performed comprehensive evaluation on characteristics and stability of silver NPs using transmission electron microscopy. The purpose of this study was to analyze the dispersability of silver NPs under conditions close to body fluids. We used Dulbecco's Modified Eagle Medium (DMEM) cell culture medium as a prominent example which was supplemented with different amounts of bovine serum albumin (BSA), a common serum protein. We have selected 7 types of silver NPs (coated with citrate, poly-L-lysine, cetyltrimethylammonium, bis(2-ethylhexyl) sulfosuccinate, Tween 20, polyvinylpyrrolidone, and dodecyltrimethylammonium) which differ according to the coating agent applied for surface modifications. For all types of NPs tested, the aggregation behaviour was evaluated upon suspension in DMEM, with and without BSA. The TEM results showed particles organized in nanometric, but also in micrometric agglomerates. Addition of BSA inhibited aggregation of NPs. Therefore, biocompatible bulky capping agents, such as BSA provided steric colloidal stabilization.

Financial support of EU FP7 grant Glowbrain (REGPOT-2012-CT2012-316120) is acknowledged.

References: This research was supported by EU FP7 grant Glowbrain (REGPOT-2012-CT2012-316120).

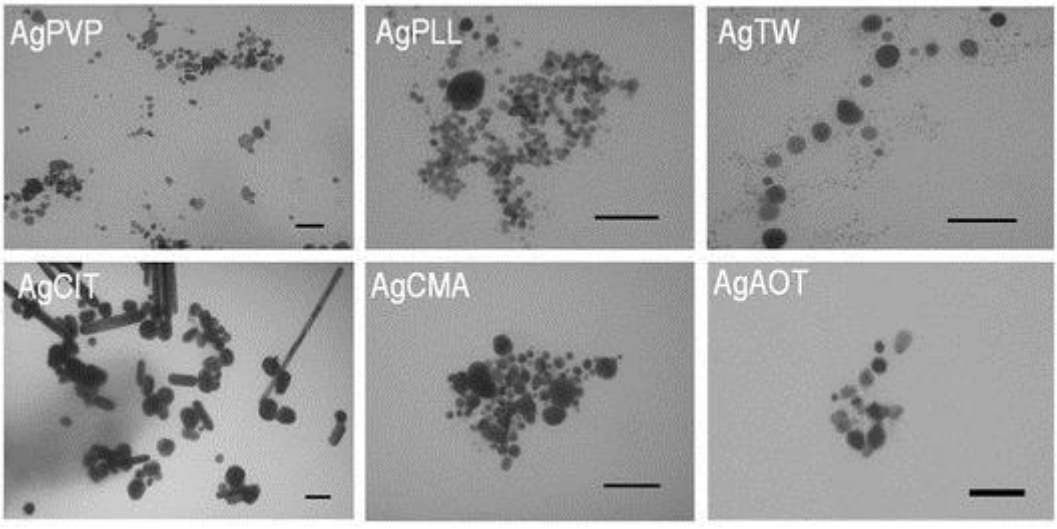

Fig. 1. Silver nanoparticles in DMEM coated by different coating agents (PVP, polyvinylpyrrolidone; PLL, poly-L-lysine; TW, Tween20; CIT, citrate; CMA, cetyltrimethylammonium; AOT, bis(2-ethylhexyl) sulfosuccinate). Bars 100 nm.

P15 Human sperm ultrastructure: revealing the structure of sperm head vacuoles

Jasna Strus (1), Magda Tušek Žnidarič (2), Nina Fekonja (1), Irma Virant Klun (3)

1) Department of Biology, University of Ljubljana, Biotechnical Faculty, Jamnikarjeva 101. SI-1000 Ljubljana Slovenia

2) National Institute of Biology, Večna pot 111, 1000 Ljubljana, Slovenia

3) Reproductive Unit, Department of Obstetrics and Gynecology, University Medical Centre Slajmerjeva 3, 1000 Ljubljana, Slovenia

Keywords: sperm cell, transmission electron microscopy, DIC microscopy, chromatin reorganization

The ultrastructure of normal (normozoospermia) and abnormal (teratozoospermia) sperm cells was investigated with differential interference microscopy (DIC) and.transmission electron microscopy. A detailed description of sperm head vacuoles, their size and number was studied in sperm samples of men involved in the in vitro fertilization program.The sperm head vacuoles observed under the high magnification of light microscopy were mostly described as "pocket-like" nuclear concavities related to failure of chromatin condensation [1, 2]. The origin and dynamics of sperm head vacuoles is not well understood and their role in sperm function is questionable. Some authors suggest that sperm vacuoles are normal features of sperm head and others describe them as degenerative structures related to male subfertility. In our study the ultrastructure of sperm head vacuoles is described and discussed in relation to sperm maturation and chromatin reorganization.

For ultrastructural investigation 10 samples of normozoospermic men and 6 samples of teratozoospermic men were fixed in 2.5 % glutaraldehyde and 1 % paraformaldehyde in 0.1 MPB, pH 7.0 for 24 h at 4°C, postfixed with 1 % OsO_4 in 0.1 MPB for 1.5 h and embedded in Agar 100 resin (Agar Scientific). Ultrathin sections were contrasted with 4 % water solution of uranyl acetate and Reynolds lead citrate and examined with Philips CM 100 electron microscope.

The observation of sperm cells with DIC microscope showed several small and larger surface concavities termed sperm vacuoles, usually located in the head of sperm cells (Fig. A). In TEM micrographs sperm head vacuoles are seen as electron lucent areas of various sizes and positions with very variable structure (Fig.B).The results of this study indicate that sperm samples of men with teratozoospermia are characterized by increased number and size of sperm head vacuoles although they are present also in sperm samples of normospermic men [3]. Large sperm head vacuoles are mostly surface bulges which contain abundant membrane whorls and fine granular material. Membrane whorls are composed of single and double membrane layers with septate electron dense molecular complexes which are continuous with the nuclear envelope (Figs.C,D).. Acrosome was fully developed in most spermatozoa with sperm head vacuoles and interconnections of the inner acrosomal membrane and nuclear envelope were observed ocasionally. The degree of chromatin condensation differed significantly between the sperm cells, with less condensed chromatin prevailing in.abnormal sperm cells. Based on our ultrastructural findings we suppose that sperm head vacuoles are the sites of removal of membranous material and proteins during chromatin reorganization. The

exact origin and role of membrane whorls in sperm head vacuoles remains to be established in relation to further ultrastructure research.

References: 1 F.Boitrelle et al. 2013. Reprod BioMed online 27 (2) : 201-211 2 A.Perdrix et al. 2011. Human Reproduction 26 : 47–58 3 N.Fekonja et al.2014 Biomed Res Int.2014, ISSN 2314-6141 This research was supported by the National Medical Ethics Committee.

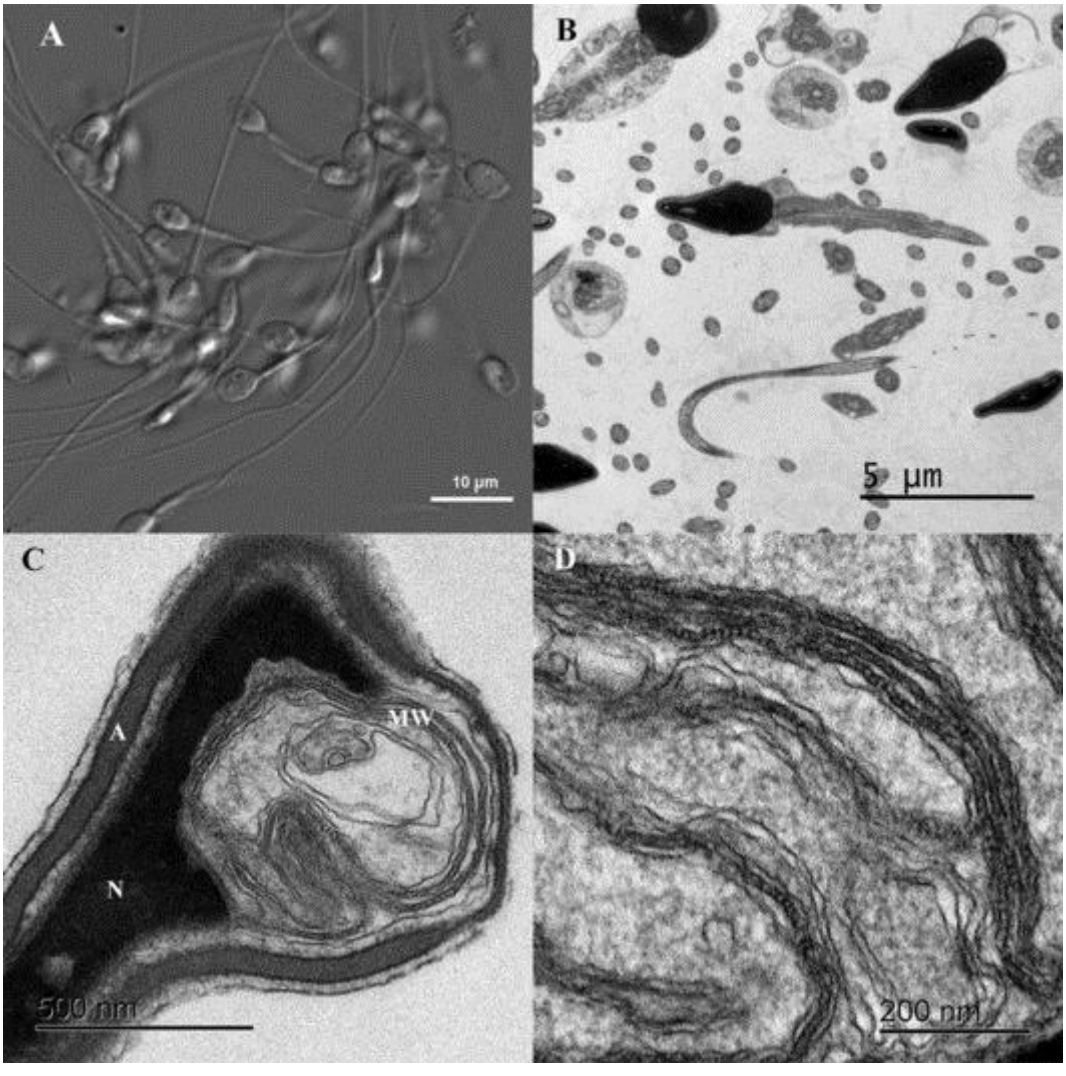

Figure 1. DIC micrograph of sperm cells with sperm kead vacuoles in normozoospermic men (A), ultrathin section of normozoospermic cells (B), invaginated sperm nucleus (N) with sperm head vacuole containing membrane whorls (MW), acrosome (A)

P16 Order and patterns in self-assembled marine gel networks: image data analysis and future perspectives

S. Habazin (1), G. Pletikapić (2), T. Mišić Radić (2), V. Svetličić (2)

1) Division of Biology, Faculty of Science, University of Zagreb, Rooseveltov trg 6, 10000-Zagreb, Croatia

2) Laboratory for bioelectrochemistry and surface imaging, Division of marine and environmental research, Ruđer Bošković Institute, Bijenička cesta 54, 10000-Zagreb, Croatia

Keywords: complexity, biopolymers, atomic force microscopy, marine biogeochemistry

Together with dissolved and particulate fractions, marine gel phase represents the third large pool of organic matter important in element cycling in the ocean [1]. It is composed of macromolecular polysaccharide networks embedded in seawater and ranges in size from nanogels to macrogels, occasionally forming meter-sized aggregates often seen during increased primary production periods in the Northern Adriatic. Extensive atomic force microscopy (AFM) imaging, determination of chemical composition and single-molecule force spectrocopy that have been performed on marine gel networks in the past decade provided extensive insight into network topography, nanomechanical properties and mechanisms governing self-assembly and cross-linking of simple fibrils to complex entangled networks [2]. However, most of the studies mentioned lack quantitative network analysis and description often seen in other fields of systems biology or polymer science. In order to improve, broaden and standardize marine gel analysis protocols spanning from field sampling to statistical analysis, in this work we propose a simple toolkit comprised of freeware image analysis software and corresponding mathematical descriptors. Because of surprising similarity with vascular networks, we have successfully employed angiogenesis analysis software (AngioTool) for network skeletonization and branching point detection [3], as well as ImageJ plugins (gijPoreanalysis and Particle Analyzer) for pore quantitation on AFM images of marine gel networks obtained in tapping or contact mode. For a series of images branching index, lacunarity, fractal dimension and pore size distribution was determined to evaluate how well and consistent the latter parameters describe marine gel network maturity and degree of its complexity. Similar networks were also seen forming by process of self-organization within extracellular polymeric substances of diatoms. Further development of our analyses could shed a new light on pattern-forming mechanisms and mathematical interpretation of self-assembled and self-organized biopolymer networks in the marine environment.

References: 1. Verdugo, P et al., Mar. Chem. 92 (2004) 67-85. 2. Svetličić, V et al., Int. J. Mol. Sci. 14 (2013) 20064-20078. 3. Zudaire, E et al., PLOS ONE 6(11): e27385. doi: 10.1371/journal.pone.0027385.

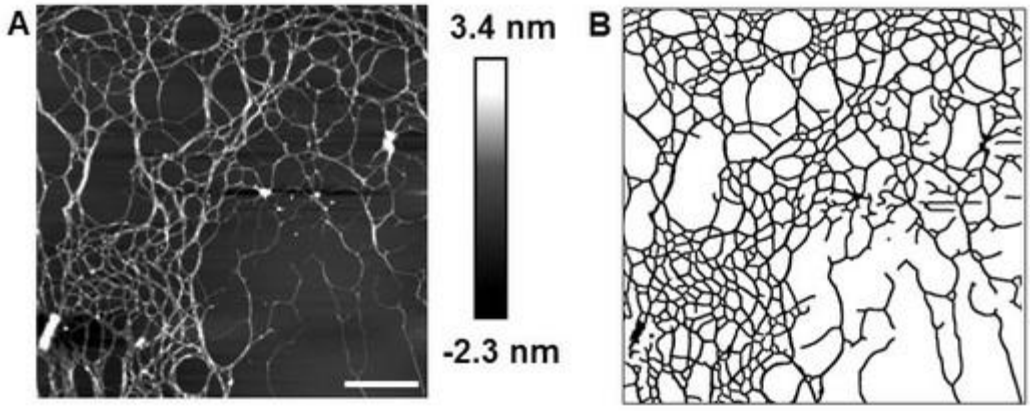

Figure 1. Typical marine gel network as imaged by AFM (A), and binary image of extracted skeleton that served as a basis for quantitative analysis (B). Scale bar: 1 μm.

P17 Analytical electron microscopy study on stability criteria of Pt/C fuel cell catalysts

Elena Willinger (1), Youngmi Yi (1), Raul Blume (2), Andrey Tarasov (1), Michael Scherzer (1), Cyriac Massué (1), Robert Schlögl (1), Marc Willinger (1)

1) Inorganic chemistry department, Fritz-Haber Institute of the Max Planck Society, Faradayweg 4-6, 14195 Berlin, Germany

2) Helmholtz-Zentrum Berlin für Materialien und Energie, Hahn-Meitner-Platz 1, 14109 Berlin, Germany

Keywords: Pt/C fuel cell catalysts, HRTEM, XPS

Durability is a key issue in the performance of Pt/C fuel cell electro catalysts for the oxygen reduction reaction (ORR). Several degradation mechanisms were suggested for Pt/C catalysts [1], which can be divided into a primary degradation process due to carbon support corrosion and a secondary loss of activity due to Pt particle detachment and sintering [2]. The detachment of Pt particles is caused by instability of the carbon support and a weak platinum-carbon interaction. Since these degradation processes occur on the nano- and even atomic level, analytical transmission electron microscopy (TEM) is ideally suited for their investigation. To develop a better understanding on how the carbon support structure can influence the degradation processes on the nanoscale, three specific Pt/C catalysts with different structural characteristics of carbon black were investigated in depth: sample A consists of a highly graphitic carbon black with a low surface area; sample B is a highly defective carbon black which contains both, high and low surface area carbon particles; finally, sample C, which is a highly functionalized and defective carbon with high surface area carbon particles. All three materials have the same platinum loading with a particle size of 3-4 nm. Differences in their performance can thus be related to the characteristics of the respective carbon support. A combination of different characterization methods, such as HRTEM, HAADF STEM, EELS, XPS, XRD, electrochemical cyclovoltammetry and thermogravimetry has been applied to provide a thorough and comparative analysis of the three samples. It will be shown how the degree of graphitization relates to the thermal and electrochemical stability of the catalysts and how the Pt support interaction varies for the different types of carbon structures (Fig. 1). High resolution imaging of the interfaces between Pt and carbon reveals differences in the respective wetting angles and associated particle shape (Fig. 1b and 1d). Based on the characteristic differences of the investigated carbon supports we can define parameters for the best compromise in terms of stability and activity.

References: [1] Shao-Horn, Y., Sheng, W.C., Chen, S., Ferreira, P.J., Holby, E.F., Morgan, D., Top. Catal. 2007; 46: 285-305 [2] Josef C.Meier, Carolina Galeano, Ioannis Katsounaros, Jonathon Witte, Hans J. Bongard, Angel A. Topalov, Claudio Baldizzone, Stefano Mezzavilla, Ferdi Schueth and Karl J.J. Mayrhofer, Beilstein J. Nanotechnol. 2014; 5: 44-67.

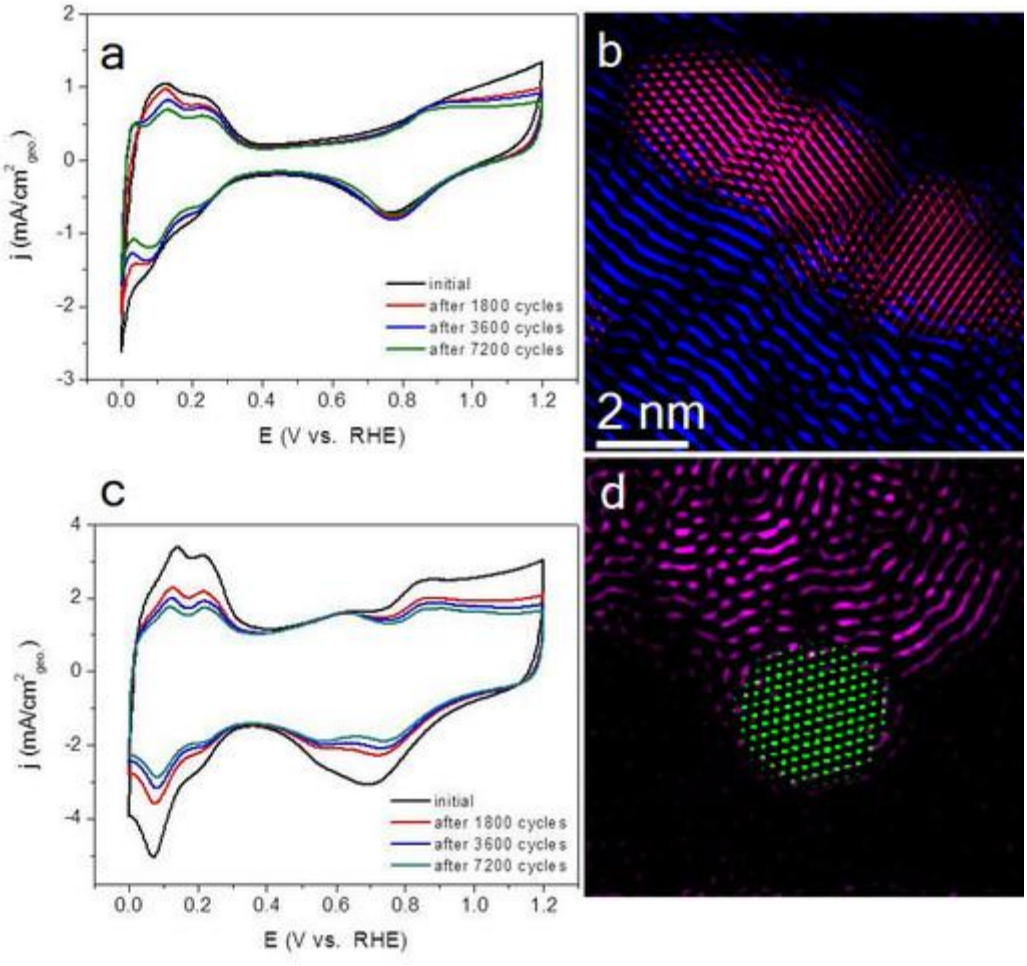

Fig. 1: Cyclovoltammetry plots and Fourier-filtered HRTEM images of Pt on carbon A (a, b) and C (c, d).

P18 High-resolution and high-speed atomic force microscopy simultaneous to advanced optical microscopy

Heiko Haschke (1), Dimitar Stamov (1), Torsten Jähnke (1)

1) JPK Instruments AG, Bouchéstrasse 12, 12435 Berlin

Keywords: AFM, bioAFM, combination with optics

In recent years, atomic force microscopy (AFM) has become a well-established technique for single molecule studies and even sub-molecular scale research. Several new developments in terms of faster AFM imaging and imaging modes, based on the phase or frequency, have been established in order to decrease the cantilever response time and increase the AFM's scan speed, e.g., for studying molecular dynamics.

The novel NanoWizard® ULTRA Speed AFM combines the latest scanner technologies and compact design allowing a full integration of AFM into advanced commercially available optical microscopy. Thus, fast AFM imaging of approximately 1 frame per second can be seamlessly combined with methods such as, fluorescence, confocal, TIRF, STED microscopy and many more. Individual molecule dynamics can now be studied with AFM and simultaneously with optical microscopy by applying JPK's tip scanner technology.

With JPK's HyperDrive™ sub-molecular resolution is achieved even on soft samples imaged in liquid environments. It allows for imaging with smallest amplitudes of often approximately 0.2 nm for lowest tip-sample interaction. Topographical images of membrane proteins and DNA-origami are presented. It has been shown that the phase response in phase modulation AFM (PMAFM) is faster allowing higher imaging speeds for the study of molecule kinetics. In conjunction with JPK's NanoWizard® ULTRA Speed AFM, a dynamic biomechanical study of Bacteriorhodopsin (bR) when interacting with photons will be discussed.

More than half a century after the first high-resolution electron microscopy images of collagen type I banding of 67 nm have been reported, now with the NanoWizard® ULTRA Speed AFM we could gain a high-resolution temporal insight into the dynamics of collagen I fibril formation and its characteristic 67 nm banding hallmark. The literature still abounds with conflicting data regarding the models of its fibril formation, structural intermediates, and kinetics. AFM is the only currently available high-resolution imaging technique amongst many to offer insight into the collagen I fibrillogenesis by operating in situ. The described technique could be instrumental for future studies of the structural dynamics of protein systems, etc.

The systems newly gained flexibility will also be demonstrated on a study of living fibroblast cells directly imaged in their culture petri dish at 37 degrees C. Here, the dynamics of individual membrane structures is investigated with AFM while simultaneously observing the individual living cell with optical phase contrast. The unambiguous correlation between AFM and optical microscopy is achieved by the DirectOverlay™ technique.

INDEX OF PARTICIPANTS

JEOL PROPOSES A NEW ANALYTICAL TEM

JEM | 2800

HIGH THROUGHPUT ELECTRON MICROSCOPE

Quick Turn Around Time

Full automation

- Auto contrast / brightness
- Auto sample height control
- Auto crystal orientation alignment
- Auto focus control
- Auto stigmator control

All-in-one for easy use by anyone

JEOL

www.jeol.com

SCAN, d.o.o., Nazorjeva 3, SI-4000 Kranj | Tel. +386 4 2750200 | Fax. +386 4 27502040 | info@scan.si | www.scan.si

Future is Cold FEG

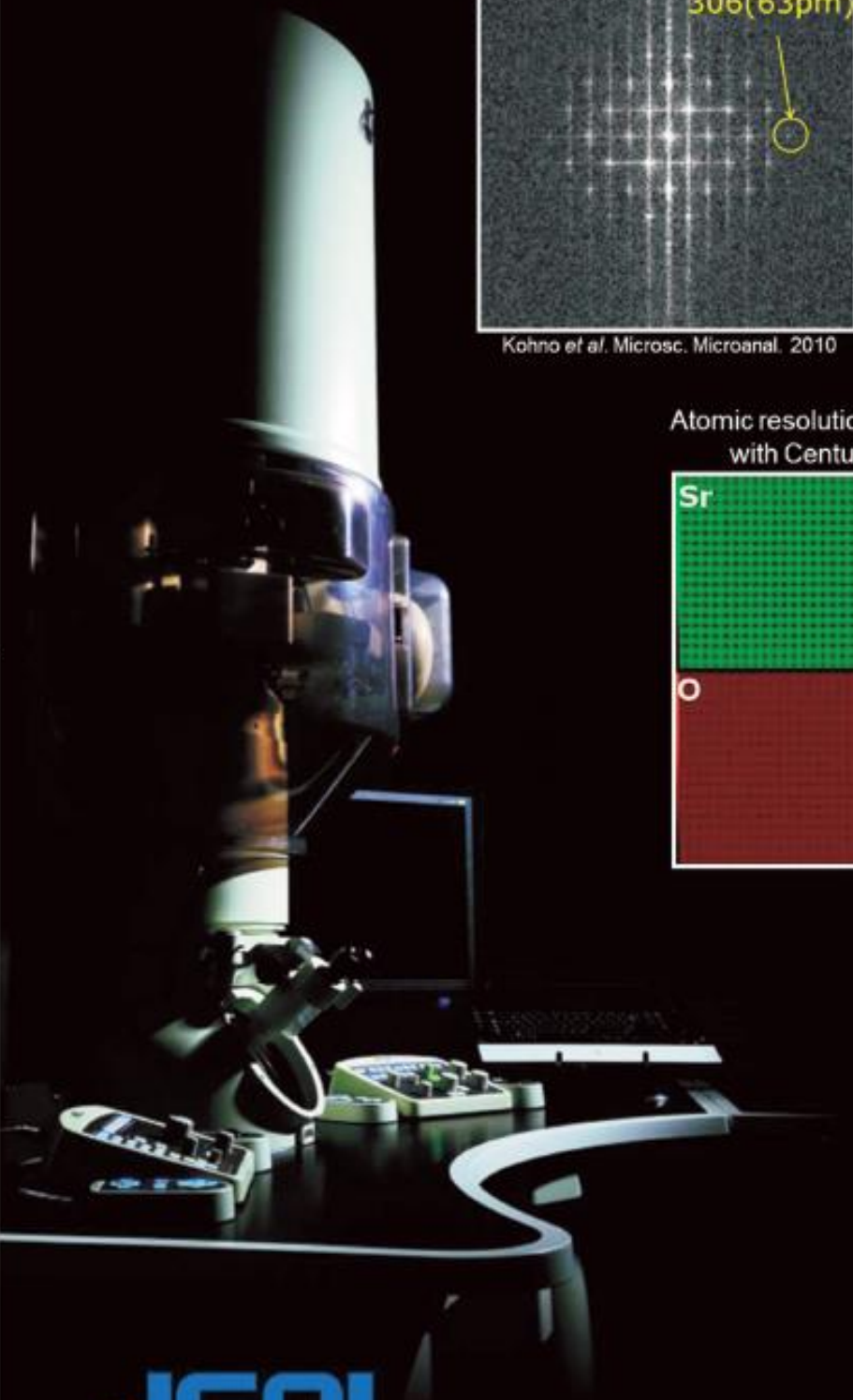

FFT pattern GaN (211)

Kohno *et al.* Microsc. Microanal. 2010

Atomic resolution EDS mapping
with Centurio detector

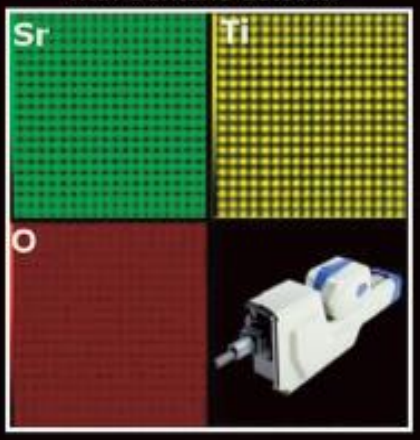

Direct imaging of hydrogene-
atom columns by ABF

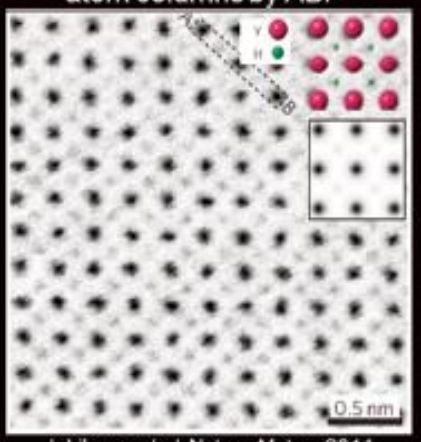

Ishikawa *et al.* Nature Mater. 2011

JEOL

Serving Advanced Technology
since 1949
www.jeol.com

SCAN, d.o.o., Nazorjeva 3, SI-4000 Kranj
Tel. +386 4 2750200; Fax. +386 4 27502040
info@scan.si; www.scan.si

Requirements for Live-Cell Imaging

Dr. Jens Peter Gabriel Product and Application Manager Widefield, Leica Mikrosysteme Vertrieb GmbH

Live-cell imaging allows researchers to study dynamic processes like protein trafficking, cell growth, mitosis, or cytoskeleton organization. With fluorescent probes that label proteins of interest, or functional probes like calcium indicators and FRET dye pairs, it can provide unprecedented insight into cellular function and organization. However, there are also challenges involved in maintaining cell viability for extended periods of time under the microscope.

Environmental conditions like temperature and CO2 concentration need to be carefully controlled in order to ensure proper function of the cells. Due to phototoxicity, exposure to fluorescence excitation light must be minimized while obtaining a sufficiently high signal-to-noise ratio. In case of fast intracellular events, high frame rates need to be achieved in order to capture them faithfully. Finally, a fast and gentle autofocus is needed to compensate for temperature drift that otherwise leads to a loss of focus in long-term recordings.

With the focus on the new Leica DMi8 inverted microscope, the presentation will show how hardware and software need to be designed to meet these special requirements for live-cell imaging. In addition to widefield microscopy, other techniques like Total Internal Reflection Fluorescence (TIRF) Microscopy, Spinning Disk Confocal Microscopy, and Super-Resolution Microscopy will be discussed.

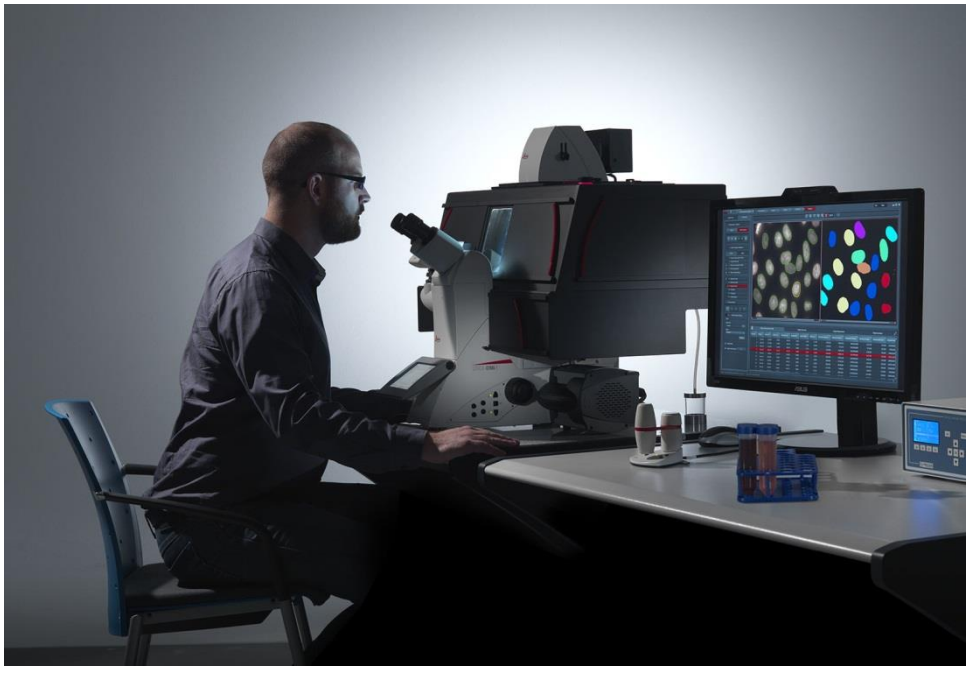

Figure "lms-dmi8": The new Leica DMi8 inverted microscope and LAS X software are perfectly suited for advanced live-cell imaging experiments.

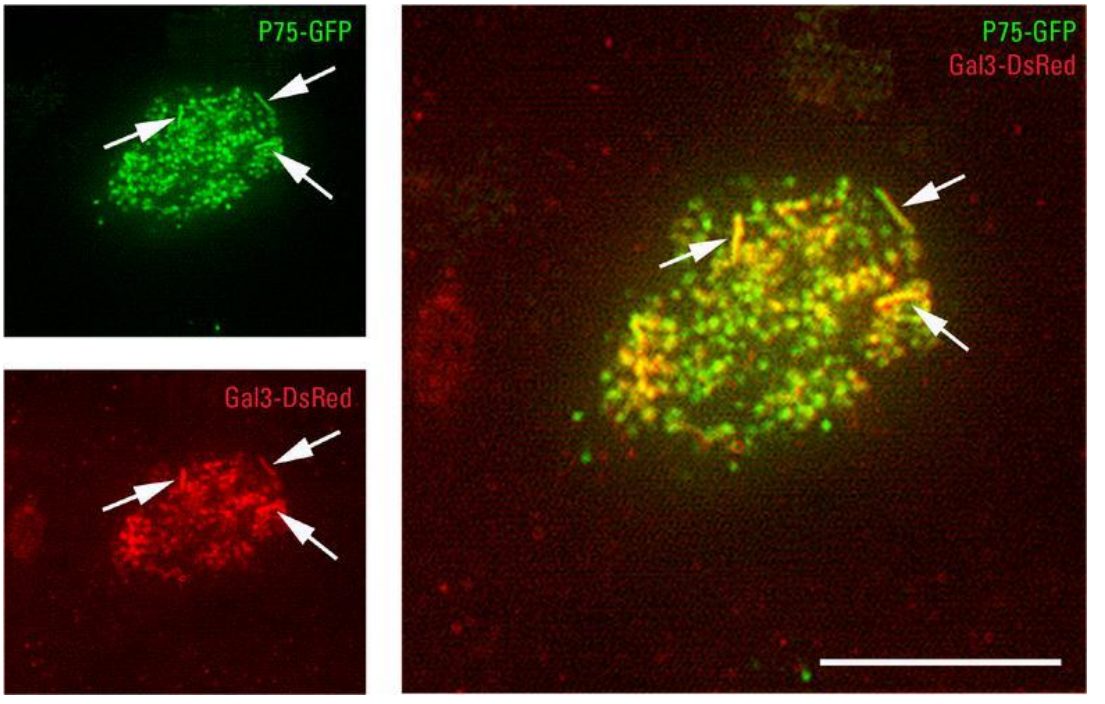

Figure „Figure-2“ Interaction of Galectin-3-DsRed and P75-GFP – P75-GFP and its sorting receptor Galectin-3-DsRed at the apical cell pole of MDCK cells shows a brought overlap of the two proteins. Scale bar 10 µm.

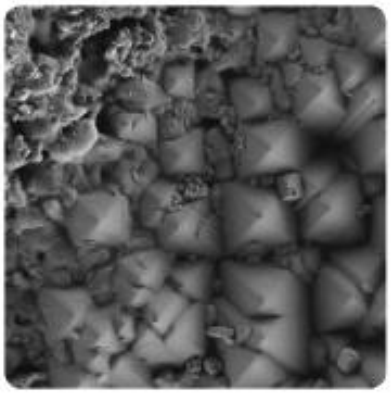
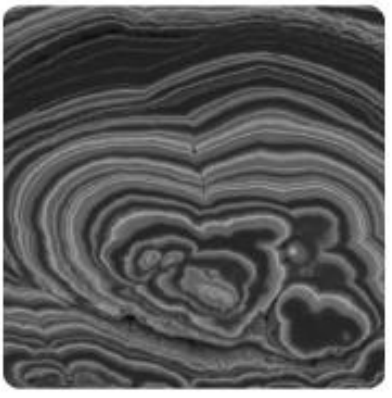
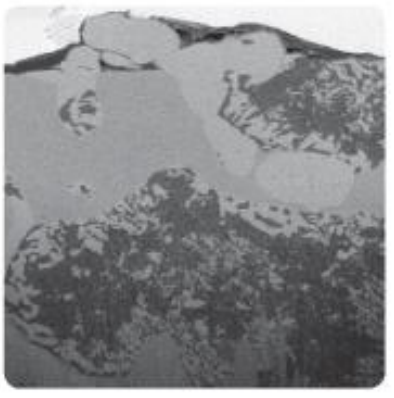
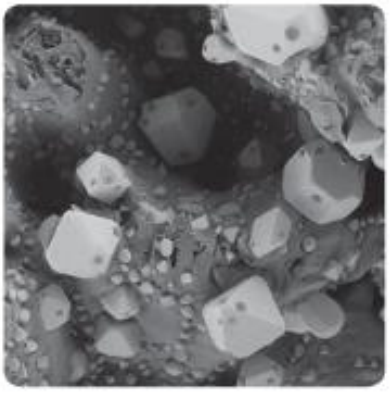

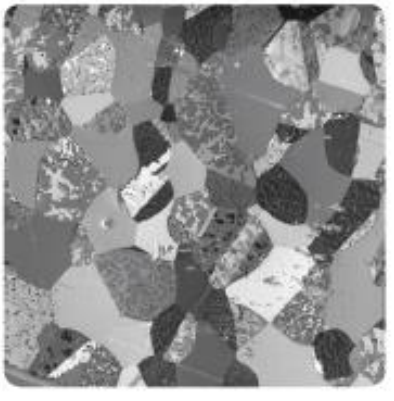

Redefining Productivity in Materials Research

Fast, thorough, and easy-to-use 2D and 3D sample characterization.

FEI's new Scios™ DualBeam™ offers high resolution, high throughput SEM and FIB imaging and analysis—even for magnetic, glass or non-conductive materials.

- **Full surface visualization:** Clearly distinguish materials and topographic contrast
- **Go deeper:** Reveal buried features or sample structure
- **Fast answers:** Rapidly create site-specific samples for S/TEM, EBSD, or atom probe when additional analysis is required

Learn more at **FEI.com/SciosDualBeam**

mikro+polo your partner in the laboratory

FEI™

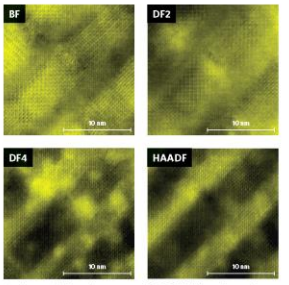

4 channel simultaneous HRSTEM imaging of $SrTiO_3$ using 4 STEM detectors.

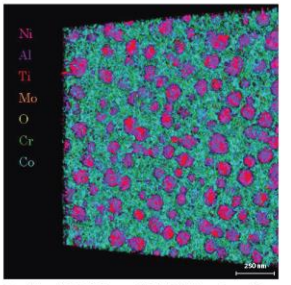

Combined 3D EDS map: Ni, Al, Ti, Mo, Cr, and Co.

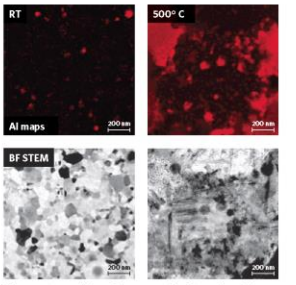

Temperature driven Al aggregation in solar cell. Sample courtesy of Dr. S. Kraschewski, U. Erlangen.

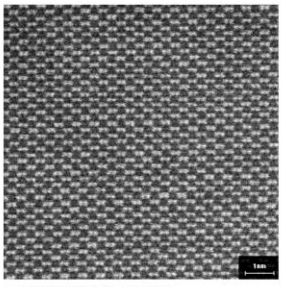

HRSTEM of Si (110) at 200kV.

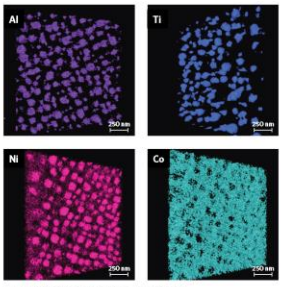

3D EDS maps at different angles.

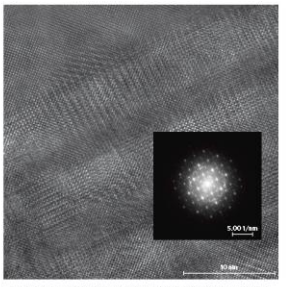

HRTEM image of $SrTiO_3$ with Ceta 16M camera.

Fast 2D & 3D Imaging and Chemical Analysis with Talos TEM

Whether you work with metals, light elements, or nanoparticles—from macro to atomic scales—Talos gives you insight into structure and composition for a complete understanding of material properties.

High speed 2D and 3D EDS analysis: Fast, multichannel, automated EDS acquisition and precise quantification to obtain multidimensional compositional maps.

Fast navigation and imaging: Highest throughput, highest resolution uncorrected S/TEM images—even for beam sensitive and challenging materials.

Space to do more: FEI TEMs have the space to accommodate additional *insitu* holders for dynamic imaging, diffraction, and tomography applications.

Watch the movie at **FEI.com/DiscoverTalos**

Explore. Discover. Resolve.

mikro+polo® your partner in the laboratory

FEI™

LIST OF PARTICIPANTS

First Name	Last Name	Email	Country
Andreja	**AMBRIOVIC RISTOV**	Andreja.Ambriovic.Ristov@irb.hr	Croatia
Jordi	**ARBIOL**	arbiol@icrea.cat	Spain
Tihomir	**BALOG**	balog@irb.hr	Croatia
Marin	**BARISIC**	marin.barisic@ibmc.up.pt	Portugal
Eva	**BARTOVA**	bartova@ibp.cz	Czech Republic
Dragutin	**BAUMAN**	dragutin.bauman@zg.t-com.hr	Croatia
Karim	**BENIHOUD**	karim.benihoud@gustaveroussy.fr	France
Ivana	**BOČINA**	bocina@pmfst.hr	Croatia
Till	**BRETSCHNEIDER**	T.Bretschneider@warwick.ac.uk	United Kingdom
Guillaume	**BRUNETTI**	brunetti@jeol.fr	France
Mia	**BUŽANČIĆ**	buzancic@izor.hr	Croatia
Alan Jenkin	**CHAN**	alan.chan@u-psud.fr	France
Vida	**ČADEŽ**	vcadez@irb.hr	Croatia
Đurđica	**ČANADI KNEŽEVIĆ**	djurdjica.canadi-knezevic@ansar-analitika.hr	Croatia
Miran	**ČEH**	miran.ceh@ijs.si	Slovenia
Marija	**ĆURLIN**	marija.curlin@mef.hr	Croatia
Igor	**DJERDJ**	igor.djerdj@irb.hr	Croatia
Ivana	**DUJMOVIĆ**	idujmovic@ffst.hr	Croatia
Paul	**DYSON**	p.j.dyson@swansea.ac.uk	United Kingdom
Jan	**FAIX**	faix.jan@mh-hannover.de	Germany
Jincheng	**FAN**	Jincheng.Fan@irb.hr	Croatia
Hrvoje	**FULGOSI**	fulgosi@irb.hr	Croatia

Jens Peter	**GABRIEL**	jens.gabriel@leica-microsystems.com	Germany
Andreja	**GAJOVIĆ**	gajovic@irb.hr	Croatia
Srećko	**GAJOVIĆ**	srecko.gajovic@hiim.hr	Croatia
Siniša	**HABAZIN**	sinisa_habazin@hotmail.com	Croatia
Maja	**HERAK BOSNAR**	mherak@irb.hr	Croatia
Paul	**HERRON**	paul.herron@strath.ac.uk	United Kingdom
Martina	**IVŠIĆ**	martina.ivsic@gmail.com	Croatia
Boštjan	**JANČAR**	bostjan.jancar@ijs.si	Slovenia
Ivanka	**JERIĆ**	ijeric@irb.hr	Croatia
Ute	**KAISER**	ute.kaiser@uni-ulm.de	Germany
Alon	**KALO**	alonkalo@gmail.com	Israel
Agnes	**KITTEL**	kittel.agnes@koki.mta.hu	Hungary
Mariana	**KLEMENTOVA**	klemari@fzu.cz	Czech Republic
Kiyoshi	**KOBAYASHI**	kkoba@yamanashi.ac.jp	Japan
Emilija	**KOSTADINOVSKA**	emilija.kostadinovska@ugd.edu.mk	Macedonia
Marijeta	**KRALJ**	marijeta.kralj@irb.hr	Croatia
Damir	**KRALJ**	kralj@irb.hr	Croatia
Guillaume	**LATHUS**	sales@jeol.fr	France
Maja	**LAZAROVA**	maja.lazarova@ugd.edu.mk	Macedonia
Adriana	**LEPUR**	Adriana.Lepur@irb.hr	Croatia
Sonja	**LEVANAT**	sonja.levanat@irb.hr	Croatia
Manca	**LOGAR**	manca.logar@ki.si	Slovenia
Alessio	**LOMBARDO**	m.malaspina@assing.it	Italy
Nikola	**LJUBEŠIĆ**	ljubesic@rudjer.irb.hr	Croatia
Jelena	**MACAN**	jmacan@fkit.hr	Croatia

Gabriele	**MAEURER**	Gabriele.Maeurer@bruker.com	Germany
Marijan	**MARCIUŠ**	mmarcius@irb.hr	Croatia
Mario	**MATOŠEVIĆ**	Mario.Matosevic@ina.hr	Croatia
Ognjen	**MILAT**	milat@ifs.hr	Croatia
Shunsuke	**MUTO**	s-mutoh@nucl.nagoya-u.ac.jp	Japan
Matej	**NOVAK**	matej.novak@mikro-polo.si	Slovenia
Bela	**PECZ**	pecz@mfa.kfki.hu	Hungary
Rainer	**PEPPERKOK**	nina.bader@embl.de	Germany
Ivo	**PIANTANIDA**	pianta@irb.hr	Croatia
Chantal	**PICHON**	chantal.pichon@cnrs-orleans.fr	France
Milivoj	**PLODINEC**	mplodin@irb.hr	Croatia
Danijela	**POLJUHA**	danijela@iptpo.hr	Croatia
Velimir	**RADMILOVIĆ**	VRRadmilovic@tmf.bg.ac.rs	Serbia
Neda	**SLADE**	slade@irb.hr	Croatia
Barbara	**SLADONJA**	barbara@iptpo.hr	Croatia
Melita	**SLAVIČEK**	melita.slavicek@inel-mt.hr	Croatia
Ljerka	**SLOKAR**	slokar@simet.hr	Croatia
Lucia	**SPASEVSKI**	mikrolux@email.t-com.hr	Croatia
Suzana	**ŠEGOTA**	ssegota@irb.hr	Croatia
Petar	**ŠENJUG**	petar.senjug@inet.hr	Croatia
Marin	**ŠOUFEK**	mikrolux@email.t-com.hr	Croatia
Jasna	**ŠTRUS**	jasna.strus@bf.uni-lj.si	Slovenia
Stefan	**TERJUNG**	terjung@embl.de	Germany
Nenad	**TOMAŠIĆ**	ntomasic@geol.pmf.hr	Croatia
Antun	**TONEJC**	atonejc@phy.hr	Croatia

Anđelka	**TONEJC**	andelka@phy.hr	Croatia
Boris	**TURK**	boris.turk@ijs.si	Slovenia
Cristian	**VAILATI**	cristian.vailati@bruker.com	Italy
Jan	**VÁVRA**	vavra@jpk.com	Germany
Oliver	**VUGREK**	ovugrek@irb.hr	Croatia
Dušica	**VUJAKLIJA**	vujaklij@irb.hr	Croatia
Zhu-Jun	**WANG**	zhujun@fhi-berlin.mpg.de	Germany
Igor	**WEBER**	iweber@irb.hr	Croatia
Elena	**WILINGER**	kudrenko@fhi-berlin.mpg.de	Germany
Marc Georg	**WILLINGER**	willinger@fhi-berlin.mpg.de	Germany
Tea	**ZUBIN FERRI**	tea.zubin@gmail.com	Croatia
Vitalijs	**ZUBKOVS**	vitalijs.zubkovs@gmail.com	Switzerland
Slavko	**ŽIŽEK**	slavko.zizek@scan.si	Slovenia